TABLE OF CONTENTS

LIST OF TABLES

LIST OF FIGURES

Page

LIST OF ABREVIATIONS

2D	Two dimensional
3D	Three dimensional
4D	Four dimensional
ATC	Air Traffic Control
ATD	Along-the-Track Distance
ATM	Air Traffic Management
BADA	Base of Aircraft DAta
BTS	Bureau of Transportation Statistics
CDA	Continuous Descent and Approach
CO_2	Carbon dioxide
CYUL	Montreal – Pierre Elliott Trudeau International Airport
CYYZ	Toronto – Pearson International Airport
DST	Decision Support Tools
EHAM	Amsterdam Airport Schiphol
EOD	End Of Descent
ETE	Estimated Time En-route
FMS	Flight Management System
GA	Genetic Algorithms
GAME	General Aircraft Modeling Environment
GARDN	Green Aviation Research and Development Network
GRIB	GRIdded Binary Format
ICAO	International Civil Aviation Organization

LARCASE	Research Laboratory in Active Controls, Avionics and Aeroservoelasticity
LFPG	Paris Charles de Gaulle Airport
NextGen	Next Generation Air Transport System
NO_x	Nitrous Oxide gases
OTS	Organized Track System
RTA	Requested Time of Arrival
T/O	Take-Off
TOC	Top Of Climb
TOD	Top Of Descent
WMO	World Meteorological Organization
XML	Extensible Markup Language

LIST OF SYMBOLS AND UNITS OF MEASUREMENTS

a	ellipse semi-major axis length (Nm)
altitude	altitude (ft)
alt1	waypoint first altitude constraint (ft)
alt2	waypoint second altitude constraint (ft)
atd	Along-the-Track Distance (Nm)
b	ellipse semi-minor axis length (Nm)
c	ellipse main-axis extension distance (Nm or deg)
cg	center of gravity position (%MAC)
CGREFDIST	aircraft center of gravity reference point's position, as a distance from the aircraft's reference point (m)
constraint	waypoint constraint type (None, At, AtOrBelow, AtOrAbove, Gradient, or Window)
Crossover altitude	altitude at which the TAS values corresponding to a Speed schedule's IAS and Mach are equal
d	half-distance between the departure and destination airports (Nm)
d_1,d_2	waypoint 1 and 2 Along-the-Track Distance values (Nm)
d_{alt}	altitude variation (ft)
e	ellipse eccentricity (dimensionless)
f	ellipse focal distance (Nm)
FPA	Flight Path Angle (deg)
ft	feet
fuel	fuel weight (Kg)
fuelburn	fuel burn or fuel consumption, (Kg)

gradient	ground-referenced segment rate of climb or descent (ft/Nm)
graph node	a graph point corresponding to the intersection of two or more graph edges
graph edge	a graph transition corresponding to a vertical flight path segment stored in the look-up structure
GND_{dist}	ground-referenced horizontal distance (Nm)
GND_{speed}	ground referenced horizontal speed (Kts)
GS	ground speed (Kts)
gw	gross weight (Kg)
h	hour
h_1, h_2	altitudes at waypoints 1 and 2 (ft)
H_{dist}	horizontal distance (Nm)
H_{speed}	horizontal speed (Kts)
IAS	indicated airspeed (Kts)
ISA_Dev	air temperature deviation from the value corresponding to the standard atmosphere (°K or °C)
LEMAC	the leading-edge, mean aerodynamic chord position with respect to the datum (m)
Look-up structure	structure storing the set of pre-computed climb, cruise and descent vertical flight path segments
Kg	kilogram
Kts	knots
lat	latitude (deg)
lb	pound
lon	longitude (deg)

min	minute
M_a	aircraft moment (Kg m)
MAC	Mean Aerodynamic Chord (m)
Mach	Mach index (dimensionless)
M_f	fuel moment (Kg m)
MIN_DIST	horizontal segment imposed minimal distance (Nm)
Nm	nautical mile
Step-climb	constant speed climb segment used for increasing the cruise altitude
Step-descent	constant speed climb segment used for decreasing the cruise altitude
TAS	true air speed (Kts)
t_{clb}	climb segment flight time (h)
t_{crz}	level-flight segment flight time (h)
V_{speed}	vertical speed (Kts)
zfgw	zero fuel gross weight (Kg)
zfwcg	zero fuel weight center of gravity position (%MAC)
α	segment climb/descent angle (deg)
γ	segment slope (ft/Nm)
θ	orthodrome heading at the center of the ellipse (deg)

INTRODUCTION

Similarly to other industries, the aviation industry is fulfilling present and future economical and environmental responsibilities by ceaselessly exploring new ways of improving the operational efficiency (fuel burn, flight times, and costs), and by reducing the volume of pollutant gas emissions.

As shown by the Bureau of Transportation Statistics (2017) (BTS), the volume of fuel consumed by the US Carriers in 2016 on domestic and international scheduled flights amounted to 17,044.7 million gallons (equivalent to 54,197.8 million kilograms), for a fuel cost of 24,654 million US dollars. According to the 2005 emission indexes presented in Kim et al. (2007, p. 332, Table 3), each kilogram of fuel burned by an aircraft produces 3.155 kilograms of Carbon Dioxide (CO_2) and 0.0142 kilograms of Nitrous Oxide gases (NO_x), respectively. This translates to a total quantity of 170,994 million kilograms of CO_2 and 769.6 million kilograms of NO_x emitted in the atmosphere in 2016. By assuming an average reduction of the fuel burn by 1%, the annual fuel cost reduction would amount to 246.54 million dollars, and determine a reduction of gas emissions of 1,709.9 million kilograms of CO_2 and 7.69 million kilograms of NO_x. Additional cost reductions would be produced by the decreases in total flight times.

Given the wide range of aircraft types currently in operation, their age and technological diversity, and by consequence their performances and capabilities variations, the fastest and most feasible method for attaining the economical and environmental objectives, applicable to all aircrafts, is the employment of optimal flight trajectories.

A flight trajectory represents the path of an aircraft in four-dimensional (4D) space – latitude, longitude, altitude, and time - from its actual position to the destination airport, and is described by a flight plan which is decomposed in two components: 1) the lateral flight plan characterizing the sequence of geographical locations overflown by the aircraft, and 2) the

vertical flight plan describing the profile of altitudes (which depends on the aircraft's performances) along the lateral flight plan.

The optimization can be performed relative to the lateral, vertical, or the entire flight plan. The actual objectives of a flight trajectory optimization are adapted to the different contexts in which they are being used. On the ground, in the context of Air Traffic Management (ATM), various Decision Support Tools (DSTs) employ trajectory optimization algorithms with objectives corresponding to reducing aircrafts' flight times and gas emissions in the control center's responsibility area, increasing the traffic flow, and reducing the number of conflicts. The optimization may be performed as a function a number of factors such as: atmospheric conditions (winds, storm activity, etc.), the aircrafts' performances, altitudes, speeds or Requested Time of Arrival (RTA) constraints, presence of No-Fly Zones, and airports' traffic limitations (Swierstra & Green, 2003).

In the context of airline operations services, the optimization algorithms are used for determining the optimal trajectories minimizing flight time, fuel burn and gas emissions, flight cost corresponding to the entire flight plan, or just to specific sections of the flight plan. However, on-board aircraft optimization functions' capabilities are not as advanced as the on-ground algorithms due to the limited computing power of the Flight Management System (FMS) (Liden, 1992a; Liden, 1992b).

In 2010, at the ETS, the Laboratory of Research in Active Controls, Aeroservoelasticity and Avionics (LARCASE) started the investigation of new FMS methods and algorithms for reducing aircrafts' environmental footprint, in partnership with CMC Electronics-Esterline, as part of a research program launched by the Green Aviation Research & Development Network (GARDN). The optimization methods were conceived, among others, to compute optimal altitudes (Dancila, Botez & Labour, 2012), optimal vertical profiles for given lateral flight plans (Murrieta Mendoza, Beuze, Ternisien & Botez, 2015), or optimal vertical and lateral flight plans (Félix Patrón, Kessaci, Botez & Labour, 2013). A detailed list of the results of the investigations conducted at the LARCASE laboratory, as part of the GARDN

program is available on the laboratory's website (http://en.etsmtl.ca/Unites-de-recherche/LARCASE/Recherche-et-innovation/Publications?lang=en-CA.)

The objective of the research presented in this thesis was to explore new methods of enhancing the performances and capabilities of the flight trajectory optimization algorithms. This research was performed as a continuation of the investigations conducted by the author during his M.Eng. program at the LARCASE laboratory (Dancila et al., 2012 ; Dancila, Botez & Labour, 2013).

The research focused on three main subjects:

1. Development and evaluation of a new method for selecting the set of candidate waypoints used by the optimization algorithm by means of determining the contour of the geographic area confining the candidate waypoints. The first hypothesis was that the proposed method of selection of the geographic area used for the computation of the optimal flight trajectory provides the means to control the size of the operational area around the departure and destination airports, and the maximal trajectory distance between the two airports. The second hypothesis was that a grid constructed to closely circumscribe this selected area would minimize the number of grid nodes considered in the trajectory optimization process, while allowing the exploration of all geographic areas that meet the criteria set relative to the trajectory maximal distance, and to the sizes of operational areas around the two airports.
2. Development and evaluation of a new method of reducing or eliminating the need for repetitive time and resource-intensive performance calculations for the computation of an optimal trajectory, by decoupling the lateral and vertical flight plan calculations, and by the employment of pre-computed vertical flight path data. The first hypothesis was that the proposed method is capable of computing and assembling the still-air performance data for vertical flight path segments corresponding to all flight phases. The second hypothesis was that the set of still-air vertical flight path segments data allows the construction of a range of full vertical flight paths necessary for flight trajectory optimization.

3. Development of a new method for geometrical construction of an optimal vertical flight plan (climb, cruise, and descent) based on the specifications of an input lateral flight plan (waypoints' Along-the-Track Distance (ATD), and altitudes constraints), and a set of preferred gradient values defined as a function of the flight phase and altitude. The hypothesis verified in this research was that the proposed method is capable of constructing an optimal vertical flight plan minimizing the number of vertical segments, using a geometrical approach.

A description of the organization of the thesis and the methodology employed in each research is presented in Chapter 2 "Approach and Organization of the Thesis".

CHAPTER 1

LITERATURE REVIEW

1.1 Flight trajectory optimization, context and objectives

A detailed description of the concepts, implementation and economical and environmental benefits of performance-based operations, represented by optimal trajectories determined function of the aircraft's performances and atmospheric conditions is presented by SESAR Joint Undertaking (2015).

Palopo, Windhorst, Suherwardy & Lee (2010) conducted a comparative study of recorded and wind-optimal flight routes, for a period of 365 days, and concluded that the wind-optimal flights yielded an overall economy of 210 lb of fuel, and 2.7 minutes of flight time reduction per flight. Their study showed that these economies were obtained without a significant impact on the airport arrival rates, and reduced the number of conflicts by an average of 29%. In another investigation, on the advantages of using continuous descents at the Atlanta airport, Wilson & Hafner (2005) showed potential flight time reductions of up to 45 hours per day, and fuel cost reductions of 80,000 dollars per day, which amounts to 29 million dollars per year, accompanied by a 50% reduction in the number of potential conflicts.

Dancila, Botez & Ford (2014), and Murrieta Mendoza, Botez & Ford (2016) studied the negative effect of a missed approach (that can be caused, among others, by approach trajectory and runway conflicts, or by adverse atmospheric conditions) on flight time, fuel burn, gas emissions, and costs. These studies show the importance of predicting flight trajectories free of conflicts, especially in the approach and landing phases of the flight.

Currently, the flight trajectory optimization is subject to intense research aiming to extend the performances and capabilities of the optimization algorithms by taking advantage of the new, and more powerful computation platforms, new navigation principles and policies, better weather predictions, advancements in aircraft modeling and performance predictions, etc.

A direction of research addressed the lateral and the vertical fight trajectory performance prediction variations due to the differences in platform implementation, as shown in the analysis performed on a set of test benches and simulators from seven different manufacturers by Herdon, Cramer & Nicholson (2009).

In their paper, Swierstra & Green (2003) noted that ATM DSTs may use various prediction algorithms, each algorithm having distinct capabilities that are dependent on the particular objective of the DST application. This variety of capabilities translates into different levels of accuracy and uncertainty of the predicted trajectories, and of the computation speeds which in turn affect the quality of the decisions, thus, the aircrafts' trajectories. Their research focused on finding the important performance and design factors to be taken into account in the development of trajectory prediction algorithms; the resulting algorithms aimed to ensure common capabilities, balance the prediction algorithms' accuracy and speed, and be applicable on a large spectrum of ATM DSTs uses.

Paglione, Garcia-Avello, Swierstra, Vivona & Green (2005) described a methodology providing common capabilities for the validation of the trajectory predictors. This methodology makes use of a database containing actual Air Traffic Control (ATC) aircraft flight data, and environmental recordings, in Extensible Markup Language (XML)

A synthetic overview of the concepts, key components, operational principles and policies defined by the Next Generation Air Transport System (NextGen) as a guideline for future improvements of the DSTs used in improving aircraft trajectories, traffic flow, and flight safety was provided by Souders, McGettigan, May & Dash (2007). The new principles and policies opened the way for user preferred routes which, in comparison with the current operational policies based on a fixed set of waypoints and airways, can take better advantage on the wind conditions and aircraft performances.

Steiner et al. (2007) presented a new theoretical solution for expanding the weather information used by the ATM DSTs by generating and incorporating probabilistic weather

information constructed from a set of 10 to 50 distinct sets of forecasts, each forecast corresponding to a time frame and a geographic area. The probabilistic information characterizes the prediction uncertainty and opens the way for better adapted flight routing, and traffic management strategies and decisions based on information that cannot be ascertained from individual forecasts.

Another important aspect of the trajectory optimization is the aircraft performance model. Suchkov, Swierstra & Nuic (2003) discussed the impact of the aircraft performance model used in trajectory prediction on the accuracy, efficiency, and safety of ATM operations. Their analysis considered four types of performance data: manufacturer data described in the aircraft manuals, look-up tables, performance model based on the dynamic model of the aircraft such as the Base of Aircraft DAta (BADA), and on a parametric-based kinematic model such as the General Aircraft Modeling Environment (GAME). They emphasized the strong influence of the aircraft's take-off weight on its performances, thus, on the trajectory prediction. The analysis of the operational data from two major airlines showed that the gross weight determined climb trajectory flight time and distances variations between 390 and 2390 seconds, and between 42 and 270 Nm, respectively. Gerretsen & Swierstra (2003) also showed that the aircraft weight has a major influence on its climb performances, but its effects on the descent performances are much smaller.

Ghazi, Botez & Tudor (2015) presented a methodology for the generation of an aircraft's look-up table-based performance model for the climb phase using the aero- propulsive model identified from the data recorded during flight tests. The method was successfully applied and validated on a Cessna Citation X aircraft model, using a number of 70 flights performed on a level D flight simulator. Murrieta Mendoza, Demange, George & Botez (2015) developed a method for the design of an aircraft's look-up table-based performance model using the fuel burn data acquired during flight tests. The method was successfully validated on a Cessna Citation X aircraft model, using a number of 66 flights performed on a level D flight simulator.

Dancila (2011) developed a method for predicting the fuel burn for constant speed and constant altitude cruise segments. This method, as opposed to the classical model allowing only the calculation of fuel burn as function of flight time on segments limited to a maximal distance, has the advantage of allowing calculation of flight time as function of specified fuel burnt and eliminating the limitations regarding the segment's length. The new method converts the classic look-up table-based performance model, requiring multi-dimensional interpolations, into a new look-up structure requiring interpolations only function of flight time (for fuel burn calculations as function of a specified flight time), or fuel burn (for flight time calculation as function of a specified fuel burn). This method was subsequently used in the development of a flight trajectory optimization algorithm determining the optimal altitude minimizing the total cost for flying a constant speed and constant altitude cruise segment, function of the aircraft gross weight at the start of the segment, and of the segment's length (Dancila, 2011; Dancila et al., 2012).

1.2 Flight trajectory optimization

Huang, Lu & Nan (2012) presented a survey of the numerical algorithms used in aircraft trajectory optimization.

Liden (1992a), and Liden (1992b) presented methods for constructing optimal flight profiles that use cruise step climbs, and the effects of the Cost Index (CI) on the minimal cost flight profile, and found two categories of discontinuities for trajectories with Requested Time of Arrival (RTA), that were caused by the modification of the optimum step climb points; Liden (1992a) further proposed approaches for removing these discontinuities.

Bilimoria & Shepard (1989) studied the performances of cruise trajectory optimization using an aircraft range and gross weight state variables–based dynamic model, and three strategies relative to the constant / variable altitude and speed. They also identified the configuration of

cruise trajectories as a function of a parameter defining the balance between the aircraft flight time and its fuel burn.

Murrieta Mendoza, Beuze et al. (2015) used a Branch-and-Bound algorithm to determine the optimal speed and altitude profiles defining the still-air optimal vertical flight trajectory. This trajectory had minimized the total flight cost of an aircraft whose performance model was described using look-up tables.

Bonami, Olivares, Soler & Staffeti (2013) investigated an aircraft trajectory optimization algorithm based on mixed integer non-linear programming, by using continuous and discrete variables representing aircraft state and decision variables, respectively. The algorithm was implemented using Gauss-Lobatto direct collocation and Branch-and-Bound algorithms.

In their paper, Tong, Schoemig, Boyle, Scharl & Haraldsdottir (2007) presented a set of factors related to the selection of a ground-referenced geometric path for a Continuous Descent and Approach (CDA), and the compromises entailed by low and idle thrust descents. Their study analyzed the characteristics of idle and constant path angle profiles for two aircraft types (B777-200 and B737-700), and a number of aircraft descent configurations. They showed that while an idle descent provided the best performances relative to fuel and gas emissions, its ground-referenced path could not be predicted due to variations in aircraft performances, configurations, and wind conditions. On the other hand, descents following a predetermined geometric path, requiring low thrust were predictable and, thus, usable in a high traffic ATC environment.

Rivas, Valenzuela & de Augusto (2012) described an aircraft global trajectory calculation tool that employed a kinetic modeling approach, and the aircraft's drag polar and engines performance models. The tool was investigated on a flight between Madrid and Frankfurt, and the results showed that the take-off weight had a major impact on the climb profile, and on the total fuel consumption. The results also showed that wind had an important effect on the predicted trajectory, while non-standard atmosphere conditions had a smaller effect.

Grabbe, Sridhar & Cheng (2006) investigated the advantages of user preferred trajectories over the East Central Pacific. For this investigation, they developed a dynamic programming algorithm (using a dynamic programming grid) capable of determining the wind-optimal trajectory minimizing the flight time. The performances of the algorithm were evaluated using flight data of 911 west and east-bound flights over the East Central Pacific. The results showed that the wind-optimal trajectories led to average flight time reductions of 9.9 minutes, and to distance reductions of 36 Nm. These results also showed that for the wind-optimal trajectories, the number of conflicts was larger than for the nominal trajectories.

Bousson & Machado (2010) presented a direct method for the optimization of 4D trajectories with time constraints at each waypoint by using a pseudo-spectral integration approach and Chebyshev polynomials.

Biljsma (2009) showed that trajectory optimization algorithms based on the control problem of Bolza were prone to convergence issues, i.e. achieving the convergence or converging to a local minimum. He proposed a new method which employs the heading and the speed as control variables, and determines the global minimal (optimal) solution every time.

Jardin & Bryson (2012) developed two methods for calculating optimal trajectories minimizing the flight time in an atmosphere characterized by strong winds, and they further analyzed their performances on a flight route between San Francisco and New York JFK airports, flown at 36,000 feet, with winds reaching 160 Kts. The first method entailed the backward computation of optimal trajectories (extremals) from each of the two airports to a set of other airports in the geographical area of interest. Subsequently, the memorized optimal trajectories were used to determine the optimal trajectory's headings and flight time as function of the aircraft's latitude and longitude, by interpolation. The second method, called "neighboring optimal wind routing", was devised by linearizing the kinematic and optimal heading angle equations near an assumed optimal route. The investigation concluded that the method generated near-optimal trajectories which closely approximated the global optimal trajectories when the wind conditions along the assumed optimal route and the

neighboring optimal route were similar. For the optimal trajectories from San Francisco to New York, the first method flight time was 252 minutes, the second method flight time was 253 minutes, and the geodesic trajectory flight time was 258 minutes. For the flight from New York to San Francisco, the first method flight time was 349 minutes, the second method flight time was 368 minutes, and the geodesic trajectory flight time was 385 minutes.

Hagelauer & Mora-Camino (1998) presented a method for computing an optimal 4D trajectory with multiple time constraints by using dynamic programming and computing time reduction techniques such as the diminution of the search space, by applying pre-execution and execution-time elimination tests, and by using neural networks for aircraft performance and flight cost computations.

Knapp, Jameson, Measure & Butler (2008) presented an aviation routing tool to predict unfavorable weather areas for a given trajectory and time period, and to determine the optimal 4D trajectory that avoids these areas.

Kamgarpour, Dadok & Tomlin (2010) presented a method for determining aircraft trajectories that circumvent adverse weather areas by employing regularly updated weather forecasts, and a receding horizon-based computation method for trajectory update and optimization.

Another research, conducted by Irvine, Hoskins, Shine, Lunnon & Froemming (2012) analyzed and classified three Summer and five Winter North Atlantic weather patterns that influence the optimal routing, and defined simple representations of the atmospheric pollution as function of the flight time, season, latitude, flight time in stratosphere etc. Their study of the optimal trajectories for the New York–London flights showed the connection between the Jetstream position and optimal trajectory latitudes, the dependency function of eastward or westward flights, and showed optimal trajectory flight times variations of up to more than 60 minutes.

Marceau Caron & Hadjaz (2011) proposed a multi-objective ATM trajectory optimization methodology that employs a description of the ground-referenced airspace as a dynamic mesh. In this mesh, all possible aircraft trajectories were defined by considering the existing airways (a static component of the mesh), and the conflict avoidance trajectories (the dynamic component of the mesh). Subsequently, the authors proposed the employment of multi- objective optimization approaches such as “lexicographic order”, or “Pareto front” to determine the optimal solutions. An implementation of the proposed method by considering a mesh covering the whole European airspace, and lexicographic order optimization criteria have resolved more than 98% of the possible conflicting flight trajectories.

Girardet, Lapasset, Delahaye, Rabut & Brenier (2013) proposed a method for generating a wind-dependent free-flight optimal trajectory minimizing the flight time, by using the Ordered Upwind algorithm. This algorithm computes the trajectory headings by minimizing the flight time, and assumes constant altitude and True Air Speed (TAS) values. The method used in the algorithm employs an unstructured triangulated mesh for wavefront calculation and propagation, and has a complexity of $O(N \log N)$ where N is the number of points composing the mesh.

Rippel, Bar-Gill & Shimkin (2005) investigated the suitability of global graph search methods such as Dijkstra, reduced-state Dijkstra, A*, and their hierarchical versions for flight trajectory prediction and optimization algorithms whose cost objective model included flight time, altitude, passengers’ comfort and pilot workload. The investigation was performed using a kinematic aircraft model and a 3D graph constructed from a 50 meters resolution grid representation of a 100 by 100 kilometers digital map. The comparison of the results for “reduced-state” and “hierarchical reduced state” versions of Dijkstra and A* algorithms with the results obtained using only the Dijkstra algorithm showed computation time improvements between 60 and 261 times with corresponding cost degradations between 2.9% and 4.4%.

Zillies et al. (2014) analyzed the effectiveness of employing wind-optimal flight trajectories in the European airspace, and the atmospheric circumstances that warrant optimal trajectories diverged from the geodesic, and the magnitude of their deviations. The optimization algorithm used in this research employed a BADA aircraft performance model, meteorological data in the GRIdded Binary (GRIB) format defined by the World Meteorological Organization (WMO) (WMO, 2003), and Dijkstra algorithm on a 4D network representation of the European airspace, with a cost objective minimizing the fuel burn. The evaluation of the algorithm was performed with respect to the fuel burn and flight time using actual air traffic data from 28,153 short, medium and long-haul flights within the European airspace, and performed during one day. The analysis showed that the wind conditions had a strong influence on the optimal trajectories, and long-haul flights warranted larger deviations from the geodesic – up to 172 Nm with fuel burn reductions of up to 0.75%, and flight time reductions of 0.83%.

Ng, Sridhar & Grabbe (2012) developed a trajectory optimization algorithm minimizing the flight time and fuel burn. This algorithm performed the computations in two steps. First, the optimal vertical flight profile is computed for a pre-defined route and altitude constraints using the BADA aircraft performance model. Then, the algorithm determines the optimal horizontal trajectory corresponding to the computed vertical profile, by interpolation using a set of extremals computed using the method presented by Jardin and Bryson (2012). The performances of the proposed algorithm were evaluated on 12,500 long-haul cargo flights from Anchorage to 10 destinations in Asia and U.S.A., performed using five types of aircrafts, and generated flight time and fuel burn decreases up to 54 minutes and 7.6 tons.

Félix Patrón, Kessaci et al. (2013) developed a flight trajectory optimization algorithm that minimizes the flight time, by using a Genetic Algorithm (GA) and a routing grid whose nodes were situated on the geodesic connecting the departure and destination airports, and on four additional “parallel” tracks – two on each side of the geodesic – for a total of five tracks. The distance between the tracks, as well as the number and distance between the nodes were adjustable.

Rodionova, Sbihi, Delahaye & Mongeau (2014) proposed a method for optimizing the aircraft flight trajectories and the traffic throughput over the North Atlantic, between Europe and North America. The method employed a GA and a grid of points constructed using a number of tracks of the Organized Track System (OTS) defined by the International Civil Aviation Organization (ICAO) (ICAO, 2013) where each track had a selected, equal number of waypoints.

Murrieta Mendoza, Botez & Félix Patrón (2015) developed an optimization algorithm for a cruise flight trajectory flown at a constant speed. The optimization algorithm used a look- up table based aircraft performance model, a 2D grid for the set of possible altitudes at each waypoint, and a GA to select the flight plan waypoints' altitudes minimizing the cost of the cruise phase.

Gil (2011) investigated a method for the optimization of cruise flight trajectories as function of the wind conditions, which used a rhomboidal-shaped routing grid. He noted that for all considered test scenarios, the nodes close to two of the corners were evaluated but not retained in the final solution, which he recognized as an algorithm inefficiency. Subsequently, the areas corresponding to the two corners were eliminated, thus, leading to a hexagonal-shape routing grid.

Devulapalli (2012) investigated flight trajectory optimization methods minimizing the flight distance, capable of achieving any of the lateral, vertical, or 3D trajectory optimizations, using an aircraft dynamics performance model, the available wind information, and observing the set of potential constraints associated with the flight such as waypoints, altitudes and zone restrictions. The methods used Dijkstra and A* algorithms for implementing the trajectory optimization. To decrease the computation time, the implementation using the Dijkstra algorithm also reduced the number of grid nodes, which were contained inside an elliptical contour constructed by setting the ellipse's foci at the departure and destination nodes, and the eccentricity value was adjusted so that the resulting

grid was compatible with the aircraft's turn performance and heading constraints at the departure and destination nodes.

1.3 Opportunities of improvement for the trajectory optimization algorithms

The reviewed literature showed the strong interest in the exploration of new optimization algorithms, and the wide range of trajectory optimization algorithms developed to date. The review also emphasized the importance of the support algorithms used by the optimization process such as the selection of the set of candidate waypoints, the aggregation of the necessary weather information, and the aircraft performance prediction computations. The capabilities of the support algorithms (such as the position and number of selected candidate waypoints, the accuracy of the weather information, or the speed and accuracy of the aircraft performance predictions) have a determining contribution to the performances (speed and accuracy) of the optimization algorithms. These observations led to the interest to also investigate new methods for improving the accuracy and capabilities of the support algorithms.

A first area that warranted further investigation was the selection of the candidate waypoints considered in the process of optimization. As shown by Gil (2011), the selection of a set of candidate waypoints disposed as a rhomboidal grid may lead to algorithm inefficiencies due to the evaluation of waypoint that will never be retained in the final trajectory. Other selection methods such as waypoint grids built based on the OTS, investigated by Rodionova et al. (2014), or on a set of parallel tracks situated on both sides of the geodesic (Félix Patrón, Kessaci et al., 2013) may lead to the exploration of geographic areas that do not take full advantage of the favorable wind conditions. These methods, too, may lead to optimization algorithm inefficiencies. The solution presented by Devulapalli (2012) allowed a better adaptation of the grid to the position of the departure and destination points, and to aircraft turn performances. However, upon an in-depth review regarding the construction of the ellipse, it could be observed that the proposed method had an important drawback – directly linking the shape of the ellipse and the grid, controlled by the eccentricity, to the aircraft's

turn performance and terminal nodes' heading constraints. Depending on the airports' positions and the aircraft's turn performances, this fact may also lead to the selection of geographic areas which could be too wide (including candidate nodes situated too far, thus, not part of the solution) or too narrow (excluding geographic areas and candidate nodes that could be part of the optimal solution). Therefore, this method may also lead to computation inefficiencies.

A second area that warranted further investigation was represented by the aircraft performance modeling and aircraft trajectory prediction methods. Irrespective of the optimization method used, a solution is selected following an iterative computation and evaluation of a series of trajectories or trajectory segments' performances. Moreover, the optimization algorithm may be executed at regular time intervals in order to update the optimal trajectory as function of the evolution of the wind conditions, aircraft position and its state parameters. Therefore, an optimization algorithm could be improved by employing new aircraft performance calculation and/or trajectory prediction methods that would provide more accurate trajectory predictions, allow the evaluation of more candidate optimal trajectories in a given time frame, and / or ensure faster optimization algorithms' response times. An example of such algorithm was presented by Dancila (2011) and Dancila et al. (2013).

A third area of interest was the trajectory optimization itself. More specifically, the investigation of a new method addressing the geometrical optimization of the vertical flight plan, having as principal objectives the reduction of the flight plan computation complexity and time. This method would facilitate the trajectory optimization when the succession of waypoints is pre-imposed. As well, this method would provide a fast and straightforward way for computing a full lateral and vertical flight plan when the set of waypoints is not imposed (such as the case with general trajectory optimization algorithms).

The three algorithms proposed in this thesis have addressed the three investigation areas identified above:

1) the selection of the candidate waypoints considered in the optimization;
2) new ways of predicting the performances of a flight trajectory;
3) the geometrical optimization of the vertical flight plan.

While the proposed algorithms were developed for their intended use on FMS platforms, their applicability could be extended to satisfy the needs of the ATM environment.

CHAPTER 2

APPROACH AND ORGANIZATION OF THE THESIS

The research exploring new methods of improving the performances and capabilities of the flight trajectory optimization algorithms, presented in this thesis, was accomplished in four phases as follows:

1. Statement of the problems addressed in the research following a review of existing optimization algorithms, their limitations and impact on optimization performances, and identification of opportunities for improvement.
2. Investigation of a new method for the selection of the geographical area used in the trajectory optimization, and construction of a routing grid circumscribing the selected area.
3. Investigation of a method for the construction of an ensemble of vertical flight path segments, covering the aircraft's flight envelope, used for flight plan prediction and optimization.
4. Investigation of a method used for the geometrical construction of an optimal vertical flight plan as a function of the flight phase and altitude-dependent preferred gradient values.

In the initial phase of the research, a review of existing optimization algorithms helped to identify the optimization strategies, the steps used by these algorithms and their limitations. Following this review, two directions of investigation aiming to improve specific elements of the optimization were identified: 1) the selection of the set of candidate waypoints considered by the optimization algorithm (geographic area and layout), and 2) the reduction or elimination of the repetitive, time and resource-intensive aircraft performance-based computations used for flight plan prediction and optimization.

In the second phase, a new proposed method addressed the selection of the geographic area containing the candidate waypoints, as a function of the size of the operational areas around the departure and destination airports, and the imposed maximal trajectory distance. An analytical investigation was used to characterize the relationship between the design parameters (mentioned above) and the geometry of the selected area. Also, the proposed method addressed the construction of a routing grid circumscribing the selected geographic area. Finally, the geographic areas selected for pairs of airports describing short and long-haul flights were compared with actual aircraft data of commercial flights connecting these airports.

In the third phase, a new method addressed the construction of an ensemble of vertical flight plan segments data, organized as a look-up structure and a corresponding graph, to be used by the optimization algorithm. This set of data eliminates the need for repetitive computations using the aircraft's performance model during the calculation of the optimal flight trajectory. A number of nine test configurations were used to investigate the influence of the input configuration parameters on the proposed method's performances. This investigation focused on the time required to generate the look-up structure and graph, the total number of vertical flight plan segments and total number of vertical flight plan trajectories described by the look-up structure, and the flight time – still-air distance distribution of the vertical flight plan trajectories.

In the fourth phase, upon the identification of the interest shown by CMC Electronics-Esterline, the research focused on the investigation of a new method addressing the construction of an optimal vertical flight plan employing a geometrical approach. Two implementations adopting distinct trade-offs, identified during the design phase, regarding the conflicting vertical flight path construction constraints were evaluated using 48 test configurations.

Chapters 3 to 5 present the set of three journal papers generated, as main author, as result of this research. The three papers were submitted for publication in peer-reviewed journals, one

paper was published and another two papers are currently in the process of review. Additionally, a number of three conference papers were published, two as main author and one as co-author. The conference papers provided a summary presentation of the results obtained in the initial stages of the investigations addressing the construction of an ensemble of vertical flight path segments, and the geometrical construction of an optimal vertical flight plan, respectively.

The research was conducted with the support and advice of Dr. Ruxandra Botez, who also co-authored the journal and conference papers generated as a result of these investigations. Mr. Benoit Beulze, as internship student, participated on the fourth phase of the research and worked on one of the algorithms' implementations presented in the third paper, which he co-authored. In the initial stage of the fourth phase of the research, Messrs. Benoit Beulze, Sammy Bottollier-Lemallaz and Soufiane Herda, internship students, worked on two out of the three implementations used in the initial exploration of different strategies for the geometrical construction of the optimal vertical flight plan. A comparative presentation of the results of the three implementations was published as a conference paper, authored by Mr Beulze, and co-authored by the author of the present thesis, Messrs. Bottollier-Lemallaz, Herda, and Dr. Botez (Beulze, Dancila, Botez, Bottollier-Lemallaz & Herda, 2015).

The first research paper, "Geographical area selection and construction of a corresponding routing grid used for in-flight management system flight trajectory optimization" (Dancila & Botez, 2016), presented in Chapter 3, was published in Proceedings of the Institution of Mechanical Engineers, Part G: Journal of Aerospace Engineering, in April 2016. It presented a method of selecting an elliptical-shaped geographic area which allowed the simultaneous control of the size of the operational areas around the departure and destination airports, and the maximal distance of the trajectory connecting the two airports. Subsequently, a method was proposed for constructing a routing grid circumscribing the selected geographical area. The mathematical equations, applied to flat surface model, were used to characterize the dependencies between the input design parameters (geodesic distance between the two airports, size of the operational areas, and maximal trajectory distance), the ellipse

constructive parameters and its shape. The method was then applied on three test cases corresponding to pairs of airports representing short and long-haul flights. For each test case, the set of geographical areas, constructed for a number of ellipse eccentricity values (controlling the maximal trajectory distance) were compared with actual trajectory data of commercial aircraft flights connecting the selected pairs of airports, retrieved from FlightAware (2014). For each test case and maximal trajectory distance value, the corresponding numbers of grid nodes were compared with the numbers of nodes of a rectangular-shaped grid covering the same maximal and minimal latitudes and longitudes, thus ensuring the same operational areas around the airports.

The second research paper, "Vertical Flight Path Segments Sets for Aircraft Flight Plan Prediction and Optimization", was submitted for review and publication to The Aeronautical Journal in November, 2016.

Firstly, the paper presented the methods currently employed for the construction of the vertical and lateral flight plan using the aircraft performance model. Secondly, the paper presented the methods used for computing the still-air parameters (flight time, still-air distance, initial and final altitudes, initial, final and average speeds, fuel burn, and aircraft gross weight) of the sets of segments composing each phase of flight (climb, constant speed level-flight cruise, climb in cruise, or descent segments) by using the aircraft performance model. Thirdly, the paper presented the assembly of the set of flight plan segments into a look-up structure organized following the aircraft's gross weight and altitude, and the generation of a corresponding vertical flight plan graph used for the selection and retrieval of the flight plan segments' data stored in the look-up structure. The set of segments composing the look-up structure and the graph describe one climb path and multiple level-flight constant speed cruise paths, climb in cruise paths, and descent paths. Fourthly, the paper proposed a method for the computation of a lateral and vertical flight plan using the vertical flight plan look-up structure, and the vertical flight plan graph. Finally, a set of nine scenarios were used to investigate the construction and properties of the resulting look-up structures and graphs including: the times required for their construction, the number of level-flight cruise, climb-

in-cruise and descent paths, the total number of graph nodes, the total number of vertical flight paths connecting the start of the climb path to the end of a descent path, the maximal and minimal vertical flight plans' flight times and still-air distances, and the flight-time versus still-air distance distribution of the vertical flight plans.

The third research paper, "Optimal Vertical Flight Plan Construction As Function Of Flight Phase And Altitude", was submitted for review and publication to The Aeronautical Journal in November, 2016.

Firstly, this paper provided a general overview of the optimization problem which included the description of the inputs (lateral flight plan, and the sets of preferred gradient values function of the flight phase and altitude), and the constraints and limitations imposed in the construction of the optimal vertical flight plan. Next, the paper presented the method used for the computing of the optimal flight plan, its decomposition into the sequence of processing steps, and the corresponding guiding logic and mathematical equations. The first step, prior to the actual optimization, performed a pre-processing of the input lateral flight plan and had two objectives: 1) generating a new representation of the lateral flight plan that would be easily interpreted and processed during the optimization calculations; 2) determining the sequence of climb, level flight, and descent domains, and the lateral flight plan waypoints delimiting them. The second step performed the actual optimization of the vertical flight plan one domain at a time, starting with the first domain, from its first waypoint to its last waypoint. Finally, two sets of results were generated and analyzed, corresponding to two implementations of the optimization algorithm each adopting distinct trade-offs regarding the precedence of one of two constraints imposed in the construction of the optimized vertical flight plan, in the situations that render them mutually exclusive. The two constraints were: 1) the gradients of the vertical flight plan climb and descent segments hade the closest possible values to the preferred values; 2) consecutive climb and descent, or descent and climb segments must be separated by a horizontal flight path segment whose length is equal or larger than a specified value. Each of the two sets of results were generated considering a

series of 48 test scenarios, and allowed the comparative analysis and identification of the effects and influence of the implementation constraints and trade-offs.

CHAPTER 3

ARTICLE 1: GEOGRAPHICAL AREA SELECTION AND CONSTRUCTION OF A CORRESPONDING ROUTING GRID USED FOR IN-FLIGHT MANAGEMENT SYSTEM FLIGHT TRAJECTORY OPTIMIZATION

Bogdan Dumitru Dancila and Ruxandra Mihaela Botez
École de Technologie Supérieure, Montréal, Canada
Laboratory of Research in Active Controls, Aeroservoelasticity and Avionics
This article was published[1] in Proceedings of the Institution of Mechanical Engineers, Part G: Journal of Aerospace Engineering, Vol. 231, No. 5, pp. 809 – 822, April 13, 2016,
Paper No. 643104 DOI:10.1177/0954410016643104

Résumé

Cet article propose une nouvelle méthode pour la sélection d'une zone géographique ayant un contour ellipsoïdal et pour la construction d'une grille de routage qui circonscrit le contour de la zone sélectionnée. La grille ainsi construite décrit l'ensemble de points utilisés par les algorithmes d'optimisation des trajectoires de vol pour la détermination de la trajectoire optimale de vol d'un avion en fonction des conditions atmosphériques. Cette méthode a été développée pour son utilisation par des algorithmes d'optimisation des trajectoires, dans le contexte des systèmes de gestion de vol, mais elle est aussi utilisable dans l'environnement de gestion du trafic aérien. La grille de routage limite la distance au sol maximale (entre les aéroports de départ et d'arrivé), maximise la zone géographique (pour une meilleure exploration des conditions atmosphériques) et minimise le nombre de nœuds de la grille. La nouveauté de la méthode proposée réside dans le fait qu'elle permet un paramétrage et contrôle de la surface totale de l'ellipse, et de la taille des zones autour des aéroports de départ et destination requises pour les procédures de décollage et d'atterrissage. Le contour elliptique construit utilisant cette méthode est donc très bien adapté à la

[1] The paper presented in this chapter contains minor modifications relative to the version printed in Proceedings of the Institution of Mechanical Engineers, Part G: Journal of Aerospace Engineering, Vol. 231, No. 5, pp. 809 – 822, April 13, 2016. These modifications were made at the request of the members of the Board of Examiners.

configuration particulière de la trajectoire pour laquelle on fait l'optimisation. L'influence de chaque variable est présentée, ainsi qu'une série de grilles de routage générées pour des trajectoires correspondantes à des distances totales de vol variées, et qui ont été par la suite comparées avec des données réelles de trajectoires de vol retrouvées à travers le site web de FlightAware.

Abstract

This paper proposes a new method for selecting an ellipse-shaped geographical area and constructing a routing grid that circumscribes the contour of the designated area. The resulting grid describes the set of points used by the flight trajectory optimization algorithms to determine an aircraft's optimal flight trajectory as a function of given particular atmospheric conditions. This method was developed with the intent of its employment in the context of Flight Management System trajectory optimization algorithms, but can be used in Air Traffic Management environments as well. The routing grid limits the trajectory's maximal total ground distance (between the departure and destination airports), maximizes the geographical area (for a better consideration of the wind conditions) and minimizes the number of grid nodes. The novelty of the proposed method resides in the fact that it allows a distinct and independent parameterization and control of the ellipse's total surface, and the required size of the take-off/landing procedure maneuvering areas at the departure/destination airports. The ellipse contour constructed using this method is, therefore, well adapted to the particular configuration of the trajectory for which the optimization is performed. Each design variables' influence is presented, as well as a set of routing grids generated for trajectories corresponding to different total flight distances, and were further compared with real flight trajectory data retrieved using the website FlightAware.

3.1 Introduction

A flight trajectory is composed of a succession of points in space, defined relative to the earth's surface, which are employed by an aircraft between a departure and destination

airport. Air navigation rules and regulations require that all commercial flights provide, in advance, a description of their intended flight trajectory – a flight plan – for approval by the authorities charged with the management of the overflown airspaces, and those flights are subsequently required to conform to their flight plan. A flight plan lists, among other items, each waypoint's geographical position (latitude and longitude), the overflying altitude and the estimated time when the aircraft reaches each waypoint (the Estimated Time En-route or ETE). Each pair of successive waypoints delimits a flight trajectory segment characterized by a ground distance and a heading or direction relative to the magnetic north. A flight trajectory optimization algorithm determines the trajectory and/or the aircraft speeds that minimize the value of a selected cost objective function for a given set of aircraft and flight configuration parameters.

The objective function itself may refer to flight time, fuel burn or total cost minimization. Each of these functions is highly dependent on the set and succession of the waypoints, the altitude and airspeed profiles employed, as well as the atmospheric conditions encountered along the flight trajectory. These factors are determined as follows: the total ground distance is the sum of the ground distances of the composing segments. At any point along the flight trajectory, the ground speed is equal to the vector summation of the aircraft's True Air Speed (TAS) and wind speed, and its value computed using the wind triangle algorithm (Hopper, 2011). The TAS itself is a function of the selected aircraft air speed, specified as an Indicated Air Speed (IAS) or Mach value, flying altitude and atmospheric conditions (air temperature, air density, etc.) (Ojha, 1995). The total flight time is equal to the integral summation, along the entire trajectory's ground distance, of the elementary flight times (1/ ground speed). The total fuel burn is computed as the integral summation of the instant fuel burn rate over the entire duration of the flight, where the instant fuel burn rate is a function of the aircraft configuration, selected air speed, altitude and atmospheric conditions (mainly the air temperature). Finally, the total cost is a weighted sum of the fuel and time- related costs (Liden, 1992b). Consequently, the selection of a set of waypoints has a major influence on many of the trajectory's parameters and on the performances of the optimization function itself, as they are affected by the total ground distance and atmospheric conditions

encountered along the flight trajectory. The ideal trajectory corresponds to a trajectory which concurrently minimizes the total ground distance, provides the most advantageous wind conditions, and employs a profile of altitudes and air speeds that maximizes the ground speed and minimizes the fuel burn rate.

The existing FMS algorithms used for trajectory computation or optimization require an explicit definition of the set, position, and sequencing of the composing waypoints. Therefore, the optimization algorithms currently implemented in the operational FMS platforms are in fact bounded to altitude and/or speed optimizations. Additionally, these algorithms consider a static description of the atmospheric conditions (wind speed, wind direction and air temperature) in which the flight is conducted. Moreover, the atmospheric parameters are associated with a set of waypoints and are generally considered constant along each segment – equal to those of the corresponding starting waypoint. However, the atmospheric parameters may change continuously as a function of the geographical location, altitude and time. Consequently, the existing algorithms only take a limited account of the dynamic nature of the atmospheric parameters. This means that the proposed flight trajectories may be sub-optimal: first due to the limitations of the atmospheric modeling, and second because the optimization algorithm cannot explore a broader range of geographical locations and corresponding altitudes that may allow an aircraft benefit from favorable wind conditions.

The increasing demand for more economical and environmentally friendly aircraft operations, the advancements in air navigation equipment and data communications, improved navigation standards such as Next Generation Air Transportation System (NextGen) (Prevot, 2009; Warren, 2000; Souders et al., 2007; de Grado & Tascon, 2011), and the availability of weather data assemblies (de Grado & Tascon, 2011; Dunn, 2008), which provide a prediction of the atmospheric parameters and their dynamics have all contributed to the development of new FMS flight trajectory computation and optimization algorithms. As part of the general effort, the Laboratory of Research in Active Controls, Avionics, and AeroServoElasticity (LARCASE) assembled a team of researchers that are

investigating new algorithms addressing or related to FMS flight trajectory optimization (Félix Patrón & Botez, 2014; Félix Patrón, Kessaci et al., 2013; Murrieta Mendoza & Botez, 2014a; Murrieta Mendoza, 2013; Sidibé & Botez, 2013; Botez & Fays, 2013; Dancila et al., 2013; Dancila et al., 2012; Dancila & Botez, 2014; Félix Patrón, Oyono Owono, Botez & Labour, 2013).

As mentioned above, one important element that influences the performance of the flight trajectory optimization algorithm is the range of geographical locations explored in the search for an optimal trajectory – i.e. the geographical area considered by the optimization algorithm. If this area is too small, points that would provide advantageous atmospheric conditions may be left out; too large, the required volume of computations and/or memory space may become impractical. Moreover, the area may include points that determine total ground distance increases, generating performance penalties which cannot be compensated for by any atmospheric conditions and that could lead to computational inefficiencies.

In his research, Gil (2011) first considered a rhomboidal-shaped geographical area with two opposed corners situated at the departure and destination airports. His investigation showed that this selection method produced an inefficient routing grid, as a considerable number of grid points, situated around the non-departure/destination corners, were never included in the resulting optimal trajectory. These ‘extra’ grid points, meanwhile, necessitated an unnecessary increase of the volume of computations. He addressed this inefficiency by selecting a hexagonal-shaped geographical area. A third type of routing grid was considered in the optimization methods investigated at LARCASE (Félix Patrón & Botez, 2014; Félix Patrón, Kessaci et al., 2013; Murrieta Mendoza & Botez, 2014a; Murrieta Mendoza, 2013), constructed using a set of tracks: the orthodrome (also known as the geodesic) corresponding to the shortest distance between the initial and final waypoints (Leick, 1985; Grafarend & Krumm, 2006; Karney, 2011; Kjenstad, 2011; Panou, Delikaraoglou & Korakitis, 2013; Sjöberg, 2009; Karney, 2013; Bowring, 1983), and a number of 4–11 equally spaced, parallel tracks situated on both sides of the orthodrome. The grid points were uniformly distributed along the set of tracks.

Another example of a routing grid used in conjunction with flight optimization algorithms is that described by Rodionova et al.(2014), constructed using a system of parallel tracks known as the organized track system (ICAO, 2013).

A routing grid constructed using a set of tracks offers two advantages. First, the tracks' and the grid points' computation algorithms are relatively simple. Second, they provide a direct relationship between the number of tracks and the number of grid nodes. However, a small number of tracks may limit the geographical coverage and may not allow the full exploration of existing advantageous wind conditions. In addition, a high number of tracks may lead to an unnecessary increase of the geographical area, and thus of grid size, leading to computation inefficiencies similar to those identified by Gil (2011).

In their investigation of an Air Traffic Management (ATM) based flow optimization method, Caron and Hadjaz (2011) considered the construction of a mesh containing the set of possible trajectories, organized as a graph, which is dynamically updated as a function of the existing airways, operational procedures, and the conflict resolution constraints. This method is more computing intensive due to the complexities associated with the conflict resolution constraints, and therefore cannot currently be used in an FMS-based environment. However, a simplified version which considers a mesh computed only as a function of the existing airways and operational procedures may be less complex and usable in an FMS environment, but would present the same advantages and disadvantages as the methods identified above.

Consequently, a judicious selection of the geographical area used by the trajectory optimization algorithm is crucial for providing a good exploration of the wind conditions and for reducing the number of computations, thus increasing the algorithm's efficiency. Devulapalli (2012) reduced the number of grid nodes, thus the optimization algorithm's computation requirements, by selecting a geographical area delimited by an ellipse-shaped contour. The ellipse was constructed placing the two foci at the departure and destination airports' position and selecting an eccentricity value as a function of the aircraft's turn radius and the departure and arrival heading constraints. This grid effectively addresses the

shortcomings specific to the rectangular and track-based grids. However, the ellipse construction method proposed by Devulapalli (2012) has the disadvantage, as detailed in the beginning of the section describing the ellipse area selection on a plane surface, of cross-linking the size of the ellipse (surface and number of grid nodes) to the radiuses of the turns at the departure and destination airports.

The atmospheric predictions are generally provided by national agencies, such as Environment Canada (2013), as a set of GRIdded Binary (GRIB) files (WMO, 2003), and may refer to a regional or global forecast. Each GRIB file describes the values of an atmospheric parameter at a set of points corresponding to a grid constructed following a specified type of cartographic projection (Grafarend & Krumm, 2006; Kjenstad, 2011; Kayton & Fried, 1997; Deakin, 2004), metric, and resolution, for a specified altitude and time. Subsequently, an atmospheric parameter's value corresponding to any location, altitude and instant of time is computed through linear interpolation.

It is, therefore, useful to utilize a grid of points specific to and circumscribing a selected geographical area, and which matches a convenient cartographic projection, metric, and resolution. Such a grid would not only help in the selection of the candidate trajectory waypoints, it may also help in organizing, and retrieving the atmospheric data limited to the area of interest and thus reducing the memory space requirements.

This paper proposes a new method for the selection of an ellipse-shaped geographical area, and for the construction of a corresponding grid which limits the trajectory's maximal total ground distance (between the departure and destination airports), maximizes the geographical area (for a better consideration of the wind conditions), and minimizes the number of grid nodes, in the context of in-FMS flight trajectory optimization. The novelty of the proposed method is embodied in its objective to eliminate the limitations imposed in the construction of the ellipse, identified in the method presented by Devulapalli (2012), that one may have control over the minimal area around the departure and destination points/maximal total distance, or of the desired ellipse's surface, but not on both requirements at the same time.

More specifically, the proposed method allows simultaneous and distinct parameterization and control of the ellipse's total surface and the required size of the maneuvering areas at the departure/destination airports. The cartographic projection used for the construction of the grid is the geographic projection (Cartesian, Latitude and Longitude representation). A set of routing grids generated for three pairs of airports Montreal (Montreal–Pierre Elliott Trudeau International Airport (CYUL)) – Toronto (Toronto Pearson International Airport (CYYZ)), Montreal – Amsterdam (Amsterdam Airport Schiphol (EHAM)), and Montreal – Paris (Paris Charles de Gaulle Airport (LFPG)) was compared with actual flight trajectory historic data.

3.2 Geographical area selection

The selection of the geographical area must consider a number of factors that are directly related to the flight trajectory and the optimization configuration parameters. First, the selected area must include the departure and destination airports, and thus, this area corresponds to a city pair. Second, it must include the direct trajectory, which corresponds to the minimal ground distance between the trajectory's departure and destination airports which ensures that the points of the trajectory presenting the minimal total ground distance will be considered in the subsequent trajectory optimization. Given that all trajectories are defined with reference to the earth's surface, which is an oblate ellipsoid (Leick, 1985; Karney, 2011; Kjenstad, 2011; Kayton & Fried, 1997; Deakin, 2004; Engels & Grafarend, 1995), a direct trajectory corresponds to the orthodrome between the two delimiting points (Leick, 1985; Grafarend & Krumm, 2006; Karney, 2011; Kjenstad, 2011; Panou, Delikaraoglou & Korakitis, 2013; Sjöberg, 2009; Karney, 2013; Bowring, 1983). Third, given that an excessive increase in the total ground distance may eliminate and even reverse any gains due to favorable wind conditions, the selected area must ensure a specified maximal total ground distance. Fourth, the selection method must provide sufficient space around the departure and arrival airports for any and all take-off and landing procedure maneuverings. Fifth, the selected area should provide equal opportunity for exploring candidate waypoints on both sides of the direct trajectory, which translates to symmetry relative to the direct trajectory. Finally, the selected geographical area should provide a good

trade-off between the maximal surface coverage (maximal exploration of the en-route wind conditions) and a minimal number of grid points.

3.2.1 Ellipse area selection on a plane surface

On a plane surface, the geometrical figure that ensures a maximal total distance between two points (foci) that are situated on its symmetry axis is an ellipse. The parameters that define an ellipse are the semi-major axis (*a*), the semi-minor axis (*b*) and the eccentricity (*e*). The maximal distance between the two foci, corresponding to a trajectory composed of two segments intersecting on the ellipse contour, is equal to 2*a*. The eccentricity is defined as

$$e = f / a \tag{3.1}$$

where *f* represents the distance between the center of the ellipse and a focal point, and whose value is

$$f = \sqrt{a^2 - b^2} \tag{3.2}$$

The value of *e* is situated between 0 and 1 ($e \in [0,1)$).

On a plane surface, the problem of selecting the geographical area translates into finding the parameters of an ellipse (the positions of focal points F_1 and F_2, and the values of *a*, *b*, *e*, and *f*) whose contour/ surface meets the set of specified criteria. The first approach, and the most direct, employed by Devulapalli (2012), is to consider that the coordinates of F_1 and F_2 are equal to those of the points of departure and the destination P_1 and P_2. The positions of F_1 and F_2 are fixed, and so the value of *f* is also fixed with respect to the origin, or center of the ellipse. Consequently, the shape of the ellipse given by its contour and its surface can only be adjusted by modifying the value of one of the *a*, *b*, or *e* parameters (the values of the other two parameters are then determined according to equations (3.1) and (3.2)). Figure 3.1 shows

that parameter *a* is closely related to the requirement of ensuring a desired maximal total distance and minimal required area around each focal point, represented by the distance between the focal point and the ellipse's contour, and therefore may be considered the principal design parameter. The principal drawback of this approach, however, is that there is a direct interdependence between the ellipse's semi-major axis *a* and its semi-minor axis *b*, its eccentricity *e*, and by consequence its surface. This means that during the construction of the ellipse, one may have control over the minimal area around the departure and destination points P_1 and P_2, or of the desired ellipse's surface, but not on all requirements at the same time.

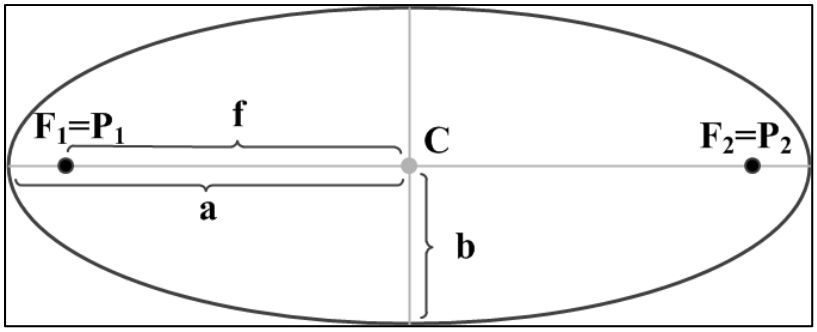

Figure 3.1 The constructive parameters of an ellipse

The ellipse construction method proposed in this paper is designed to eliminate this drawback by separating the positions of the ellipse's foci (F_1 and F_2) on Figure 3.1 from those of the departure and the destination points P1 and P2, respectively, as illustrated in Figure 3.2.

Consequently, the first step is the computation of the distance ($2d$) between P_1 and P_2. The ellipse's semi-major axis lies on the line determined by P_1 and P_2, and the center of the ellipse (C) is situated halfway between P_1 and P_2 ($\overline{P_1C} = \overline{P_2C} = d$). This ensures that the desired symmetry relative to the direct trajectory P_1P_2 is transversal as well as longitudinal. The selection of the ellipse's parameters, and finally of its surface as well as the area around

the departure and destination points, is controlled using two parameters: the main-axis extension distance (*c*) and the ellipse eccentricity (*e*).

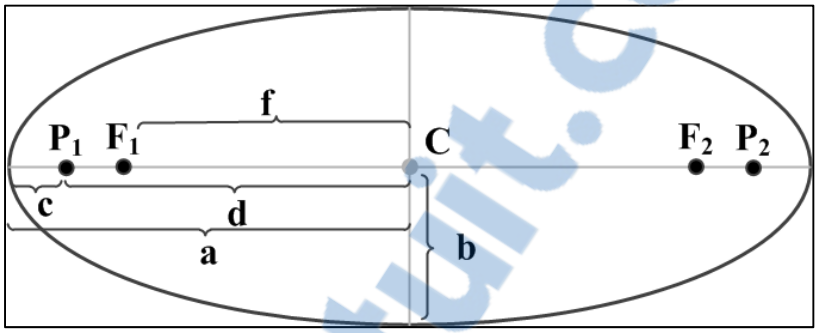

Figure 3.2 The elements of the ellipse considered
for the construction of the routing grid

The relationship between *a*, *c*, and *d* is described by equation (3.3)

$$a = c + d \tag{3.3}$$

The main-axis extension distance (*c*) is used to adjust the size of the area around the departure and destination points, and the eccentricity (*e*) is used to adjust the ellipse' surface by changing the position of the two foci F_1 and F_2, therefore, the value of f as a function of *c*, *d*, and *e* (see equations (3.1) to (3.3)).

To summarize, for a given set of *c*, *d*, and *e* values, the remaining set of ellipse parameters (*a*, *b* and *f*) is determined using equations (3.1), (3.2), and (3.3).

For any point I situated on the contour of the ellipse, as depicted in Figure 3.3, its coordinates (*x*, *y*) defined with respect to the center C are satisfying the general equation of the ellipse:

$$\frac{x^2}{a^2} + \frac{y^2}{b^2} = 1 \tag{3.4}$$

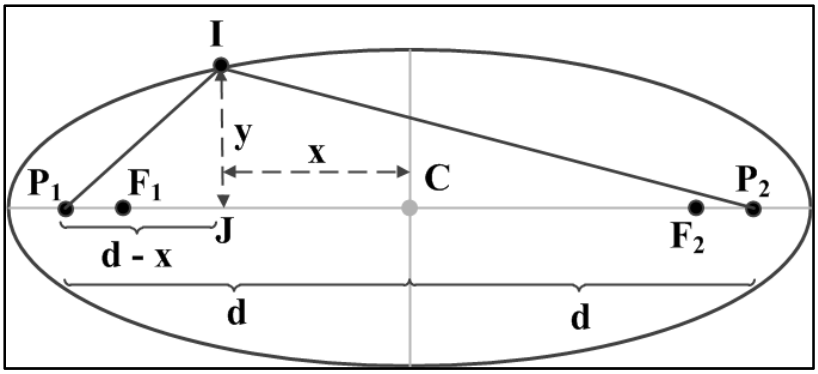

Figure 3.3 The segments composing a trajectory between P1 and P2 intersecting the contour of the ellipse

The total distance between P_1 and P_2, on any trajectory composed of two segments intersecting the contour of the ellipse in a point I (P_1IP_2), as depicted in Figure 3.3, is computed as the sum of P_1I and IP_2, which are determined using the Pythagorean theorem for the triangles P_1JI and IJP_2. Consequently, the equation used to compute the total distance is

$$P_1IP_2 = P_1I + IP_2 = \sqrt{(d-x)^2 + y^2} + \sqrt{(d+x)^2 + y^2} \tag{3.5}$$

The general properties of an ellipse say that when the positions of P_1 and P_2 coincide with the positions of F_1 and F_2, respectively, $P_1F_1 = P_2F_2 = 0$ and the total distance between P_1 and P_2 on any trajectory composed of two segments intersecting the contour of the ellipse in a point I is constant and equal to $2a$, and does not depend on the position (x, y) of the intersection point I. However, when P_1 and P_2 do not coincide with F_1 and F_2, the total distance is not constant as it is a function of positions of P_1 and P_2 and of the coordinates x and y of the point I where the trajectory intersects the contour of the ellipse.

Using equation (3.5) and the notations presented in Figures 3.2 and 3.3, the final form of the equation describing the total distance is obtained by firstly expanding the expressions of the two square roots

$$P_1IP_2 = P_1I + IP_2 = \sqrt{d^2 - 2dx + x^2 + y^2} + \sqrt{d^2 + 2dx + x^2 + y^2} \tag{3.6}$$

Then expressing y^2 as function of a^2, b^2, and x^2 using equation (3.4), we obtain

$$P_1IP_2 = \sqrt{x^2\left(1 - \frac{b^2}{a^2}\right) - 2dx + d^2 + b^2} + \sqrt{x^2\left(1 - \frac{b^2}{a^2}\right) + 2dx + d^2 + b^2} \tag{3.7}$$

Subsequently, expressing the terms multiplying x^2, and b^2, as functions of a and e, by use of equations (3.1) and (3.2), leads to

$$P_1IP_2 = \sqrt{e^2x^2 - 2dx + d^2 + a^2\left(1 - e^2\right)} + \sqrt{e^2x^2 + 2dx + d^2 + a^2\left(1 - e^2\right)} \tag{3.8}$$

and, finally replacing a as function of c and d using equation (3.3). Therefore, the equation describing the distance between P_1 and P_2 becomes

$$P_1IP_2 = \sqrt{e^2x^2 - 2dx + d^2 + (c+d)^2\left(1 - e^2\right)} + \sqrt{e^2x^2 + 2dx + d^2 + (c+d)^2\left(1 - e^2\right)} \tag{3.9}$$

As noted, P_1 and P_2 are positioned symmetrically relative to C, therefore, $d \in [0, a]$. The case when $d = 0$ corresponds to a scenario in which the trajectory's start and end points coincide ($P_1 = P_2 = C$), and in the case when $d = a$, P_1 and P_2 which are the trajectory's start and end points are situated on the ellipse's contour, at both ends of semi-major axis.

An analysis of the variation of the total distance (P_1IP_2) as a function of the position x of point I, using equations (3.4) and (3.5), showed that for $d = 0$ ($a = c$ given by equation

(3.3)), the total distance varies between 2*a* for $x = \pm a$ (thus, $y = 0$, equation (3.4)), and 2*b* for $x = 0$ (thus $y = \pm b$, equation (3.4)). Similarly, for $d = a$ ($c = 0$ from equation (3.3)), the total distance varies between 2*a* for $x = \pm a$ (thus, $y = 0$, equation (3.4)), and $2\sqrt{a^2 + b^2}$ for $x = 0$ (thus $y = \pm b$, equation (3.4)). A more detailed characterization of the total distance (P_1IP_2) as a function of *d* and *x* is presented in Appendix I, Figure-A I-1 to Figure-A I-6, corresponding to six ellipses, each with distinct eccentricity values, and whose parametric relationships and shapes are presented in Table 3.1 and Figure 3.4.

In order provide a general characterization, a description which is independent of the actual value of the ellipse' semi-major axis, *a*, the data presented in Table 3.1, Figure 3.4 and Appendix I, Figure-A I-1 to Figure-A I-6 are normalized to the value of *a*.

Table 3.1 The relationship between the ellipse's parameters for the cases described in Figure 3.4 and Appendix I, Figure-A I-1 to Figure-A I-6

$e = \frac{f}{a}$	$\frac{b}{a}$	$\frac{\sqrt{a^2 + b^2}}{a}$	**Figures**
0	1	1.414214	Figure 3.4, Appendix I, Figure-A I-1
0.1	0.994987	1.410674	Figure 3.4, Appendix I, Figure-A I-2
0.5	0.866025	1.322876	Figure 3.4, Appendix I, Figure-A I-3
0.9	0.43589	1.090871	Figure 3.4, Appendix I, Figure-A I-4
0.99	0.141067	1.009901	Figure 3.4, Appendix I, Figure-A I-5
0.999	0.04471	1.000999	Figure 3.4, Appendix I, Figure-A I-6

Table 3.1 mainly describes the relationship between an ellipse's eccentricity (*e*) and the normalized value of its semi-minor axis (*b*), for a number of six eccentricity values. Figure 3.4 provides a description of the shapes and (normalized) sizes of the contours corresponding to the ellipses described in Table 3.1.

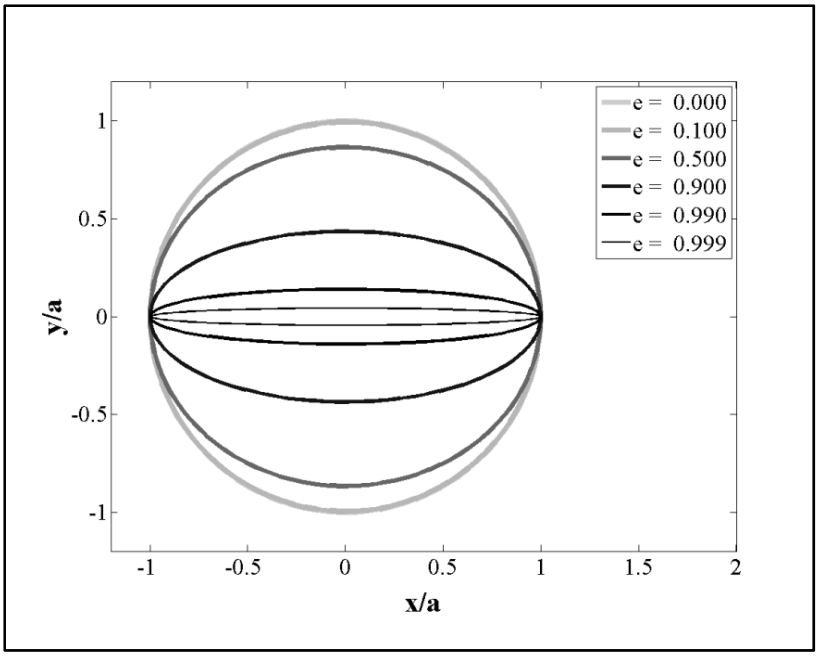

Figure 3.4 The shape of an ellipse as a function of its eccentricity (*e*) values presented in Table 1

In Appendix I, Figure-A I-1 to Figure-A I-6 illustrate, for each ellipse configuration presented in Table 3.1, the relationship between the normalized values of the total distance (P_1IP_2), described by equation (3.9), and the normalized value of the *x* coordinate of the point (I) in which the trajectory intersects the ellipse's contour, for a number of 11 normalized values of the half-distance between P_1 and P_2 (*d*).

3.2.2 Area selection on an ellipsoid

For any and all aircraft navigation and flight trajectory prediction/optimization computations, the set of waypoints composing the flight trajectory is situated on and defined with respect to the surface of the earth. Therefore, on the reference ellipsoid, the desired contour corresponds to that of the selected surface-plane ellipse which is subsequently ‘‘molded’’ on the ellipsoid such that P_1 and P_2 map to their corresponding geographical coordinates by using a process known as conformal mapping (Leick, 1985; Grafarend & Krumm, 2006; Kayton & Fried, 1997; Deakin, 2004; Agard & Gehring, 1965). Consequently, the surface-plane ellipse's P_1P_2

segment and its major axis translate into the orthodrome between P_1 and P_2, and a segment of the ellipsoid's grand circle passing through P_1 and P_2, respectively. Also, the center of the surface-plane ellipse translates into a point situated on the orthodrome, at mid-distance between P_1 and P_2. The heading at each point along the orthodrome is not constant, thus it changes continuously (Karney, 2013). The orthodrome's heading at the mid-point C between P_1 and P_2 represents the surface-plane ellipse's rotation angle relative to the meridian passing through C, prior to its molding onto the ellipsoid (Leick, 1985).

Consequently, the ''geographical area selection algorithm'' must determine the geographical coordinates of a set of points situated on the surface of the reference ellipsoid that correspond to the contour of an ellipse which satisfies the set of pre-defined criteria:

- its major axis is centered on the orthodrome linking the two airports – thus including the trajectory of minimal total ground distance and ensuring a symmetrical exploration of the area wind conditions;
- it ensures a prescribed maximal total ground distance between the two airports; and
- it provides a specified range around the airports for take-off and landing maneuvers.

Appendix I, Figure-A I- 7 to Figure-A I-9, illustrates the orthodromic trajectory between Montreal (CYUL) and Amsterdam (EHAM), the position of the center of a selected ellipse, and its contour (including the areas around the Montreal airport (CYUL)).

3.2.3 Implementation

The ellipsoid-surface contour selection algorithm was implemented in Matlab using functions provided by the Mapping Toolbox ('ellipse1', 'track1', 'distance' and 'legs'). First, the orthodrome's parameters were computed using the geographical coordinates of the departure and the arrival airports P_1 and P_2. They include the orthodrome's length ($P_1P_2 = 2d$) in nautical miles and arc degrees, the corresponding geographical position (*lat*, *lon*) of the center of the orthodrome (C), and the orthodrome's heading (θ) at C. These parameters are fixed and depend only upon the position of the two airports P_1 and P_2. Subsequently, the values of two additional parameters, which determine the shape of the ellipse, were selected:

the orthodrome extension (*c*) in nautical miles or arc degrees, and the ellipse eccentricity (*e*). As in the case of the plane surface, the ‘‘orthodrome extension’’ provides the additional routing area that may be explored for the take-off and landing procedures when the runway heading is opposite to that of the orthodrome connecting the departure to the destination airport.

The resulting target ellipse parameters were obtained as follows:

- center position (*lat*, *lon*) – the coordinates of the center of the orthodrome C;
- tilt angle (θ) – the orthodrome heading at the center of the orthodrome C;
- major ellipse axis (*a*) – in nautical miles and in arc degrees, as described by equation (3.3); and
- eccentricity (*e*).

The optimal values for *e* and *c* are generally chosen as a function of the particular pair of airports for which the geographical area is being selected, and they have a direct and strong influence on the shape of the ellipse. For each pair of airports, the correlation between the values of *e*, *c*, and the selected geographical area, and thus the selection process, can be fine-tuned using historical records of actual flight trajectories between the two airports and/or wind conditions.

Subsequently, the mapping of the target ellipse (defined by the *lat*, *lon*, θ, *a*, and *e* parameters) on the reference ellipsoid, and thus the computation of the actual geographical coordinates of the series of points composing the contour delimiting the desired geographic area, was performed using the ‘‘ellipse1’’ function of the Matlab Mapping Toolbox. The number of points composing the contour is selected using the ‘‘*npts*’’ input parameter of the ‘‘ellipse1’’ function, which has a default value of 100.

3.3 Construction of the routing grid

The routing grid is constructed using the specified latitude and longitude axial resolution required by the flight trajectory computation or optimization algorithm; it circumscribes the contour delimiting the selected geographical area.

Depending on the selected ellipse's major axis length, eccentricity, center position and tilt angle, the shape of the orthodrome, and by consequence the shape of the contour delimiting the selected geographical area with respect to the ellipsoid surface's reference coordinate system represented in a geographic projection (a Cartesian, Latitude and Longitude projection) can be concave, convex or symmetric. It can be noted that irrespective of the contour' shape, a maximum of two contour points can exist at each longitude. On the contrary, depending on the ellipse's major axis length, eccentricity, center position and tilt angle, the contour of the selected geographical area can take a strong concave shape which makes that the number of contour points corresponding to a selected latitude could reach a value of four (as illustrated in Appendix I, Figure-A I-11 and Figure-A I-12). Moreover, on its orthodromic flight from the departure to the destination airport, the aircraft's longitude variation is generally uniform (with exceptions related to take-off and landing procedure maneuverings), whereas its latitude variation may not be. Therefore, it seemed appropriate to organize the grid data following the longitude, i.e. the range of longitudes covered by the selected geographical contour and the corresponding range of latitudes for each longitude.

The selected contour's minimal and maximal longitude and latitude values are identified and subsequently used in conjunction with the grid's required resolution for determining the sets of latitude and longitude values specific to the desired grid. By travelling the contour in a clock-wise direction, starting with the point situated on the top (northern) side at the longitude corresponding to the center of the ellipse, the algorithm determines the corresponding grid point coordinates (longitude and latitude) by performing an ‘‘upward’’ or ‘‘downward’’ rounding.

The direction of the rounding depends on the particular point's position on the ellipse. It must account for the fact that the shape of the ellipse contour's representation on a Cartesian, latitude-longitude plane may not be uniform – as it may have alternating convex and concave regions. The logic guiding the rounding process, presented in Table 3.2, must therefore ensure that the corresponding grid point's position is situated on or exterior to the selected contour (where i designates the current contour point, $i+1$ designates the next contour point, and the latitude and longitude values and variations respect the standards and conventions used in navigation and geodesics).

Table 3.2 Selected contour point's latitude and longitude rounding logic used for determining the routing grid's coordinates structure

sign(Lon_{i+1} - Lon_i)	**sign(Lat_{i+1} - Lat_i)**	**Lon_i rounding direction**	**Lat_i rounding direction**
+	+	Down	Up
+	-	Up	Up
-	+	Down	Down
-	-	Up	Down

The set of unique, rounded longitude values of the selected contour points represents the routing grid's longitude vector. A determination of the minimal and maximal latitude values is then made for each longitude in the set. Consequently, the routing grid's longitude vector, combined with the minimal and maximal latitude values at each longitude, completely describes the grid contour. Any grid point is situated at a longitude whose value is contained in the routing grid's longitude vector, and at a latitude whose value is a multiple of the routing grid's latitude resolution, situated between the corresponding minimal and maximal routing grid latitudes.

Depending on the particular utilization, the structure describing the routing grid can store the information at different levels of detail. One example is a structure listing the routing grid's longitude vector, and the minimal and maximal latitude values at each longitude in the set. Another example is a structure listing the routing grid's longitude vector and a set of vectors containing latitude values with one latitude vector for each routing grid longitude value. Additionally, the structure may store information regarding the geographical coordinates of the departure and arrival airports, the set of points composing the orthodromic trajectory between the two airports, the ellipse's center position and its tilt angle, and the ellipse's major axis and eccentricity values.

3.4 Results

The algorithm's performance was analyzed on a set of flight trajectories covering a wide range of distances. Actual aircraft trajectory data, retrieved from FlightAware (2014), were used to investigate the relationship between the departure and arrival airports' location, the orthodrome's length, the constructive parameters of the ellipse used in the selection of the routing area, the routing grid size and the maximal geographical area covered by the flight trajectories.

This information was taken from three flight trajectories for which at least one daily regular flight service was provided from Montreal (CYUL–CYYZ, CYUL–EHAM and CYUL–LFPG). The aircraft trajectories were plotted using the raw positioning data retrieved from FlightAware (2014), and might have contained position estimation errors introduced by the tracking system due to the unavailability of actual aircraft or ground station data (for instance over certain oceanic areas), which could be illustrated as spurious fluctuations in the aircraft trajectory tracks.

The drawings presented in Appendix I, Figure-A I-10 to Figure-A I-12 illustrate the relationship between the departure and destination points' positions, the corresponding orthodrome, the selected geographical contour, and the area covered by the routing grid

circumscribing the selected contour for the three flight trajectories, where $c = 0.25°$ (the semi-major axis extension distance was equal to the length of an arc of $0.25°$ of the grand circle containing the orthodrome), $e = 0.99$, and the grid's axial resolutions were $0.5°$. They also illustrate the differences, in terms of the shape and surface, between the grids circumscribing the selected contour, and rectangular grids constructed using the minimal and maximal latitude and longitude values of the selected geographical contour.

In Appendix I, Figure-A I-13 to Figure-A I-15 show the performances of the algorithm in terms of routing grid size reduction, described as the percentage ratio of the number of points of a routing grid circumscribing the selected contour relative to the number of points of the corresponding rectangular routing grid constructed using the geographical contour's minimal and maximal latitude and longitude values, for all three flight trajectories and a range of eccentricity and orthodrome extension values.

It can be observed that, as expected, for the shortest trajectory CYUL–CYYZ (Appendix I, Figure-A I-10 and Figure-A I-13), the variation of the eccentricity (e) and orthodrome extension values (c) determined a smaller variation and reduction of the geographical area and routing grid's size than it was the case for longer trajectories such as CYUL–EHAM and CYUL–LFPG. It can also be observed that, as illustrated in Appendix I, Figure-A I-13 to Figure-A I-15, the eccentricity had a higher influence on the routing grid size reduction than the orthodrome extension value. Moreover, the influence of the eccentricity increases with the distance between the departure and destination airports. The influence of the orthodrome extension value, however, lessens with the increase of the distance between the departure and destination airports, to the point where it becomes negligible (Appendix I, Figure-A I-14 and Figure-A I-15).

In Appendix I, Figure-A I-16 to Figure-A I-18 present a comparative illustration of actual aircraft flight trajectories for the three city pairs considered in this article (retrieved from FlightAware (2014)), and the corresponding selected ellipse routing areas for which $c = 0.25°$ and for a number of four eccentricity values (e = 0.9, 0.95, 0.99, and 0.999). For

each case, the detailed view of the area surrounding CYUL illustrates the relationship between the orthodrome extension value (*c*), the eccentricity value (*e*), the size of the maneuvering area around the airport and the actual take-off and landing trajectories.

Comparing the actual flight trajectories and the selected geographical contours, it can be observed that for all three cases, an orthodrome extension value of $0.25°$ was proven sufficient for all of the required procedural maneuverings. It can also be observed that for the longer flight distances (Appendix I, Figure-A I-17 and Figure-A I-18), the set of flight trajectories was entirely contained inside surfaces delimited by geographical contours constructed using lower eccentricity (*e*) values than those corresponding to shorter flight distances (Appendix I, Figure-A I-16). This can be explained by the relative increase in total distance (the longer deviations from the orthodrome for identical relative increases in total distance), and consequently the possibility of using favorable wind conditions in areas situated further away from the orthodrome.

In Appendix I, Figure-A I-16 shows that for the flight trajectory corresponding to a shorter flight distance (CYUL– CYYZ), the actual aircraft flight trajectories were generally contained within a geographical contour corresponding to an eccentricity value of $e = 0.99$; the exceptions being represented by segments of the take-off/landing procedure maneuverings. It can be observed that the exceeding instances were not related to the size of the orthodrome extension but to a combination of geographical area's wideness around the departure/destination airports and the runways' headings relative to those of the orthodrome.

3.5 Conclusions

This paper proposes a new method for the selection of a geographical region and the construction of a corresponding grid used by flight trajectory computation and optimization algorithms. The advantage of this method is that for any pair of departure and destination airports, the process is controlled using only four parameters (orthodrome extension, eccentricity, and latitude and longitude grid resolution). Each parameter has a distinct

contribution to the grid construction. Moreover, the selected area and the routing grid ensures a maximal total trajectory distance, a high level of symmetry relative to the orthodrome, and also minimizes the number of grid points. Consequently, the grid symmetry relative to the orthodrome allows for a better exploration of the geographical area's wind conditions, while the minimal number of grid nodes leads to a reduction of the number of computations required for the flight trajectory optimization.

The algorithm's performance, in terms of the reduction of the number of grid nodes, was evaluated as the ratio between the number of points of the grid determined by the proposed algorithm (circumscribing the selected geographical contour) and the number of points of a rectangular grid circumscribing the minimal and maximal latitude and longitude values of the selected geographic contour. The results showed that, as expected, for identical eccentricity and orthodrome extension values, the algorithm's performance increases as the distance between the two airports increases. Also, the results showed that the eccentricity has a greater influence on the size of the selected grid than the orthodrome extension value. Moreover, the influence of the orthodrome extension on the number of grid nodes diminishes as the distance between the two airports increases.

The comparative study of actual aircraft flight trajectories and families of selected geographical contours showed that generally, lower values of eccentricity (larger ellipse surfaces and total distance values) are employed as the distance between the two airports increases. This is consistent with the fact that for longer flight distances, comparative to shorter flight distances, identical relative increases in the total distance correspond to larger deviations from the orthodrome, allowing for a larger exploration of favorable wind conditions. The study also showed that for shorter flight distances, such as illustrated in Appendix I, Figure-A I-16, while the majority of the aircraft's flight trajectory was situated inside a geographical area corresponding to a high eccentricity value (narrower ellipse surface), the take-off/landing maneuverings may extend to areas corresponding to ellipses with lower eccentricity values (larger ellipse surfaces) due to the combination of contour

wideness in the terminal areas and the relative angle between the orthodrome and the runway heading.

In conclusion, the results have shown that the proposed method is capable of constructing a routing grid which is adapted to the particular set of departure and destination airports, one that has a reduced number of grid points. While the results indicated good performances for long flight trajectories, it also shown that for some short trajectory cases, even better performances may be achieved by separating the terminal area (take-off and landing areas) selection and grid construction from that corresponding to the cruise phase.

Based on this analysis, the authors have identified two main research directions. The first one relates to the investigation of a flight trajectory optimization algorithm employing a routing grid constructed using the method presented in this paper, and is the subject of a distinct research and publication. The second direction refers to the research of a new geographic area selection method (especially tailored to shorter trajectories), separating the selection of the take-off and landing areas from the cruise area, and the construction of the resulting routing grid.

CHAPTER 4

ARTICLE 2: VERTICAL FLIGHT PATH SEGMENTS SETS FOR AIRCRAFT FLIGHT PLAN PREDICTION AND OPTIMIZATION

Bogdan Dumitru Dancila, and Ruxandra Mihaela Botez.
École de Technologie Supérieure, Montréal, Canada
Laboratory of Research in Active Controls, Aeroservoelasticity and Avionics
This article was submitted to The Aeronautical Journal
November 21st, 2016

Résumé

Cet article présente une méthode pour la construction d'un ensemble de segments du profil vertical de vol composant l'enveloppe du profil vertical de vol d'un avion en utilisant le modèle de performance d'un avion. Cette méthode a été développée pour son utilisation dans des algorithmes de prédiction et optimisation des plans de vol des avions. Le but principal est de réduire le volume de calculs récurrents des paramètres de performance des segments requis pour la prédiction ou l'optimisation des plans de vol. La méthode présentée dans cet article est applicable à des scenarios de type «free-flight». Les segments composant l'enveloppe verticale de vol appartient à l'une des phases de vol suivantes : montée non-contrainte; vol horizontal à vitesse constante; étape de montée en croisière, et descente continue. Les vols de segments sont effectués à des valeurs prescrites de consignes de vitesse pour la montée, croisière, et descente; ainsi qu'à des valeurs prescrites de température de l'air. La méthode emploie un modèle de performance des avions qui utilise des tableaux d'interpolation linéaire. Neuf scénarios de test ont été utilisés pour évaluer les performances des enveloppes de vol en fonction du nombre d'altitudes de croisière et de profils de descente. L'ensemble de paramètres de performance évalués incluent la gamme de temps total de vol et des distances de vol en air calme, ainsi que les profils verticaux correspondant aux valeurs minimes et maximes pour les temps de vol et pour les distances de vol en air calme.

Les avantages de la méthode proposée sont nombreux. Premièrement, le besoin d'exécuter les calculs de performance d'une façon répétitive pour des segments identiques du plan vertical de vol est éliminé et les moyens pour la récupération rapide des données de performance nécessaires dans la construction d'un plan de vol complet sont mis en place. Deuxièmement, la structure de recherche des segments du profil vertical de vol et le graphe des profils verticaux de vol décrivent un ensemble de profils verticaux de vol qui prennent en considération les paramètres de configuration de l'avion et du plan de vol et qui couvrent l'enveloppe de vol maxime de l'avion. Troisièmement, la structure de recherche et le graphe mettent en place un moyen rapide et clair pour l'identification des options disponibles pour la construction d'un segment du plan de vol et aussi pour la détection des points associés aux changements des phases de vol, incluant la montée, la croisière, l'étape de montée en croisière et la descente.

Abstract

The paper presents a method for constructing a set of vertical flight path segments, that would compose an aircraft's vertical flight envelope, by using an aircraft performance model. This method is intended to be used for aircraft flight plan prediction and optimization algorithms. The goal is to reduce the volume of recurring segment performance computations currently required for flight plan prediction or optimization. The method presented in this paper applies to a free-flight scenario. The flight path segments composing the vertical flight envelope belong to one of the unrestricted climb, constant-speed level flight, step-climb and continuous descent segments, performed at the consigned climb, cruise and descent speed schedules and at the consigned air temperature values. The method employs an aircraft model using linear interpolation tables. Nine test scenarios were utilized to assess the performances of the resulting flight envelopes as function of the number of cruise altitudes and descent flight paths. The set of evaluated performance parameters includes the range of total flight times and still-air flight distances, and the vertical profiles describing the minimum and maximum flight times, and still-air flight distances.

The advantages of the proposed method are multiple. Firstly, it eliminates the need for repetitive aircraft performance computations of identical vertical flight plan segments, and provides the means for quick retrieval of the corresponding performance data for use in the construction of a full flight plan. Secondly, the vertical flight path look-up structure and the vertical flight path graph describe a set of vertical flight paths that consider an aircraft's and flight plan's configuration parameters, and cover its maximum flight envelope. Thirdly, the look-up structure and the graph provide the means for rapid and clear identification of the available options for constructing a flight plan segment, as well as for detecting the points associated with changes in the flight phases, including climb, cruise, step-climb and descent.

4.1 Introduction

An aircraft's flight plan defines its flight path as a sequence of points in space that the aircraft is mandated to follow from its current position to its destination, where each point is characterized by a geographic location and altitude. Generally, the flight plan is decomposed into three phases: climb, cruise, and descent. For each phase, the corresponding flight path is described by a lateral flight plan concentrated on the geographic routing, and a vertical flight plan defining the flying altitudes along the lateral flight plan (Liden, 1992b; Liden, 1985). The vertical flight plans are constructed as a function of the aircraft's performance, and its configuration. The set of flight plan parameters computed by a FMS usually contains the geographic locations, altitudes, gross weights, fuel burns, ground and TAS, segment lengths, bearings and flight times, etc. (Liden, 1992b; Liden, 1985). Once computed, these parameters are employed by the FMS for aircraft navigation and guidance. The FMS flight plan computation algorithms may also be used to perform flight path optimizations, with objectives such as total flight-time, fuel-burn or total cost minimization (Liden, 1992b; Liden, 1985). Other research shows that there was a distinct interest in expanding the set of functionalities and capabilities of the flight path prediction algorithms, including areas such as the augmentation of a crew's situational awareness as described by Benavides, Kaneshige, Sharma, Panda & Steglinski (2014).

The flight plan data can also be computed by ground-based algorithms, such as the algorithms used by the ATM for traffic prediction, planning, and supervision. These algorithms have expanded the series of functions used for aircraft flight path computation (Rivas et al., 2012; Swierstra & Green, 2003; Paglione et al., 2005; Mondoloni, Paglione & Green, 2002; Mondoloni, Swierstra & Paglione, 2005; Warren, 2000; Lee, Weygandt, Schwartz.& Murphy, 2009) by facilitating specific tasks such as conflicts detection and resolution (Granger, Durand & Alliot, 2001; Tomlin, Pappas & Sastry, 1998), circumventing areas affected by adverse weather (Lee et al., 2009; Brunilde, Lapasset, Delahaye, Rabut & Brenier, 2013; Palopo et al., 2010; Nilim, El Ghaoui & Duong, 2002; Krozel, Mitchell, Prete, Smith & Andre, 2007), route selection (Brunilde et al., 2013; Palopo et al., 2010; Nilim et al., 2002; Krozel et al., 2007; Suzuki, Tsuchiya & Andreeva, 2009), and developing of routing strategies for traffic flow augmentation (Granger et al., 2001; Tomlin, Pappas & Sastry, 1998; Brunilde et al., 2013; Palopo et al., 2010; Nilim et al., 2002; Krozel et al., 2007; Suzuki et al., 2009; Prevot, Palmer, Smith & Callantine, 2001; Wichman, Klooster, Bleeker & Rademaker, 2007; Jackson, Gonda, Mead & Saccone, 2009; Tomlin, Pappas, Košecká, Lygeros & Sastry, 1998; Cano, Dorado & Sánchez-Escalonilla, 2007).

Flight path prediction and flight path optimization algorithms are not exclusively reserved for conventional aircraft or traffic management applications. The advancements in the development of Unmanned Aerial Vehicles (UAV) have led to an exponential increase of the type and range of missions on which they are employed. Consequently, UAV flight path optimization algorithms, such as those developed using a clothoid planner (Wilburn, Perhinschi & Wilburn, 2013b), or the concept of Dubins' particle (Wilburn, Perhinschi & Wilburn, 2013a), can be further used to construct flight paths that ensure the desired mission performance.

Studies conducted at MIT have shown the opportunities and potential of savings in flight path optimization, as many aircraft do not fly at their optimal speed or/and altitude (Jensen, Hansman, Venuti & Reynolds, 2013; Jensen, Hansman, Venuti & Reynolds, 2014). Those studies were based on the comparisons between the speeds and altitudes of over 200,000

flights within the continental United States, using Enhanced Traffic Management System data, and optimal speeds and optimal altitudes from models developed with information obtained using Lissys Piano-X (http://www.piano.aero/). A different study, conducted by Bonnefoy & Hansman (2010), analyzed the data provided by the BTS and investigated the influence of cruise speed reduction in terms of fuel burn benefits and airline scheduling consequences, and proposed how to mitigate these consequences.

The computing power of on-board platforms is very limited. Moreover, all on-board algorithms - including the FMS algorithms - must be predictable. The aircraft performance and flight path calculations using the classic model based on the aircraft's equations of motion are too complex and too computing-intensive to be employed on these platforms. Therefore, on-board algorithms generally use a simplified aircraft performance model constructed based on a set of linear interpolation tables (Liden, 1992b; Liden, 1985). Taking advantage of the use of advanced computation systems, the ground-based algorithms, such as ATM path prediction and optimization algorithms, employ an accurate performance model that relies on the aircraft's equations of motion (Rivas et al., 2012; Swierstra & Green, 2003; Nuic et al., 2005).

An on-board algorithm re-calculates the flight plan at regular time intervals, which ensures that the flight plan and its corresponding flight path parameters are always in synchronization with the aircraft's configuration, and the predicted speeds, altitudes, and atmospheric conditions. The flight path computations are performed successively, one segment at a time, from the aircraft's location to its destination. For each segment, the lateral and vertical flight plan components are calculated simultaneously in order to account for waypoint positions (geographical location), altitude restrictions or imposed procedural navigation segments. In addition, the performance model used by the on-board algorithms restricts the maximum length of a cruise segment on which the calculations can be performed (Liden, 1992b; Liden, 1985). Segments longer than a predefined value (usually 50 to 100 Nm) are parsed into a sequence of sub-segments whose lengths are limited to a predefined value. This means that for these algorithms, any flight plan update requires a full (lateral and vertical) flight path

computation, including the cases in which the vertical flight plan profile does not change. This inefficiency ultimately translates into longer flight plan calculation times, which has even more impact on flight optimization algorithms that may entail the computation of a larger set of potential optimal flight paths.

The investigations and the development of flight path optimization algorithms at the ETS' Research Laboratory in Active Controls, Avionics and Aeroservoelasticity (LARCASE) (Dancila et al., 2013; Dancila et al., 2012; Félix Patrón, Botez & Labour, 2013; Gagné, Murrieta Mendoza, Botez & Labour, 2013; Dancila, Botez & Ford, 2014; Murrieta Mendoza, 2013; Sidibé & Botez, 2013; Félix Patrón, Kessaci et al., 2013; Félix Patrón, Oyono Owono et al., 2013; Botez & Fays, 2013; Murrieta Mendoza & Botez, 2014a; Murrieta Mendoza & Botez, 2014b; Félix Patrón & Botez, 2014; Félix Patrón, Berrou & Botez, 2015; Félix Patrón, Kessaci & Botez, 2014) provided a good understanding of the tradeoffs and limitations imposed on the optimization algorithms with respect to run times and the size of the set of potential paths, and thus, to the general performance of the optimization algorithm. This research inspired the quest to find faster, less computing-intensive flight path computation algorithms.

The method presented in this paper aims to decrease the number of computations associated with the generation of a flight plan by disconnecting the vertical path computations from the lateral computations, thereby allowing the reuse of the already-computed vertical flight path data. The method employs a fuel burn prediction algorithm developed at the LARCASE (Dancila et al., 2013), and is used in conjunction with free-flight navigation scenarios, along the lines of the impending Next Generation Air Transportation System (NextGen) (Warren, 2000; Cano et al., 2007; Prevot, 2009; Erzberger & Paielli, 2002; Pappas, Tomlin, Lygeros, Godbole & Sastry, 1997; Haraldsdottir et al., 2006).

The method presented in this paper was developed for scenarios where the aircraft speed is defined by a constant speed schedule in each flight phase (climb, cruise or descent). Also, in each flight phase, the temperature profile of the air function of altitude is characterized by a constant value (ISADev), in degrees Celsius, representing the difference relative to the

corresponding standard atmosphere temperature. The "climb" and "descent" paths also take into account the speed and altitude restrictions specific to each phase (such as "thrust-reduction", "acceleration" or "speed restriction" altitudes) as well as the position of the crossover altitude. The aim was to investigate the generation, and use of pre-computed vertical flight path data in a simpler context (comparative to a more complex scenario considering multiple temperatures and speed schedules). The results of an initial and limited evaluation of the present method performed for a single test case (different than the cases considered in this paper) were presented in (Dancila & Botez, 2014).

The assembly and use of pre-computed vertical flight path data in a more complex scenario that considers multiple speed schedules and air temperature deviation values may be the subject of future research.

4.2 Existing algorithms' vertical and lateral flight path segment parameters' computation

As previously mentioned, existing flight plan computation algorithms perform a simultaneous determination of a flight path's lateral and vertical parameters, sequentially – one segment at a time, from the aircraft's position to the destination airport. These algorithms assume that winds have no vertical component; therefore, the winds have no direct influence on the set of aircraft performance parameters corresponding to the vertical profile. This means that for unconstrained climb, descent, acceleration, or deceleration segments (no waypoint-imposed segment length limitations), the wind will only affect the segment's horizontal distance. For constant-speed level-flight segments, given their maximum segment length limitation of up to 50-100 Nm, and the given performance modeling (hourly fuel burn rate), the wind only affects the segment flight time. The examples below illustrate the wind effects for climb (Appendix II, Figure-A II-1 to Figure-A II-4) and for constant-speed level-flight segments (Appendix II, Figure-A II-5 and Figure-A II-6).

The climb or descent performance data provides the values for a segment's *fuelburn* and still-air horizontal distance (H_{dist}) as a function of a given aircraft configuration (i.e. weight and

center of gravity position) at the beginning of the segment, the segment's airspeed (IAS or Mach), the air temperature (ISADev), the initial altitude, and the final altitude. The horizontal component of the aircraft' speed (H_{speed}) and the distance H_{dist} value are calculated relative to the mass of air in which the flight is performed; for still-air conditions, they are equal to the segment's ground speed (GND_{speed}) and the ground distance (GND_{dist}).

Consequently, the set of equations characterizing a still-air climb/descent segment are:

$$GND_{dist} = H_{dist} \tag{4.1}$$

$$d_{alt} = final_{altitude} - initial_{altitude} \tag{4.2}$$

where segment H_{dist} (and *fuelburn*) is computed using the aircraft climb performance data. Considering the diagram presented in Appendix II, Figure-A II-3), the still-air Flight Path Angle (*FPA*) for a climb segment is computed using the equation:

$$FPA_{still-air} = \arctan\left(\frac{d_{alt}}{H_{dist}}\right) \tag{4.3}$$

Subsequently, the aircraft's average vertical (V_{speed}) and horizontal speed (GND_{speed}) components (presented in Appendix II, Figure-A II-1) are computed using the equations:

$$V_{speed} = TAS_{avg} * \sin(FPA_{still-air}) \tag{4.4}$$

$$GND_{speed} = H_{speed} = TAS_{avg} * \cos(FPA_{still-air}) \tag{4.5}$$

where TAS_{avg} represents the average *TAS* value for the climb segment. The use of the average *TAS* value is considered acceptable given that the climb and descent segments are computed for small altitude differences.

The segment climb time is computed using the equation:

$$t_{clb} = \frac{d_{alt}}{V_{speed}} \tag{4.6}$$

During the lateral flight path segment computations, the wind influences the value of the ground speed, computed as a vector summation of the H_{speed} and the wind speed using the "wind triangle algorithm" (Hopper, 2011). The V_{speed} and t_{clb} values remain unchanged. Consequently, the segment ground distance computed as a function of the wind conditions ($GND_{dist\text{-}wind}$) is found by:

$$GND_{dist-wind} = GND_{speed} * t_{clb} = \frac{GND_{speed}}{V_{speed}} * d_{alt} \tag{4.7}$$

Given the fact that the segment's flight time is identical for still-air and wind conditions, the relationship between the ground distances corresponding to still air and wind conditions is described by the following equation:

$$\frac{GND_{dist-wind}}{H_{dist}} = \frac{GND_{speed}}{H_{speed}} \tag{4.8}$$

As shown in equation (4.8), the wind determines a segment ground distance that is a scaled value of the still air horizontal distance (H_{dist}) by a factor equal to the ratio between the average ground and still-air speed values. Consequently, in the presence of winds, the ground-referenced segment flight path angle (FPA_{wind}) is:

$$FPA_{wind} = \arctan\left(\frac{d_{alt}}{GND_{dist-wind}}\right) = \arctan\left(\frac{H_{speed}}{GND_{speed}}\frac{d_{alt}}{H_{dist}}\right) \tag{4.9}$$

For descent, the relationship between a flight path segment's parameters in still-air and under wind conditions is identical to that of climb; therefore, equations (4.3)-(4.9) are also valid for determining a descent segment's wind performance parameters.

For cruise level-flight segments flown in still-air conditions (Appendix II, Figure-A II-5), the ground speed is identical to the *TAS* value computed as a function of the set of *IAS*/*Mach*, altitude and air temperature values.

Consequently, for a segment of a given length (GND_{dist}), the corresponding flight time is computed as:

$$t_{crz-segm-still-air} = \frac{GND_{dist}}{TAS} \tag{4.10}$$

The aircraft's level-flight ground speed as a function of the wind conditions is computed similarly to a climb segment, by adding the *TAS* and the wind vectors (Appendix II, Figure-A II-6). Therefore, the flight time can be computed as:

$$t_{crz-segm-wind} = \frac{GND_{dist}}{GND_{speed}} \tag{4.11}$$

For a flight path segment defined with respect to a given flight time ($t_{crz-segm-still-air} = t_{crz-segm-wind}$), the relationship between the segment's still-air parameters and ground speeds and distances is described by the equation:

$$\frac{GND_{dist-wind}}{GND_{dist}} = \frac{GND_{speed}}{TAS} \tag{4.12}$$

which is similar to the equation corresponding to climb and descent segments.

The existing algorithms therefore compute the cruise level-flight path segment's fuel burn by multiplying the corresponding segment's flight time and fuel burn rate. The cruise constant-speed level-flight segment fuel burn computation algorithm developed at LARCASE (Dancila et al., 2013) determines a segment's fuel burn as a function of the aircraft's initial gross weight at the start of the segment and the segment's flight time. It also eliminates the limitations relative to the maximum length of the segment.

4.3 Description of the proposed method

The proposed method addresses the computation and assembly of a set of vertical flight path segments that may be utilized for the construction of an aircraft's lateral and vertical paths composing the flight plan as a function of the aircraft's performance model, and the aircraft and flight plan configuration parameters (departure and destination airports' altitudes, End of Descent (EOD) position, take-off weight and balance configuration, selected range of cruise altitudes, standard air temperature deviation, climb, cruise and descent speeds, and the set of expected landing or EOD gross weights). Furthermore, the proposed method employs a graph (a vertical flight path graph) to characterize the relationship between the set of segments assembled in the vertical flight path look-up structure. The method takes into consideration cruising altitudes situated at multiples of 1,000 ft.

This set of flight path segments, assembled in a vertical flight path look-up structure, describes all the phases of a flight (climb, cruise, and descent), and covers the limits of the aircraft's flight envelope. The climb, cruise, acceleration and deceleration vertical flight paths are computed according to the implementation of the aircraft's performance model, described by a set of performance and limitation parameters, and a set of linear interpolation

tables. The cruise, constant-speed level-flight vertical flight paths are computed using the fuel burn computing method developed at LARCASE (Dancila et al., 2013). The pre-computed vertical flight path segments' parameters (such as horizontal distance, fuel burn or fuel burn rate, flight path angle, or flight time) correspond to still-air flight conditions.

Similarly to the classic computation of a flight plan, the present method considers that the atmospheric winds do not have vertical components; therefore, the winds have no influence on the aircraft's vertical speed. Instead, they influence the ground-referenced segment flight path angle (FPA_{wind}) and the flight path parameters associated with lateral plan, such as the ground speed, flight time and the ground distance, as illustrated in the examples presented in Appendix II, Figure-A II-1 to Figure-A II-6, and in equations (4.1) - (4.12). Consequently, for the climb, descent, acceleration or deceleration segments, the corresponding still-air average speeds, flight path angles, and flight times determined using equations (4.1) – (4.6) are stored along with the matching vertical flight path segments' performance data and used during the lateral flight plan profile computations, generating a full lateral and vertical flight plan.

A cruise, constant-speed level-flight segment connects two consecutive non constant-speed level-flight segments (climb, descent or deceleration segments). It is characterized by the cruising altitude and the gross weight values described in the two delimiting segments' vertical path performance data for that particular cruising altitude. The corresponding still-air cruise distance is computed by multiplying the cruise segment's *TAS* by the segment's flight-time computed as a function of the cruising altitude and the initial and final aircraft gross weight (thus the fuel burn) using the algorithm developed at LARCASE (Dancila et al., 2013):

$$t_{crz-segm-still-air} = f\left(alt_{crz}, \mathrm{gw}_{initial}, gw_{final}\right) \tag{4.13}$$

$$H_{still-air-dist-cruise} = TAS_{cruise} * t_{crz-segm-still-air} \tag{4.14}$$

For each set of aircraft and flight configuration parameter values, the vertical flight paths are computed once, and subsequently employed in all flight plan computations. This, in turn, provides an important reduction of the volume of computations associated with the recurrent flight plan calculation, update or optimization.

Each flight path data set describes, among others, the aircraft's gross weight variation with altitude (for climb/descent segments), and the range and variation of its gross weight values for a given cruise altitude (for constant-speed level-flight segments). Consequently, for each altitude value in the range of altitudes characterized by the look-up structure, there are only a limited set or range of gross weight values which correspond to the pre-computed flight paths. A valid "gross weight – altitude binomial" represents a pair of values comprised of an aircraft gross weight and a flying altitude belonging to at least one pre-computed flight path segment.

The "vertical flight path graph", illustrated in Figure 4.1, is built using the flight path segments' data assembled in the vertical flight path look-up structure (their construction is described in detail in section 4.3.7).

A "graph node" represents a gross weight – altitude binomial belonging to at least two pre-computed vertical flight path segments. It represents the intersection of two or more pre-computed lookup table flight paths. A "graph edge" represents a vertical flight path segment stored in the look-up structure, which starts at the initial altitude and gross weight values (the "initial node"), and ends at the final altitude and gross weight values (the "final node"). During the construction of a flight plan, the vertical flight path graph can be used for identifying the available segments options, and for extracting the corresponding vertical flight path segment's performance data from the look-up structure.

At each stage of a flight plan construction, the position of the start point on the vertical flight path graph (the corresponding graph edge/node, altitude, gross weight etc.) is known as it represents the end of the last computed segment. If the start point is situated on an edge the

only option available is to continue on the same edge. If the start point corresponds to a node, the construction of the vertical flight plan can continue using any of the available edges staring at the respective node. The information regarding the selected edge, starting altitude and gross weight are used to extract the vertical flight plan segment performance data from the vertical flight path look-up structure.

The vertical flight path look-up structure and vertical flight path graph were described and organized with respect to the aircraft's altitude and gross weight values, an arrangement which is analogous to the aircraft performance model.

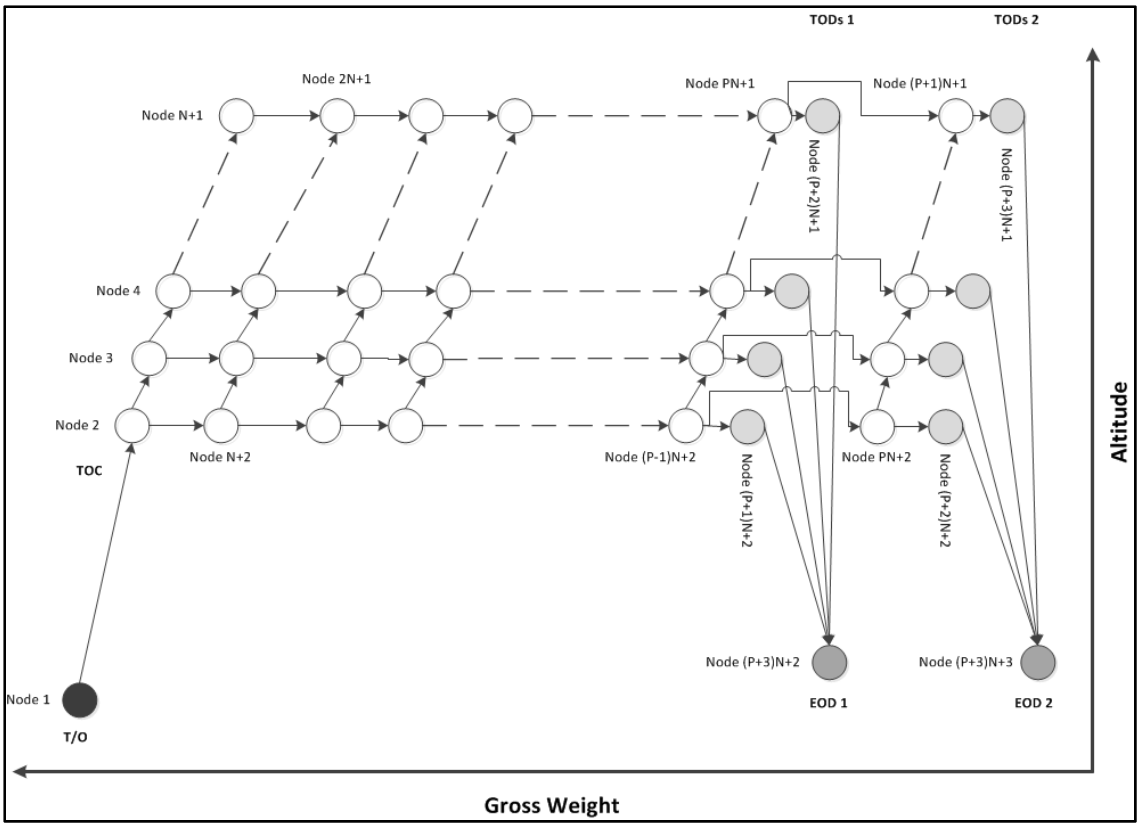

Figure 4.1 The vertical flight path graph corresponding to a look-up structure describing a climb path, a cruise phase composed of N cruising altitudes, P step-climb flight paths, and two sets of descent flight paths corresponding to two expected landing gross weights

4.3.1 Input configuration data

Each part of "configuration data" employed by the present method corresponds to one of the following categories:

- **Aircraft performance** – aircraft-specific linear interpolation tables and data.
- **Aircraft configuration** – the zero-fuel gross weight (*zfgw*), fuel weight (*fuel*), zero-weight center of gravity position (*zfwcg*), and one or more values of the expected landing or EOD gross weight.
- **Atmosphere** – the air temperature, defined by the corresponding standard temperature deviation (*ISADev*).
- **Navigation** – the departure and destination airports' and EOD altitudes; minimum and maximum cruise altitude limitations; climb, cruise and descent speed schedules, EOD speed (a "speed schedule" denotes a pair of IAS and Mach index values).

An aircraft's performance model (Liden, 1992b; Liden, 1985) supplies all the data necessary for the calculation of aircraft and flight path parameters, such as the maximum flight altitudes, fuel burn, altitudes, and still-air flight distances and flight path angles. Each calculation employs one or more linear interpolation tables specific to the particular performance parameter and flight phase, and the calculation may depend on one or a combination of parameters such as aircraft weight and balance configuration, altitude, speed, air temperature etc. The present method considers that for each flight phase, the air temperature (defined using the standard temperature deviation) is constant, thus, it does not change with the geographical position and time.

The advantage of considering the set of expected landing/ EOD gross weight values as an input to the method is that it allows the advanced computation of the set of expected vertical descent paths to be stored in the vertical flight path look-up structure and in the vertical flight path graph. The selection of these values may be performed following an analysis of historical flight data corresponding to the aircraft's type, departure and destination airports etc. Moreover, it is known that the "descent" flight paths' performance parameters are less

sensitive with respect to gross weight variation (and thus, the estimated landing/EOD gross weight variation) than those corresponding to “cruise” and especially “climb” flight path performance parameters (Gerretsen & Swierstra, 2003). Therefore, a judiciously chosen set of landing gross weights may also allow the use of pre-computed descent paths for performance computations corresponding to other landing gross weight values, by employing interpolation algorithms, which will result in path predictions within an acceptable error margin.

4.3.2 Gross weight and center of gravity position

For some aircraft models, the performance interpolation tables may impose calculations as function of the center of gravity position. Consequently, the expression linking the fuel weight, the total weight, and the center of gravity position must be established prior to the construction of the vertical flight path look-up structure. This expression is a function of the aircraft’s take-off weights and balance configuration, and relies on a set of aircraft performance tables. It does not change for the entire extent of the flight, thus for any flight phase, segment type, flight speed, altitude or atmospheric conditions.

As illustrated in the literature (Dancila et al., 2013; Federal Aviation Administration, 2007), the aircraft’s total gross weight *gw* and the position of its center of gravity *cg* specified as a percentage of the mean aerodynamic chord length (% MAC) are dependent on the aircraft’s zero fuel gross weight *zfgw*, zero fuel weight center of gravity position *zfwcg*, and fuel weight *fuel*, as described in equations (4.15) and (4.16):

$$gw = f_1\left(zfgw,\ fuel\right) \tag{4.15}$$

$$cg = f_2\left(M_a\left(zfgw, zfwcg\right), M_f\left(fuel\right), CGREFDIST, LEMAC, MAC\right) \tag{4.16}$$

where M_a is the aircraft moment, M_f is the fuel moment, *MAC* is the length of the mean aerodynamic chord, *LEMAC* is the leading edge mean aerodynamic chord position, and *CGREFDIST* is the position of the aircraft's center of gravity reference point.

4.3.3 Maximum flying altitude as function of the gross weight

The vertical flight paths assembled in the vertical flight path look-up structure must conform to a set of minimum two conditions: account for the aircraft's performance and their limitations, and cover the maximum set of altitude and gross weight configurations (the maximal flight envelope). Both conditions require a proper characterization of the maximum flying altitude, which depends on the aircraft's performance, and which could also be a function of one or more parameters related to the particular aircraft's configuration (*gw*, *cg*), and flying conditions (speed, air temperature, etc.).

The proposed method addresses these requirements firstly by determining the relationship between the maximum altitude and the aircraft's gross weight, and for the flying conditions for each phase (climb, cruise, and descent) using the appropriate set of aircraft performance data. Secondly, for each flight phase, a table is constructed that provides the maximal set of altitudes and the corresponding maximum allowed aircraft gross weight.

For the cruise phase, the table provides the necessary information regarding the maximum altitude envelope for the particular aircraft configuration and flying conditions, as well as the maximum *gw* value (earliest point) at which a flight is possible, as function of the cruise altitude. This information in turn allows the computation of the earliest climb start points (*gw* values), and the earliest possible climb flight paths that lead to each cruise altitude, thereby maximizing the range of flight paths available for the flight plan computation phase.

4.3.4 The climb flight path and the Top Of Climb

The climb phase extends from the take-off altitude or from the aircraft's initial altitude to the Top of Climb (TOC), reached at the point where the climb flight path arrives at the minimum cruise altitude. The proposed method considers that the climb path is an unconstrained, continuous climb, meaning that there are no waypoint-imposed altitude and speed restrictions, nor mandatory level-off segments.

The climb path is decomposed in sub-segments, and its parameters are computed for these sub-segments corresponding to altitude differences of a maximum of 1,000 ft. Therefore, each such sub-segment usually starts and/or ends at an altitude multiple of 1,000 ft. and is characterized by a set of parameters which may include:

- The aircraft's initial and final flying altitudes;
- The aircraft's initial and final *gw*, *cg*, and *fuel weight*;
- The aircraft's initial and final *IAS*/*Mach* and *TAS* values;
- The sub-segment's still-air horizontal distance and flight path angle (*FPA*); and
- The sub-segment's flight time, fuel-burn, and average *TAS*.

As mentioned above, the climb flight path computation takes into account all procedural speed and altitude constraints, including the take-off speed as well as the thrust reduction, acceleration, speed restriction, and crossover altitudes. The sequence of steps employed for the computation of the climb vertical flight path and the TOC parameters is presented in Figure 4.2, below.

An illustration of a climb vertical flight path, including its altitude-based segmentation, and the corresponding performance parameters is presented in Figure 4.3.

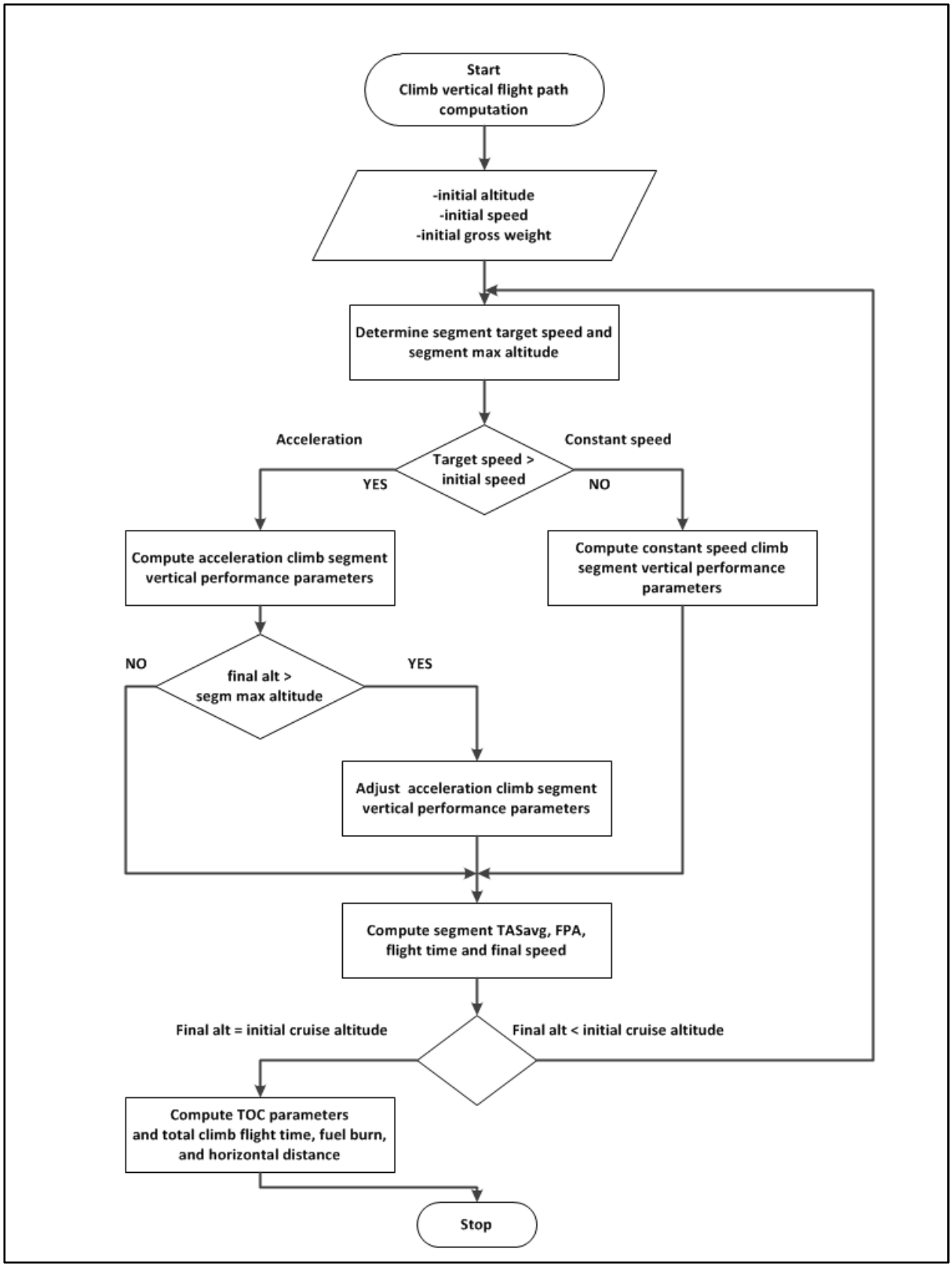

Figure 4.2 The climb vertical flight path computation workflow

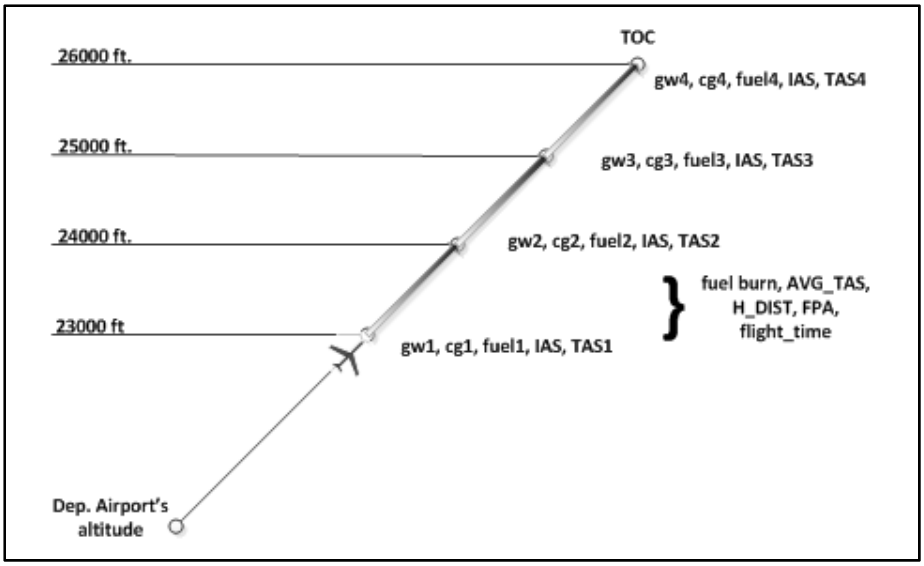

Figure 4.3 The pre-computed climb vertical flight path parameters

Complementary to the climb vertical flight path data, an additional set of parameters associated with the TOC characterizes the climb path as a whole and may include:

- TOC *altitude*;
- TOC *gw*, *fuel*, and *cg*;
- TOC *IAS*/*Mach* and *TAS*;
- Still-air, horizontal distance measured from aircraft location to the TOC, as the sum of the still-air horizontal distances of the composing climb segments;
- Time to TOC as the summation of the composing climb path segments' flight times; and
- Climb fuel-burn as the sum of the fuel burns of the composing climb path segments.

The individual segments' flight times as well as the time to TOC computed in still-air conditions remain valid during the lateral path calculations, as the winds are assumed to have no vertical components. However, during the lateral path computations, the still-air, vertical path-computed speed, horizontal distance, and flight path angle parameters are adjusted as function of each segment's particular wind conditions, as illustrated in Appendix II, Figure-A II-1 to Figure-A II-4, and equations (4.7) - (4.9).

4.3.5 Descent flight paths and the set of Top of Descent points

For the descent phase, the set of computed descent vertical flight paths are connecting the EOD altitude to the maximum valid cruise altitude. They may incorporate the required level-flight deceleration segments at each cruise altitude, which correspond to the aircraft's deceleration from cruise to the descent speed. The set of points situated at the start of the deceleration segments represents the set of Top of Descent (TOD) points. The number of descent vertical paths is equal to the number of expected EOD gross weight values provided as input data. For each descent path, the number of TOD points is identical to the number of altitudes, positioned in the selected range of cruise altitudes, provided as input data, which meet the aircraft's maximum altitude and gross weight flight envelope limitations.

Each descent vertical flight path's parameters are divided in two groups. The first group characterizes the set of "level-flight deceleration segments", one segment per valid cruise altitude, and the second group characterizes the "actual descent path", which is performed at the descent speed schedule, from the corresponding maximum valid cruise altitude to the EOD altitude. The approach used in the construction of the descent paths ensures that for any selected TOD (corresponding to a descent flight path and cruise altitude), the aircraft's parameters at the end of the deceleration segment are equal to those of the selected actual descent flight path at the TOD's cruise altitude (as illustrated in Figure 4.1).

Figure 4.4 illustrates the sequence of steps employed for the construction of the descent paths, from the EOD altitude up to the maximum cruise altitude, which include the actual descent and the flight paths' level-flight deceleration segments.

An example of a descent vertical flight path and the relationship between the TODs, the deceleration segments, the actual descent, and the EOD is presented in Figure 4.5, where k represents the index of the selected landing/EOD gross weight value, and $N+i$ represents the index of the selected cruise altitude value.

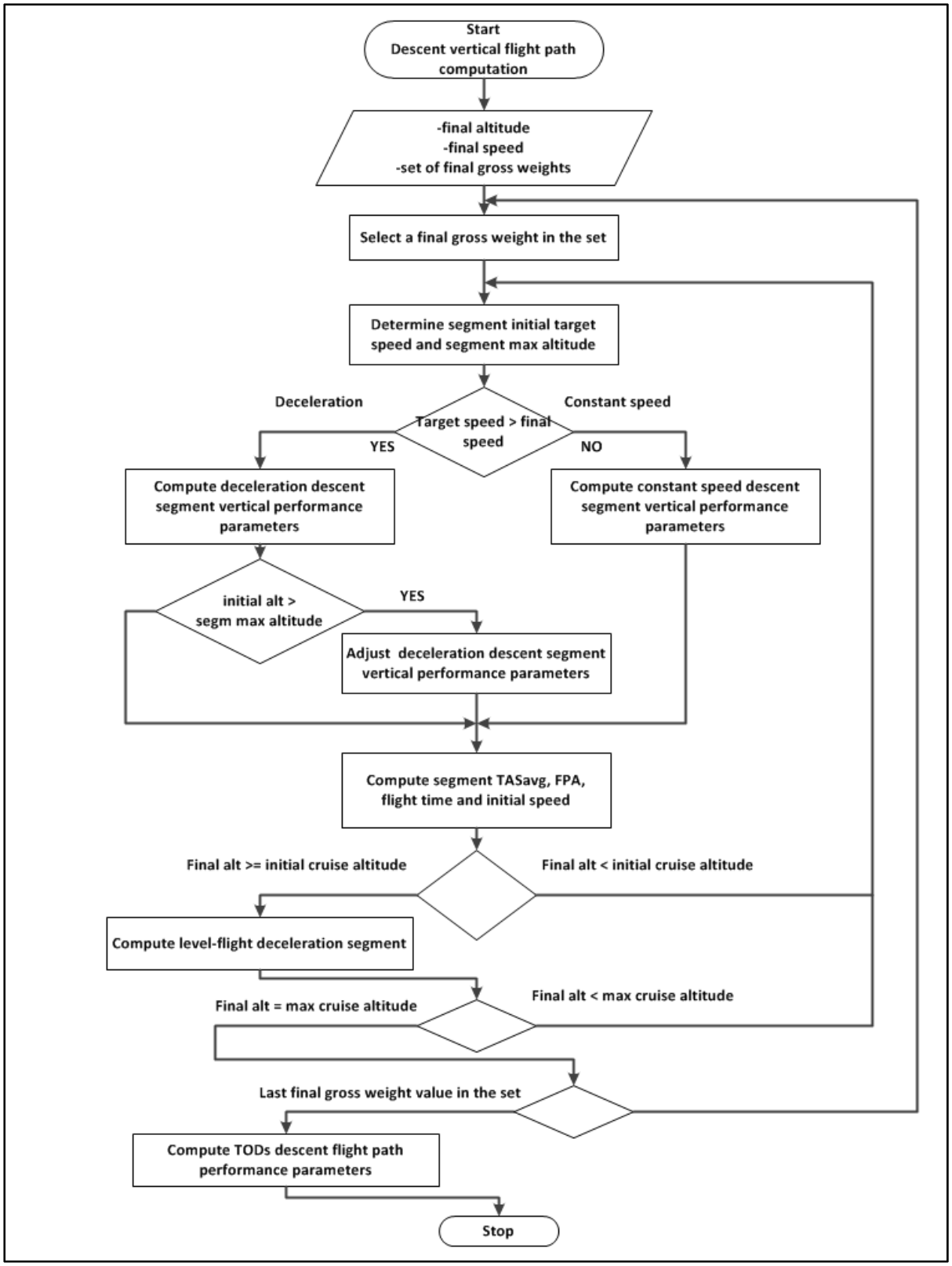

Figure 4.4 The descent vertical flight paths' computation workflow

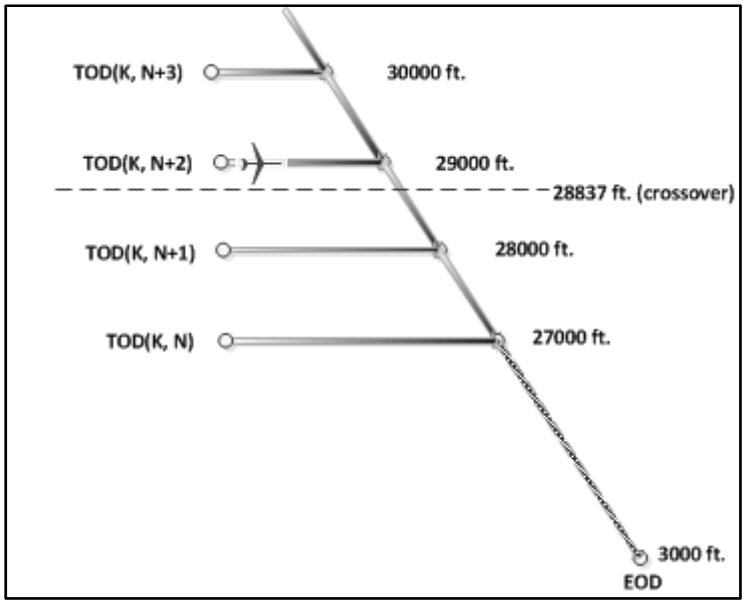

Figure 4.5 Example of a descent flight path – the deceleration and descent segments

The actual descent vertical flight path data is similar to the climb vertical flight path data in terms of number and type of parameters, as well as in terms of the sub-segments' 1,000 ft. altitude decomposition.

Each "level-flight deceleration" segment represents the flight path segment connecting the corresponding pair of level-flight constant speed cruise, and actual descent paths. The deceleration segment is characterized by a set of parameters which include:

- Aircraft's altitude;
- Aircraft's initial and final *gw*, *cg*, and fuel weight;
- Aircraft's initial and final *IAS*/*Mach* and *TAS* values;
- Segment's still-air horizontal distance; and
- Segment's flight time, fuel-burn, and average *TAS*.

The resulting descent vertical flight paths' data can be assembled as a 2 x *K* x *N* structure, where *N* represents the number of cruise altitudes, and *K* represents the number of descent paths (expected gross weight landing/EOD values). The element (1, *i*, *j*) stores data

characterizing the “deceleration segments” corresponding to the descent path *i* “at” the cruise altitude *j*, and the element (2, *i*, *j*) stores the data characterizing the “actual descent segments” corresponding to the descent path *i* “from” the cruise altitude *j*.

Complementary to the descent segments’ vertical flight path data, an additional set of parameters corresponding to the computed TODs provides a global characterization of the set of available descent paths. The TOD data may be organized as a function of the EOD gross weight and initial cruise altitude, where the parameters describing each TOD may include:

- TOD *gw*, *fuel*, and *cg*;
- TOD *IAS*/*Mach* and *TAS*;
- Still-air distance from the TOD to the EOD as the sum of still-air horizontal distances of the ”deceleration in cruise” and “descent” segments;
- TOD to EOD flight time, as the sum of the corresponding ”deceleration in cruise” and “descent” flight times; and
- Descent fuel-burn as the sum of the fuel burns of the corresponding ”deceleration in cruise” and “descent” flight path segments.

4.3.6 Cruise vertical flight paths

For the cruise phase, the set of vertical flight paths consists of flight path segments that may be employed to link the TOC (if the aircraft is in climb) or the actual aircraft position (if the aircraft is already in cruise) with the set of TODs. These segments are positioned between the minimum cruise altitude and the maximum altitude in the set of TOD altitudes. The present method limits the cruise segments’ types to “constant-speed level-flight” and “constant-speed step-climb”. As previously mentioned, the proposed method considers constant climb, cruise and descent speed schedules. As well, it considers only climb in cruise segments in accordance with the usual tendencies of searching higher cruise altitudes which yield better flight performance. Cruise step-descents are usually performed as a consequence of an ATC request or extreme weather avoidance maneuvers, and are not a part of pre-planned flight paths. Thus, cruise “step-descents”, acceleration or deceleration segments are not considered.

4.3.6.1 Step-climb vertical flight paths

The actual number of step-climb vertical flight paths stored in the look-up structure is dependent on the relationship between the desired step-climb vertical flight path resolution and the platform's processing time and memory space limitations. These paths may include the earliest climbs to each cruise altitude (the climb paths reaching the cruise altitudes at gross weights corresponding to the maximum gross weight values allowed at each cruise altitude). Each step-climb vertical flight path is decomposed into sub-segments corresponding to maximum 1,000 ft. altitude differences, and takes into consideration the position of the crossover altitude. All step-climb sub-segments are computed in the same manner, and are described by the same set of parameters as the climb sub-segments.

4.3.6.2 Level-flight cruise vertical flight paths

The level flight cruise vertical flight paths are constructed for altitude multiples of 1,000 ft. The performance parameters of the segments composing the level-flight cruise path were calculated using the fuel burn computation algorithm developed at the LARCASE laboratory (Dancila et al., 2013). This algorithm constructs and uses a fuel burn look-up table that describes the correlation between the gross weight at the beginning of the segment, cruise altitude, segment flight time, and the aircraft's gross weight at the end of the segment -- the fuel burn. Figure 4.6 illustrates the sequence of steps employed for the construction of the level-flight cruise vertical path data.

The constant-speed level flight look-up table is calculated once and is valid for the entire cruise flight. This table makes it possible to perform more flexible fuel burn computations than the existing on-board fuel burn algorithms (i.e. "fuel burn" as a function of the "flight time", and "flight duration" as a function of the "fuel burn"), and eliminates the restrictions presently imposed on the maximum length of a level-flight cruise segment (50 to 100 Nm.) by the existing FMS algorithms (Liden, 1992b; Liden, 1985).

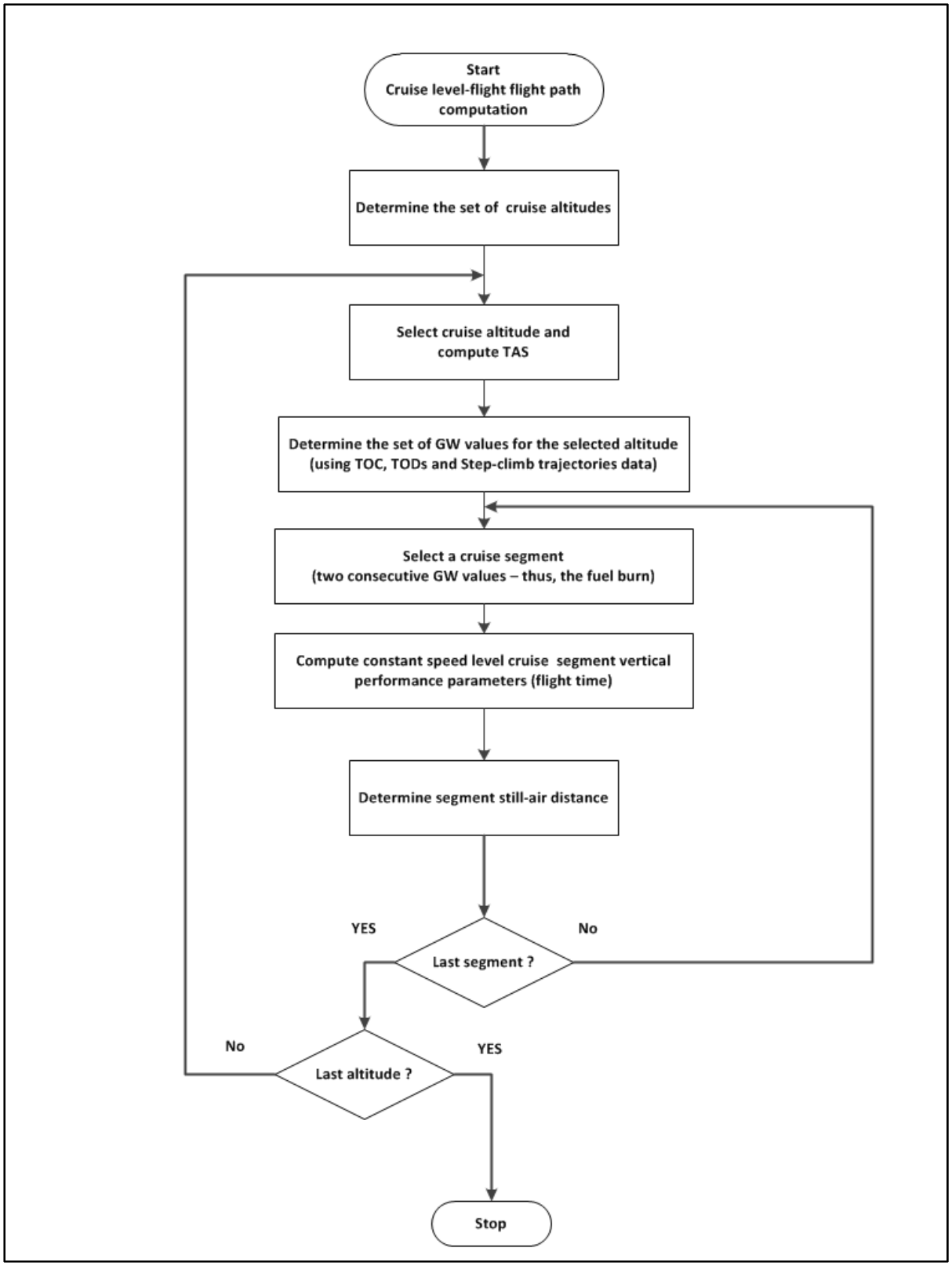

Figure 4.6 The level-flight cruise vertical flight path computation workflow

As illustrated in Figure 4.1, each level-flight cruise flight path segment starts at a gross weight value equal to that at which the climb flight path or a step-climb flight path reaches the corresponding cruise altitude, and ends at a gross weight value equal to that at which the immediately succeeding step-climb or descent flight path reaches the same cruise altitude.

The set of parameters that characterizes a level-flight cruise vertical path segment may include:

- Altitude;
- Initial and final *gw*, *cg*, and *fuel weight*;
- *IAS*/*Mach* and *TAS* values;
- Segment's flight time and fuel burn; and
- Segment's still-air horizontal distance.

4.3.7 The vertical flight path look-up structure and the vertical flight path graph

The assembly of climb, cruise, and descent flight path segments' performance data can be compiled into a look-up structure. The sets of climb-in cruise and descent paths are organized sequentially, in a reverse order of the gross weight at the start of the vertical flight path (minimum cruise altitude and the EOD, respectively), similar to the usual aircraft's gross weight reduction along a flight path.

The global topological relationships between the climb, cruise, and descent paths (as well as the corresponding path segments) can be described using the vertical flight path graph. Its nodes (Figure 4.1) are represented by the gross weight–altitude binomials corresponding to the T/O, TOC, TODs, and the EODs, as well as by all the "intersection" points between the pre-computed cruise vertical flight paths (level flight and step-climb). These intersection points are situated in the cruise phase, between the TOC and the TODs, at altitude multiples of 1,000 ft.

A succinct representation of the succession of steps employed for the construction of the vertical flight path look-up structure and the vertical flight path graph is presented in Figure 4.7.

For any flight phase, given an aircraft's vertical flight plan position defined by an altitude and gross weight, the vertical flight plan graph provides a way for detecting whether that position is situated at a graph node or on a edge and consequently, the number and type of vertical path segments that can be employed for building the subsequent vertical and lateral flight path segment. It also facilitates the detection of the transition points from one flight phase to the next. For example, the graph node corresponding to the TOC designates the transition point from climb mode to cruise. Similarly, upon reaching any graph node corresponding to a TOD, its set of parameters can be used by itself or in conjunction with other parameters (such as the distance to the EOD/destination airport) to decide whether the exploration of a "descent path" is appropriate.

Once the vertical path segment is selected, the vertical flight path graph facilitates the retrieval of the corresponding performance information from the vertical flight path look-up structure, either as general segment description data (say for the entire descent segment as a whole) or as detailed segment description data (say for the set of data of each sub-segment composing the selected descent vertical flight path).

The two sets of data describing the ensemble of available vertical path segments also allow the construction of a complete stand-alone vertical flight plan and the computation of the corresponding set of altitudes, still-air distances, flight times, fuel burns, and flight costs. The construction of the vertical flight plan may also target specific goals including flight time, fuel burn, or flight cost minimization. However, knowing that such a vertical flight plan is constructed for still-air conditions, its suitability for the construction of the final lateral and vertical flight plan is dependent on the flight's particular navigation (composing segments' lengths and headings), and wind conditions.

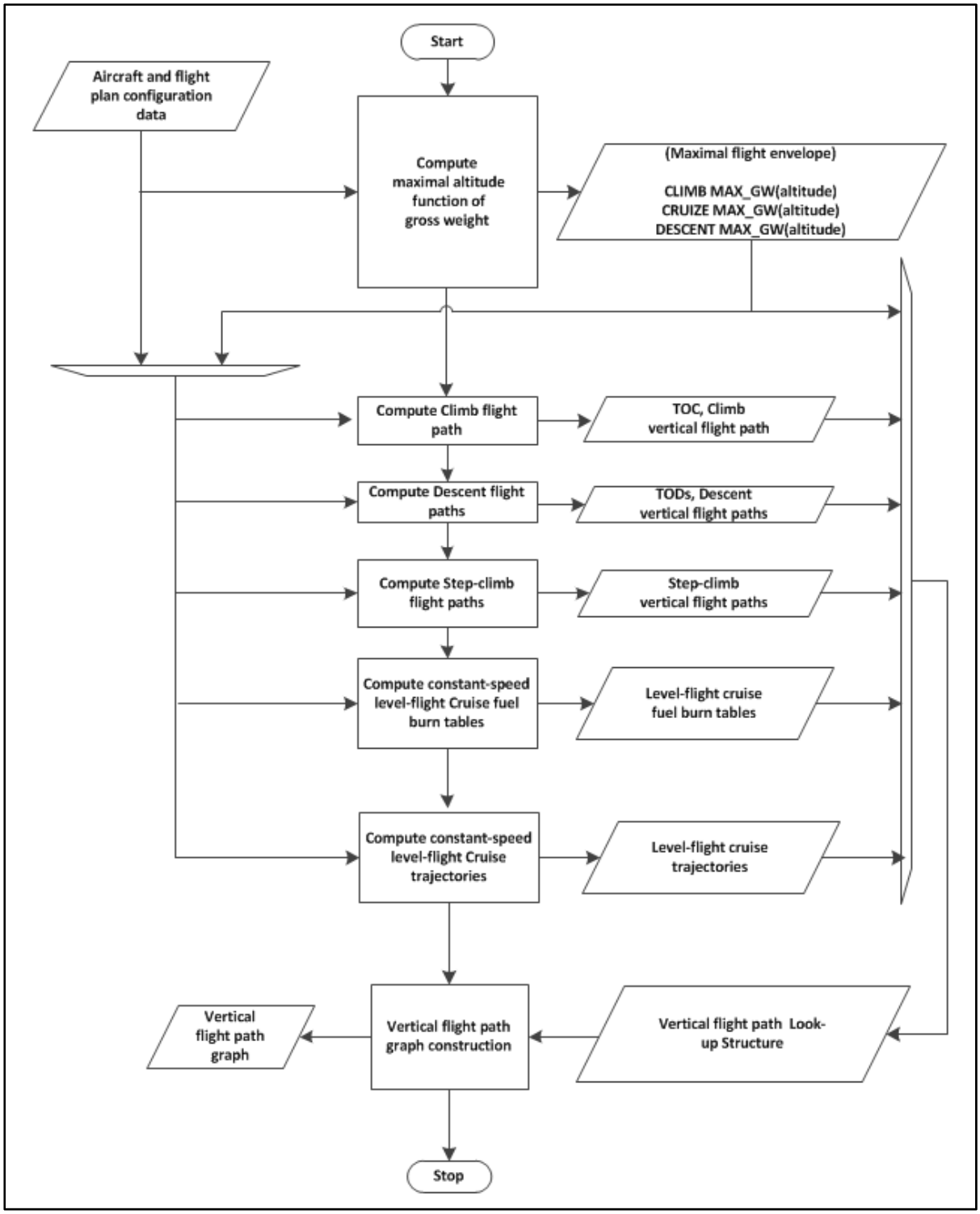

Figure 4.7 The vertical flight path look-up structure and vertical flight path graph computing workflow

Nonetheless, the ability to construct and evaluate such profiles may provide useful insight regarding the relationship between the criteria used for the selection of a vertical flight path and an aircraft's performance, configuration, and navigation conditions.

4.3.8 The vertical and lateral flight plan computation using the vertical flight plan look-up structure and the vertical flight plan graph

The proposed method considers that the vertical flight path look-up structure and graph are employed in a scenario in which the full vertical and lateral flight plan parameters are computed in a manner similar to the scenario considered by the existing on-board algorithms, one segment at a time, from the aircraft's actual position to the destination airport. The performance parameters of the vertical flight plan segments, however, are not recalculated at every reconstruction/evaluation of the corresponding flight plan segments. Instead, the segment's performance parameters are extracted from the look-up structure and processed along with the corresponding lateral navigation and wind data to determine the full vertical and lateral flight path description (flight plan).

The flight plan computations may be performed with respect to the selected vertical flight path look-up structure segment's entire still-air horizontal distance (H_{dist}), or for just a fraction (k) of it. For the climb, step-climb, and descent segments, the computations may also be performed relative to the look-up structure segment's entire altitude difference (d_{alt}), or for just a fraction (k) of it. These computations allow the determination of the aircraft's parameters at a particular location or altitude on the flight plan.

The actual computation of the flight plan parameters for a fraction k of a look-up structure flight path segment depends on the type of the segment itself, and takes advantage of the fact that the look-up structure and the composing segments were computed considering the linearity domains of the aircraft's performance model. Therefore, some of the fractional (k) still-air flight path segment parameters' values (such as the fuel burn, altitude difference, and horizontal distance) are equal to the same fraction k values of the corresponding full-length

still-air flight path segment's parameters. If the segment is flown at constant *IAS*/*Mach*, the final *TAS* is computed using the corresponding speed conversion equation as a function of the final altitude; the segment flight time is equal to the quotient between the segment's still-air distance fraction and its average *TAS*.

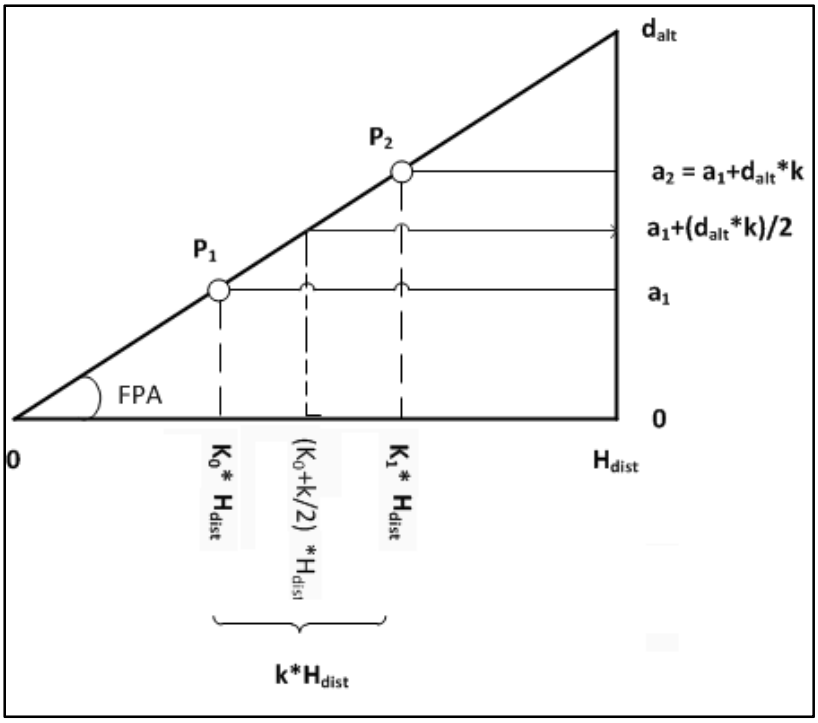

Figure 4.8 Example of fractional constant-speed climb segment performance computation

For the constant speed climb segment example presented in Figure 4.8, considering the *fuelburn* and H_{dist} values retrieved from the look-up structure, the still air performance parameters for the segment P_1P_2 (representing a *k* fraction of the entire constant speed climb segment) are computed as follows:

$$K_1 = K_0 + k \tag{4.17}$$

$$P_1P_{2-hdist} = k * H_{dist} \tag{4.18}$$

$$P_1P_{2-fuelburn} = k * fuelburn \tag{4.19}$$

$$P_1P_{2-dalt} = k * d_{alt} \tag{4.20}$$

$$a_1 = K_0 * d_{alt} \tag{4.21}$$

$$a_2 = a_1 + k * d_{alt} \tag{4.22}$$

$$TAS\_P_2 = TAS(IAS / Mach, a_2) \tag{4.23}$$

$$TAS_{avg\_P_1P_2} = TAS(IAS / Mach, a_1 + d_{alt}\frac{k}{2}) \tag{4.24}$$

$$t_{still-air\_P_1P_2} = \frac{P_1P_{2-hdist}}{TAS_{avg\_P_1P_2} * \cos(FPA)} = \frac{k * H_{dist}}{TAS_{avg\_P_1P_2} * \cos(FPA)} \tag{4.25}$$

where *FPA* is computed using equation (4.3).

"Acceleration-in-climb" and "deceleration-in-descent" segments consider a uniform variation of the *IAS*/*Mach*. Consequently, the segment's final speed is calculated as a function of the initial and final *IAS*/*Mach* values, as well as of the fraction of the look-up structure flight path segment for which the computations are performed. The corresponding final *TAS* value is computed using the corresponding speed conversion equations. The flight time for the fraction of the segment is computed as the quotient between the actual still-air horizontal distance fraction and its average *TAS*.

Considering the look-up structure segment presented in Figure 4.8, the acceleration-in-climb and deceleration-in-descent segments are characterized by an additional set of parameters: initial speed IAS_0/$Mach_0$, and final speed IAS_f/$Mach_f$, and thus the *IAS*/*Mach* speed variation d_{IAS}/d_{Mach}. The *IAS* fractional segment's final and average speed values, and the flight time are computed using the following equations (similarly for Mach segments):

$$IAS\_P_1 = IAS_0 + K_0 * d_{IAS} \tag{4.26}$$

$$IAS\_P_2 = IAS\_P_1 + k * d_{IAS} = IAS_0 + (K_0 + k) * d_{IAS} \tag{4.27}$$

$$TAS\_P_1 = TAS(IAS\_P_1, a_1) \tag{4.28}$$

$$TAS\_P_2 = TAS(IAS\_P_2, a_2) \tag{4.29}$$

$$IAS_{avg\_P_1P_2} = IAS\_P_1 + \frac{k * d_{IAS}}{2} \tag{4.30}$$

$$TAS_{avg\_P_1P_2} = TAS\left(IAS_{avg\_P_1P_2}, \mathrm{a}_1 + d_{alt}\frac{k}{2} \right) \tag{4.31}$$

$$t_{still-air\_P_1P_2} = \frac{P_1P_{2-hdist}}{TAS_{avg\_P_1P_2} * \cos(FPA)} = \frac{k * H_{dist}}{TAS_{avg\_P_1P_2} * \cos(FPA)} \tag{4.32}$$

The final *gw* and *cg* values are computed using equations (4.15) and (4.16).

For a level-flight constant-speed cruise segment the look-up structure data provides the values corresponding to the flying altitude, *IAS*/*Mach* speed, initial gross weight, *fuelburn*, *TAS*, still-air flight time, and horizontal distance. The corresponding (P_1P_2) fractional flight path segment parameters' computation can be performed relative to a selected fraction (*k*) of the *fuelburn* value, flight time or still-air horizontal distance. The fuelburn-based computations are performed using equations (4.13) and (4.14), where $gw_{initial}$ and gw_{final} are replaced by the actual gross weight at the start and at the end of the fractional segment (gw_{P1} and gw_{P2}, respectively). Thus,

$$gw_{P2} = gw_{P1} + k*fuelburn \tag{4.33}$$

For the fractional flight time or horizontal distance-based still-air computations, the relationship between the flight time and still-air horizontal distance is described by equation (4.14), and therefore:

$$P_1P_{2-still-air-dist} = k * H_{dist} \tag{4.34}$$

and

$$P_1P_{2-still-air-time} = k * t_{crz-segm-still-air} \tag{4.35}$$

The final *gw* and *fuelburn* values are computed from the cruise fuelburn look-up tables as functions of the initial *gw*, *altitude*, and actual segment flight time (Dancila, 2011; Dancila et al., 2012):

$$gw_{P2} = f\left(alt_{crz}, \mathrm{gw}_{P1}, P_1P_{2-still-air-time}\right) \tag{4.36}$$

For a selected fraction of a level-flight deceleration segment, situated between a TOD and the corresponding actual descent path, the horizontal flight distance and fuel burn values are equal to the same fractional value of the total segment's H_{dist} and *fuelburn* found in the look-up structure. The computation of the flight path segment's complete set of still-air parameters is performed in a manner similar to that used for the climb-acceleration or descent-deceleration segments, using equations (4.17) – (4.22) and (4.26) – (4.32), where $d_{alt} = 0$. The final *gw* and *cg* values are computed using equations (4.15) and (4.16). The final speed, average segment speed, and actual segment flight time are computed considering a uniform deceleration relative to the aircraft's *IAS*/*Mach*.

Figure 4.9 presents a simplified description of a typical use of the vertical flight path graph and look-up structure, and Figure 4.10 presents the processing steps employed for the translation of the vertical path segment data into lateral and vertical flight plan segment data.

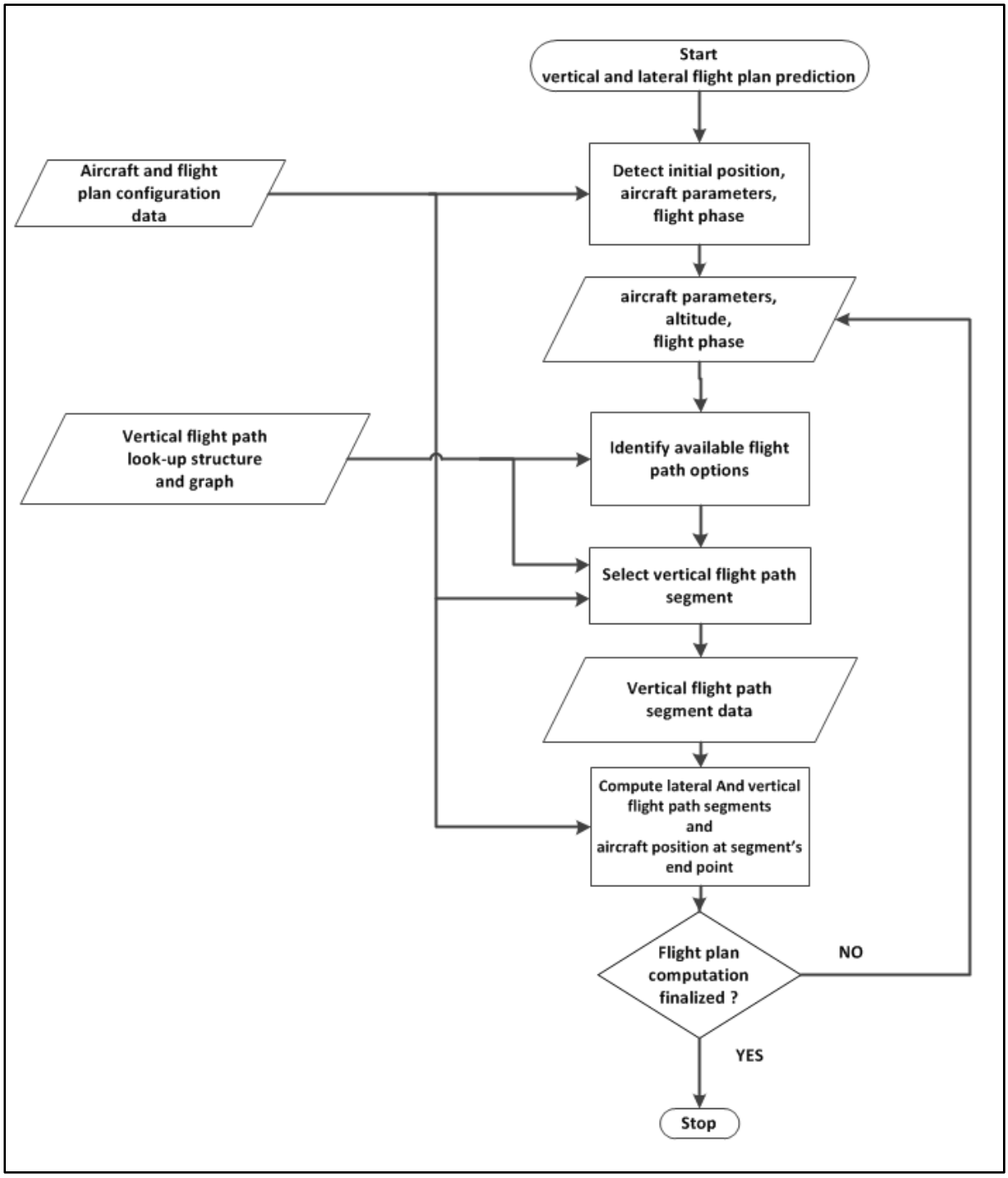

Figure 4.9 The flight plan computation workflow

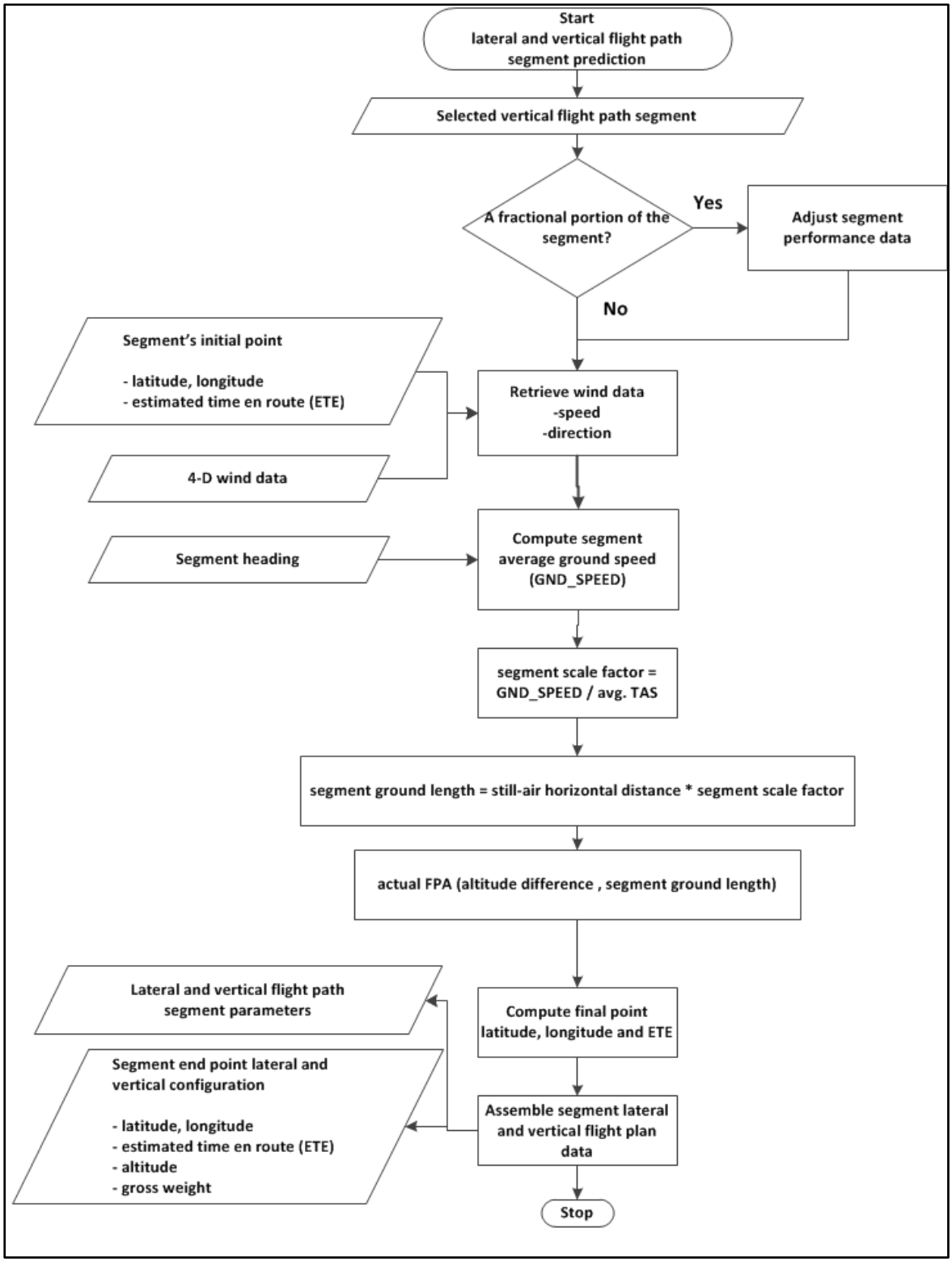

Figure 4.10 The flight plan segment's computation workflow

4.4 Results

The method described in this paper was investigated using a performance model dependent upon the center of gravity position on nine test scenarios corresponding to flight plans connecting the T/O and EOD points. The principal objective was the determination of the characteristics and parameters of the resulting flight envelopes, and the influence of the number of cruise altitudes and descent paths on the flight envelope's performance; namely, the range of total flight times and still-air flight distances, and the vertical flight paths describing the minimum and maximum flight times and still-air flight distances. The nine scenarios, designated as A11, A12, A13, A21, A22, A23, A31, A32, and A33, shared the same aircraft take-off weight and balance configuration, minimum cruise altitudes, as well as speed schedules, and standard temperature deviation values. These scenarios employed three values of the maximum cruise altitude (three test cases for each maximum cruise altitude value), and three sets of EOD gross weight values (identical for each maximum cruise altitude value). The set of configuration parameters for the nine test cases are presented in Table 4.1 and Table 4.2.

The topologies of the sets of flight paths described by the resulting vertical flight path look-up structures and vertical flight path graphs, calculated using the proposed methodology, are presented in Table 4.3. A graphical representation of the set of vertical flight paths stored in each vertical flight path look-up structure (and vertical flight path Graph) is presented in Appendix II, Figure-A II-7 to Figure-A II-15. It can be observed that for each case presented in Appendix II, Figure-A II-7 to Figure-A II-15, the set of paths composing the corresponding vertical flight path graph is similar to that described in Figure 4.1: a climb path connecting the take-off to the minimum cruise altitude, a set of cruise constant altitude segments, a set of step-climb segments connecting each pair of consecutive cruise altitudes for a number of cruise gross weight configurations, and a set of descent segments connecting each cruise altitude to each of the landing/EOD altitude and gross weight configurations.

Table 4.1 The set of test configuration parameters common to the nine scenarios

Parameter Name	Value
T/O Gross Weight (% of T/O Gross Weight)	100
T/O Altitude (ft)	600
Minimum Cruise Altitude (ft)	28000
Climb Speed Schedule (IAS, Mach)	310 Kts., 0.81
Cruise Speed Schedule (IAS, Mach)	330 Kts., 0.83
Descent Speed Schedule (IAS, Mach)	280Kts., 0.78
EOD Altitude (ft)	3000
ISA_Dev (°C)	0

The data showed that, as expected, the values of the minimum cruise altitudes (selected as an input parameter) and maximum cruise altitudes (determined as function of the aircraft's configuration and performance) had an influence on the number of vertical flight path graph nodes. Moreover, they also showed that the selected number of descent paths, and more importantly their corresponding EOD gross weight values, had an important influence on the number of step-climb vertical flight paths and on the number of vertical path graph nodes.

The influence of the EOD gross weight values is twofold: firstly, as function of the aircraft's performance, the EOD GWs determine the maximum altitudes of the TODs, and thus the maximum cruise altitude (an example of maximum cruise altitude differences due to the EODs' gross weight values' selection is illustrated in Table 4.3 and Appendix II, Figure-A II-8 and Figure-A II-9, for test cases A12 and A13). Secondly, the set of TOD gross weight values determines the minimum gross weight at each cruise altitude, thus the vertical flight path look-up structure's (and vertical flight path graph's) total number of step-climb paths.

Table 4.2 The sets of test configuration parameters specific to each test case

Test Case	Maximum Cruise Altitude (ft)	Number of Descent Paths	EOD Gross Weight Values (% of the T/O Gross Weight)
A11	36000	11	71.43, 72.14, 72.86, 73.57, 74.29, 75, 75.71, 76.43, 77.14, 77.86, 78.57
A12	36000	5	71.43, 72.14, 72.86, 73.57, 74.29,
A13	36000	5	75.71, 76.43, 77.14, 77.86, 78.57
A21	34000	11	71.43, 72.14, 72.86, 73.57, 74.29, 75, 75.71, 76.43, 77.14, 77.86, 78.57
A22	34000	5	71.43, 72.14, 72.86, 73.57, 74.29
A23	34000	5	75.71, 76.43, 77.14, 77.86, 78.57
A31	33000	11	71.43, 72.14, 72.86, 73.57, 74.29, 75, 75.71, 76.43, 77.14, 77.86, 78.57
A32	33000	5	71.43, 72.14, 72.86, 73.57, 74.29
A33	33000	5	75.71, 76.43, 77.14, 77.86, 78.57

It can be observed that for test cases A11 and A12 (and similarly for test cases A21 and A22, or A31 and A32), the number of step-climb flight paths was identical although the number of descent flight paths was different. This can be explained by the fact that for the two test cases (similarly for the other two pairs of test cases), the EOD gross weight minimum values were identical, and thus the minimum gross weight values at each cruise altitude and, by consequence, the number of step-climb paths were also identical.

Table 4.3 The topologies of the sets of flight paths described by the resulting vertical flight path look-up structures and vertical flight path graphs

Test Case	Climb Paths	Cruise Altitudes	Step-Climb Paths	Descent Paths	Vertical Flight Path Graph Nodes
A11	1	8	44	11	443
A12	1	8	44	5	395
A13	1	7	37	5	297
A21	1	7	43	11	381
A22	1	7	43	5	339
A23	1	7	37	5	297
A31	1	6	42	11	321
A32	1	6	42	5	285
A33	1	6	36	5	249

Subsequently, the investigation aimed to determine the total number of distinct flight paths that could be constructed using the vertical flight path graph, the minimum and maximum flight times and still-air distances, as well as the corresponding vertical flight path trajectories, using a "depth first" exhaustive exploration of the vertical flight path graph. The results corresponding to each of the nine test cases investigated in this article are presented in Table 4.4 and Appendix II, Figure-A II-16 to Figure-A II-24.

These results showed that, as expected, the total number of distinct flight paths described by a vertical flight path graph is directly dependent on the number of graph nodes and the graph's topology (the particular disposition of the graph nodes). Moreover, the parameters defining the graph topology (the number of cruise altitudes and the number of step-climb and descent paths) do not have the same influence in determining the total number of distinct flight paths. The parameter having the largest influence is the number of "step-climb" flight paths, while the number of "descent" flight paths has the least influence. This can be explained by the fact that the number of possible descent paths (as function of the combination of cruise altitude and EOD GW) is much smaller than the possible number of

cruise flight paths (as function of the combination of constant speed level flight, and climb in cruise segments).

Table 4.4 The vertical flight path graphs' total number of flight paths, the minimum and maximum flight times and still-air distances

Test Case	Number of flight paths	Min. flight time (h)	Max. flight time (h)	Min. still-air distance (Nm)	Max. still-air distance (Nm)
A11	115927565	5.274	7.746	2517.24	3687.362
A12	108146993	6.355	7.746	3049.451	3687.362
A13	5273451	5.274	6.417	2517.24	3050.248
A21	32811375	5.274	7.721	2517.24	3677.852
A22	25030804	6.355	7.721	3049.451	3677.852
A23	5273451	5.274	6.417	2517.24	3050.248
A31	5911543	5.274	7.669	2517.24	3657.096
A32	3980908	6.355	7.669	3049.451	3657.096
A33	1441797	5.274	6.405	2517.24	3046.001

The analysis also showed that the minimum and maximum values of the flight time and still-air distance are dependent on the sets of cruise altitudes, cruise-in-climb flight paths, and EOD gross weight values composing the vertical flight path graph. Moreover, each of the four values were attained on corresponding flight paths, each path being composed of a particular combination of consecutive segments from the set of level-flight cruise, step-climb, and descent segments of the vertical flight path graph (Appendix II, Figure-A II-7 to Figure-A II-15), and described by the succession of the vertical flight path graph nodes delimiting these segments.

As illustrated in Appendix II, Figure-A II-16 to Figure-A II-24, for all test cases, the maximum flight times and still-air distances were attained on flight paths employing a number of step-climb segments leading to the maximum cruise altitude, and descents segments corresponding to the minimum EOD gross weight values (and thus, maximum fuel burn). The minimum flight times and still-air distances, on the other hand, were attained on

flight paths employing a single step-climb to altitudes different than the maximum altitudes, and on descent paths ending at the maximum EOD gross weight values (and thus, minimum fuel burn). The two vertical profiles are generally different because of the fact that they employ different cruise altitude values; one cruise altitude value corresponds to the maximum fuel burn rate, and the other value corresponds to the minimum TAS. However, it can be observed that for the T/O configuration and the set of cruise altitudes used in this paper, the profiles for the minimum flight times and still-air distances were identical.

An additional point of interest was the investigation of the flight path's flight time and the still-air distance distribution as a function of the set of cruise altitudes (corresponding to each test case) and the EOD gross weight values. Consequently, for each test case, the corresponding range of flight times was decomposed into a set of 30-seconds intervals; the range of still-air distances was also decomposed into a set of 1 Nm intervals. Subsequently, an exhaustive exploration of the flight paths described by the vertical flight path graph was used to determine the number of flight paths leading to each sub-domain corresponding to a flight time and still-air distance interval as a function of the EOD gross weight value. A statistical analysis of the data allowed the identification of the flight time – still-air distance domain covered by the vertical flight path graph as a function of the EOD gross weight. Moreover, the statistical analysis provided the number of flight paths associated with each EOD gross weight, as well as the flight time – still-air distance domains attainable by flight paths corresponding to two or more EOD gross weight values. The results of the statistical analysis are presented in Appendix II, Figure-A II-25 to Figure-A II-33, and Table-A II-1 to Table-A II-9.

In each of the nine tables (Appendix II, Table-A II-1 to Table-A II-9), each cell C(i, j) of a row i describes the number of vertical flight paths that the flight time – still-air distance domain corresponding to EOD(i) shared with the flight time – still-air distance domain corresponding to EOD(j). For $i = j$, C(i, j) describes the total number of vertical flight paths corresponding to EOD(i). As each of the three sets of test cases (A1x, A2x, and A3x) described a different set of cruise altitudes, a comparison of the data tables depicts the

variation of the number of vertical flight paths corresponding to each EOD gross weight as function of the set of cruise altitudes. The plots presented in Appendix II, Figure-A II-25 to Figure-A II-33, illustrate, for each test case, the flight time – still-air distance domains covered by the sets of flight paths ending at each of the EODs defined by the corresponding look-up structure. The plots presented in Appendix II, Figure-A II-25 to Figure-A II-33 also illustrate, for each test case, the flight time – still-air distance domains common to pairs of EODs corresponding to consecutive gross weight values. These plots showed that, for each test case, the flight time – still-air distance domain covered by the ensemble of flight paths corresponding to all EODs defined in the corresponding look-up table did not have discontinuities. Moreover, each EOD flight time – still-air distance domain presented areas which overlapped with the domains corresponding to the adjacent EODs (identified distinctively in each test case plot)

An investigation regarding the values of the total time required for the generation of the vertical flight path look-up structures and the vertical flight path graphs using the same aircraft and flight plan configurations as depicted in Tables 4.1, 4.2, 4.3 and Appendix II, Figure-A II-7 to Figure-A II-15, as well as their decomposition as a function of the processing module are presented in Appendix II, Table-A II-10. The processing times correspond to a code developed in Matlab and executed on an AMD Phenom(tm) II X4, 2.80 GHz platform.

Most of the processing time (approximately 62% to 69.4% of the total processing time) was consumed for the generation of the level-flight fuel burn tables. Although this is a large proportion, this time is spent only once, and advanced generation strategies may reduce its overall impact on the construction and availability of the set of pre-computed vertical flight path segments.

The other two modules which required significant processing time were those computing the step-climb and the descent flight path segments, taking between 15.92% and 21.98%, and 5.7% and 8.5% of the total processing time, respectively. Knowing that their processing

times were dependent on the selected number of step-climb and descent flight paths, a careful selection of their number and configurations would likely reduce the impact on the availability of the set of pre-computed vertical flight path data while ensuring the desired range of step-climb and descent vertical flight path options.

4.5 Conclusions

The paper presents a method for constructing a set of vertical flight path segments, assembled as a vertical flight path look-up structure and a corresponding vertical flight path graph, encompassing an aircraft's climb, cruise, and descent phases and covering the full range of altitudes allowed by an aircraft's performance envelope. The paper also describes the envisaged utilization of the structure and graph for constructing a full lateral and vertical flight plan. The principal advantage of the proposed method over the existing flight plan computation algorithms is that it reduces the volume of repetitive resource-intensive calculations that use the aircraft performance model, limiting them to the construction of the look-up structure. This reduction is especially important for flight path optimization, which entails repetitive computations and evaluations of the cost objective function values of a number of different flight paths. Another advantage is the availability, through the graph data, of advanced information (aircraft altitude and gross weight values) identifying critical points of the vertical flight plan (such as the TOC, the start of a step-climb segment, or a TOD), and the available options for constructing the vertical flight segments composing the flight paths.

The main limitation of this method is that the flight paths described by the look-up structure are constructed by considering only a single value of the temperature deviation, and the speed schedule for each of the three flight phases (climb, cruise, and descent). This limitation facilitated an initial evaluation of the look-up structure and vertical flight path graph computation complexity, and of the performance of the corresponding set of vertical flight paths. This limitation also facilitates the exploratory investigation of flight path optimization algorithms employing a vertical flight path look-up structure and a vertical flight path graph,

which is the object of a subsequent research and will be the subject of a distinct publication. The construction and performance of a vertical flight path look-up structure and vertical flight path graph encompassing multiple temperature deviation and speed schedule values may also be the subject of future research.

Another limitation is the fact that the range of step-climb and descent flight path segments available for the construction of a vertical flight plan are limited to those stored in the vertical flight path look-up structure. However, practical navigation constraints relative to the execution of consecutive step-climb maneuverings presently restrict the actual number of step-climbs that can be employed during a flight. This limitation could therefore be diminished by a careful selection of the set of set-climb flight paths stored in the look-up structure.

The results of the investigation showed that the total number of distinct vertical flight paths that can be constructed using the set of vertical flight path segments stored in the look-up structure can be extremely large – up to more than 115.9 million (Table 4.4). It must be noted, however, that some of these flight paths may not be usable on real flights due to practical limitations, such as the minimum flight time between two consecutive climb steps. The investigation also showed that this number is dependent on the topology of the vertical flight path graph, as the parameters determining it are (ordered according with their weight) – the number of climb-in cruise flight paths, the number of cruise altitudes and the number of descent flight paths.

The results indicate that for a given aircraft Take-Off (T/O) and flight plan configuration parameters, the number of step-climb flight paths is influenced by the minimal value in the set of the EOD gross weight values, given that it determines the minimal values of the TOD gross weight at each cruise altitude. They also show that the maximum flight time and still-air flight distance were attained on vertical flight plans employing a number of step-climbs leading to the maximum cruise altitude, and on the descent flight paths leading to the minimum EOD gross weight value (maximum fuel burn). The minimum flight time and still-

air flight distance were attained on vertical flight plans employing a single cruise altitude and a descent flight path leading to the maximum EOD gross weight value (minimum fuel burn).

The results of the statistical analysis performed on each set of vertical flight paths, constructed using the vertical flight path look-up structures, have shown the influence of the number and range of the EOD gross weight values, as well as the influence of the range of cruise altitudes on the number of flight paths and the flight time/still-air distance distribution function of their EOD gross weight value. The results showed that the flight time/still-air distance domains of two sets of flight paths, corresponding to two EOD gross weight values, may intersect – the corresponding common range of flight times/still-air distances and the number of flight paths corresponding to each EOD gross weight value depending on the particular flight plan configuration parameters. The results indicated that for a given flight plan configuration, the flight time/still-air distance domain corresponding to an EOD gross weight value increases when the maximum cruise altitude increases and/or the EOD gross weight value decreases. For the set of configurations considered in this paper, the domains corresponding to an EOD gross weight described flight time ranges of between approximately 0.3 and 0.7 hours, and still-air flight distances between 150 and 250 Nm. A more advanced analysis may allow the identification of the relationship between the flight configuration parameters, EOD gross weight, and the corresponding domain's range of flight times and still-air distances, which in turn may allow the determination of the optimal number and set of EOD gross weight values as a function of the desired range of flight times and still-air distances.

The processing times required for generating the look-up structure and the vertical flight path graph are large compared to the times associated with the construction of a single vertical flight plan. However, the time required for retrieving the data from the look-up structure is much smaller than the actual calculation using the aircraft performance model and interpolation algorithms. In the context of multiple, repetitive flight plan computations, this time difference may result in significant processing time reductions. Moreover, a judiciously

chosen set of flight paths and advanced generation strategies may further contribute to reducing the general computing times.

The availability of the vertical flight path data (look-up structure and graph) opens the way for the investigation of flight plan optimization strategies and algorithms based on the vertical flight path graph exploration, namely the investigation and selection of the vertical flight plans that are best-suited to achieve the flight time, fuel burn, or total cost objective as a function of the aircraft and flight plan configuration parameters. It also allows for the analysis of the influence of the lateral position of the start and destination points, and of the wind conditions in the selection of the optimal still-air vertical flight path profile.

CHAPTER 5

ARTICLE 3: OPTIMAL VERTICAL FLIGHT PLAN CONSTRUCTION AS FUNCTION OF FLIGHT PHASE AND ALTITUDE

Bogdan Dumitru Dancila, Benoit Beulze, and Ruxandra Mihaela Botez.
École de Technologie Supérieure, Montréal, Canada
Laboratory of Research in Active Controls, Aeroservoelasticity and Avionics
This article was submitted to The Aeronautical Journal
November 29th, 2016

Résumé

Cet article présente une méthode, développée au LARCASE, utilisée pour la construction géométrique d'un plan vertical de vol optimisé, associé à un plan de vol horizontal désigné. Un plan de vol horizontal est défini comme une succession de points de cheminement où chaque point de cheminement est caractérisé par sa distance «along-the-track» relative au première point de cheminement, ainsi que par sa contrainte d'altitude. L'objectif principal de l'optimisation est la minimisation du nombre total de segments du plan de vol vertical, desquels les valeurs de gradients (ou pentes) sont égales ou le plus proche possibles des valeurs consignées pour les phases de vol et les altitudes correspondantes. L'avantage principal de la méthode proposée est le fait qu'elle permet la construction du plan de vol vertical optimisé sans faire appel aux calculs intensifs en temps et ressources, comme c'est le cas avec les calculs utilisant le modèle de performance des avions. Aussi, l'algorithme proposé a l'avantage de générer des plans de vol verticaux fixés par rapport au sol, donc, contrairement aux algorithmes utilisant le modèle de performance, les plans latéraux et verticaux restent inchangés sous l'effet des variations des conditions de vent. Cette caractéristique donne un avantage important pour les vols dans des espaces aériens congestionnés où un niveau élevé de prédictibilité des trajectoires est désirable. De plus, l'algorithme proposé est capable de respecter les contraintes opérationnelles diverses imposées sur les points de cheminement du plan de vol, comme les limitations d'altitude et de gradients. Deux implémentations correspondant à deux compromis relatifs aux contraintes

de valeurs du gradient préférable et de la longueur minimale du segment ont été comparées. Ces algorithmes sont prédictibles et minimisent le nombre de calculs en effectuant des optimisations du plan de vol vertical seulement sur des sous-domaines sur lesquels de tels calculs sont nécessaires. Les résultats montrent que les paramètres d'un segment sont dépendants de l'ensemble de paramètres de la séquence de segments du plan de vol qui le précèdent, à cause de la manière séquentielle dans laquelle on construit le plan de vol vertical. Aussi, les résultats montrent que pour une majorité de cas de test; les plans de vol calculés utilisant les deux implémentations ont été identiques. De plus, même quand les plans de vol n'ont pas été entièrement identiques, beaucoup de leurs segments correspondants étaient identiques.

Abstract

This paper presents a method for the geometrical construction of an optimal vertical flight plan associated to a provided lateral flight plan, developed at LARCASE. A lateral flight plan is defined as a succession of waypoints, each waypoint characterized by its Along-the-Track Distance relative to the first waypoint, and its altitude constraints. The principal objective of the optimization is the minimization of the total number of vertical flight plan segments, whose gradient (or slope) values are equal or closest to the values set for their corresponding flight phase and altitude. The main advantage of the proposed method is that it allows the construction of the optimized vertical flight plan without employing time - and resource-intensive computations, as it is the case when using aircraft performance models. Also, the proposed algorithm has the advantage of generating ground-fixed vertical flight plan, thus, unlike the model-based algorithms, the lateral and vertical flight plans remain unchanged under varying wind conditions. This feature provides an important advantage when flying into congested airspaces where improved trajectory predictability is desired. Additionally, the proposed algorithm is capable of observing various operational constraints imposed on the flight plan waypoints, such as altitude limitations and gradients. Two implementations corresponding to different trade-offs between conflicting preferred gradient and minimal segment length constraints were compared. These algorithms are predictable and minimize

the number of computations by performing vertical flight plan optimizations only on the sub-domains on which such computations are necessary. The results show that a segment's parameters are dependent on the set of parameters of the sequence of flight plan segments that precede it, due to the sequential manner in which the vertical flight plan is constructed. In addition, the results show that for a majority of the test cases, the resulting flight plans computed using the two implementations were identical. Moreover, even when the flight plans were not completely identical, many of the corresponding segments were identical

5.1 Introduction

As one of the contributors to the generation of atmospheric gas pollutants, the aviation industry is actively seeking to find new ways to reduce its environmental footprint. These efforts are driven by the introduction of ever stricter environmental regulations, and by the pursuit of improved economic performance. Aircraft manufacturers are developing technologies and manufacturing procedures leading to lighter aircraft, better aerodynamics, improved engine efficiency, and advanced avionics which lead to improved aircraft performance (Asselin, 1997).

The airline companies, are operating fleets composed of different generations of aircraft, thus, the most economically feasible approach relies on the employment of operational procedures and methods that minimize costs, fuel burn and gas emissions. One of the methods that have had a major effect on all three performance targets is the determination and use of optimal flight trajectories (Liden, 1985; Liden, 1992b; Rivas et al., 2012; Warren, 2000; Suzuki et al., 2009). These trajectories are determined as functions of the wind, air temperature and storm conditions (Souders et al., 2007; de Grado & Tascon, 2011; Dunn, 2008; WMO, 2003) in the geographic area in which the flight is performed, and of the aircraft's capabilities (Liden, 1985; Liden, 1992b; Dancila et al., 2013; Gerretsen & Swierstra, 2003; Nuic et al., 2005). The optimal trajectories must also observe the set of rules and standards imposed by the aircraft navigation regulations (Souders et al., 2007; RTCA

Inc., 2002; ICAO, 2013; Prevot, 2009; Erzberger & Paielli, 2002; Haraldsdottir et al., 2006) in effect at the time of a flight.

A flight plan describes an aircraft's planned, or desired flight trajectory and characterizes the succession of an aircraft's state parameters (speed, gross weight, fuel burn, heading etc.) and positions in space (geographical coordinates and altitude) from its actual location to its destination. The algorithms computing the flight plan's parameters can be executed in a ground-based environment or in an aircraft on-board-based environment. Ground-based algorithms can be deterministic or non-deterministic. They rely on high-performance computing systems and generally use aircraft flight dynamics equations. They can be used by airline companies for planning purposes, and by the ATM for conflict and traffic flow management (Prevot, 2009; Erzberger & Paielli, 2002; Granger et al., 2001; Tomlin, Pappas & Sastry, 1998; Palopo et al, 2010; Krozel et al., 2007; Jackson et al., 2009; Tomlin, Pappas, Košecká et al., 1998; Swierstra & Green, 2003; Mondoloni et al., 2002; Cano et al., 2007).

On-board flight plan computation algorithms, on the other hand, are deterministic, and thus predictable (Liden, 1985; Durrieu et al., 2014) – similarly to all avionics algorithms. They are executed on a specialized platform, the FMS, whose computing resources are limited (Liden, 1985; Durrieu et al., 2014) relative to ground-based platforms, concurrently with other processes that implement various functionalities including aircraft navigation and guidance. Moreover, all processes running on the FMS are constrained by strict execution times. As a consequence, FMS algorithms that require aircraft performance parameters' computation, including flight plan calculations, minimize the system workload by utilizing a linear interpolation-based aircraft performance models (Liden, 1985; Liden, 1992b; Dancila et al., 2013; Dancila et al., 2012). The FMS uses the computed flight plan parameters for guidance purposes. Therefore, the flight plan parameters are decomposed into two sets of data. The lateral plan is used for lateral guidance (geographical routing), and the vertical plan is used for vertical guidance.

Flight optimization algorithms compute flight plans that achieve a particular purpose, which may include the minimization of the total flight time, cost, environmental footprint, or noise pollution (Liden, 1985; Liden, 1992b; Suzuki et al., 2009). The optimization objective can be achieved by controlling one or a combination of parameters, such as altitude, speed, or geographical waypoint location, and may be implemented using a large variety of optimization algorithms (Liden, 1992b; Granger et al., 2001; Tomlin, Pappas & Sastry, 1998; Palopo et al, 2010; Dancila et al., 2012; Félix Patrón, Kessaci et al., 2013; Murrieta Mendoza & Botez, 2014a; Sidibé & Botez, 2013; Félix Patrón, Oyono Owono et al., 2013; Rodionova et al., 2014; Nilim et al., 2002; Lovegren, & Hansman, 2011; Jensen et al., 2014; Liden, 1992a; Knapp et al., 2008; Ardema & Asuncion, 2009; Brundile et al., 2013; Félix Patrón, Botez & Labour, 2012; Jensen et al., 2013; Visintini, Glover, Lygeros & Maciejowski, 2006; Miyazawa, Wickramasinghe, Harada & Miyamoto, 2013; Wirth, Oettershagen, Ambühl & Siegwart, 2015; Sorensen, Morello & Erzberger, 1979; Sorensen & Waters, 1981; Erzberger, McLean & Barman, 1975; Erzberger & Lee, 1978; Sorensen, 1979; Erzberger & McLean, 1981; Schreur, 1995; Bonami et al., 2013; Tong et al., 2007).

Many of the optimization algorithms presented in the literature were developed using the aircraft point mass dynamic model characterized by a series of non-linear differential equations. These equations are generally solved using calculus of variations, and iterative algorithms such as dynamic programming which can be time and computing-resource intensive, and may require a particular level of experience (Sorensen, Morello & Erzberger, 1979; Sorensen & Waters, 1981). One approach aiming to simplify the trajectory computation is based on the energy-state method (Erzberger et al., 1975; Erzberger & Lee, 1978; Sorensen, 1979). The algorithm implementing the energy-state method presented in Sorensen (1979) considers a vertical trajectory composed of three segments (climb, cruise, and descent) constructed only function of the aircraft's performance model (its corresponding dynamic equations), and the boundary conditions (the initial state and the final adjoint variables). The construction itself of the vertical flight plan is performed in a sequence of seven steps, each step entailing complex, iterative calculations (Sorensen, 1979). This approach is complex relative to the FMS computing power.

Some optimization methods described in the literature make use of simplified dynamic models, and fast-time integration algorithms as the ones presented in Erzberger & McLean (1981) and Schreur (1995), or are using Ordinary Differential Equation systems constructed from aircraft drag polar and engine performance model (Rivas et al., 2012), that are solved using traditional numerical methods, such as the Runge–Kutta method. Other examples of vertical flight plan optimization algorithms presented in the literature use Multiphase Mixed-Integer Optimal Control techniques (Bonami et al., 2013), where the discrete variables control the steering decisions, and the continuous variables are modeled using differential equations to characterize the aircraft state.

Optimization algorithms that employ linear-interpolation table-based performance models may use various search algorithms such as the golden section (Félix Patrón et al., 2012), or genetic algorithms (Félix Patrón, Oyono Owono et al., 2013).

In addition to the complexity of the methods based on the aircraft performance model, the research presented in Tong et al. (2007) showed that the trajectories computed using such methods are sensitive to wind variations, thus, may lead to important differences between the predicted ground-referenced flight plan and the actual aircraft flight trajectory. These differences may affect the traffic flow in congested airspaces, as well as in terminal and airport areas. The research (Tong et al., 2007) also showed that geometrically-constructed descent trajectories, using carefully-selected gradient values were capable of achieving flight time, fuel burn, or total cost performances that were close to the performances of idle descent trajectories.

One of the limitations of the existing FMS algorithms is that the functions used to compute the total cost (Liden, 1985; Liden, 1992b) are limited to considering only the fuel burn and flight time. However, other costs such as the maintenance costs caused by engine wear due to thrust changes may have a significant contribution to the total flight costs. These costs may prove significant, especially on flight trajectories with repetitive changes in air speed and or flight path angle. Moreover, as a function of an aircraft's performance, for each configuration

there are particular thrust settings and flight path angles which yield minimal engine wear and/or fuel burn.

The method presented here is part of the authors' efforts to address this limitation by researching new methods capable of geometrically constructing an optimal vertical flight plan (Beulze et al., 2015; Dancila, Beulze& Botez, 2016) minimizing the number of vertical plan' segments, and thus the number of flight path angles (gradients), thereby reducing the computation workload by eliminating the need for aircraft performance model-based calculations. Also, while the vertical flight plan constructed by the proposed algorithm may be sub-optimal (from the point of view of flight time, fuel burn or cost) relative to a vertical flight plan constructed using the aircraft performance model (as noted in Tong et al. (2007)), it has the advantage of being ground-fixed; thus, the lateral and vertical flight plans computed by this ground-fixed algorithm remain unchanged under varying wind conditions, unlike the model-based algorithms. This feature may prove important for flying into congested airspaces where improved trajectory predictability is desired. Moreover, the proposed algorithm was capable of observing various operational, altitude and gradient constraints imposed on the flight plan waypoints.

5.2 The Optimization Methodology

The method presented in this paper performs the geometrical construction of an optimal vertical flight plan associated to a provided lateral flight plan defined as a succession of waypoints. Each waypoint is characterized by a set of five parameters: the along-the-track distance relative to the first waypoint of the lateral flight plan (*atd*), first and second altitude values (*alt1* and *alt2*, respectively) which characterize the range of altitudes associated with the waypoint, the waypoint constraint type (*constraint*) defining the waypoint configuration, and the gradient value (*gradient*) defining the imposed gradient (also known as the flight path angle) value for the segment reaching the corresponding waypoint. The interpretation of the *alt1* and *alt2* parameters are dependent on the waypoint's constraint type as follows: "*None*" – no altitude or gradient limitations, and thus, the *alt1*, *alt2*,and *gradient* values are

disregarded; "*At*" – the aircraft's altitude at the corresponding waypoint must be equal to that described by *alt1*, and can employ any flight path angle; "*AtOrBelow*" - the aircraft's altitude at the corresponding waypoint must be equal to or lower than that described by *alt1*, and can employ any flight path angle; "*AtOrAbove*" - the aircraft's altitude at the corresponding waypoint must be equal to or above that described by *alt1*, and can employ any flight path angle; "*Window*" - the aircraft's altitude at the corresponding waypoint must be between *alt1* and *alt2*, and can employ any flight path angle; and "*Gradient*" - the aircraft's altitude at the corresponding waypoint must be equal to that described by *alt1*, and must arrive on a flight path angle equal to the value described by the corresponding *gradient* parameter.

The principal objective of the optimization is represented by the minimization of the total number of vertical flight plan segments, whose gradient values are equal to or closest to the preferred values set for their corresponding flight phase and altitude. The second objective is the ability to construct optimal flight plans without having to perform the time and resource-intensive computations associated with aircraft performance models – a goal made possible by the employment of the preferred gradients.

A set of flight phase and altitude-dependent preferred gradient values are provided as two distinct input tables, one for climb and another for descent. These tables are constructed as a function of an aircraft's climb and descent performances, and may take into account the wind conditions along the selected lateral flight plan segments. For each phase, the corresponding table describes the list of altitudes and the associated preferred gradient values. A preferred gradient value is to be employed on altitudes situated at or below the corresponding altitude value. Therefore, a preferred gradient value is used on an altitude domain delimited by the corresponding altitude and that defined by the table's preceding altitude limit.

Additionally, the proposed method observes a set of constraints. Firstly, the vertical flight plan segments must reside inside the *altitude-atd* domain determined by the altitude limitations defined by the set of waypoints. This domain is delimited by two boundaries; the upper boundary constructed by connecting the superior altitude limitations of each pair of

successive waypoints, and the lower boundary constructed by connecting the inferior altitude limitations of each pair of successive waypoints. Secondly, the absolute value of any segment's gradient should be smaller than a predefined value, provided as input. Thirdly, a horizontal segment must be inserted between consecutive climb and descent, or descent and climb segments. Fourthly, the length of the inserted horizontal segments, as well as of the segments corresponding to the "*Gradient*" waypoints, must be equal to or higher than a predefined value (*MIN_DIST*), provided as input. Fifthly, whenever possible, a direct segment is constructed between initial and final waypoints or between two consecutive "*At*" waypoints. Finally, the vertical flight plan is constructed even when one or more constraints cannot be satisfied, and a corresponding warning is issued.

5.2.1 Pre-processing

The method presented in this paper aims to reduce the volume of computations required for the construction of the optimized flight plan. As presented in the preceding paragraph, the construction employs a pure geometrical approach as a function of the waypoints' *atd*, *altitude* and gradient *limitations*. It relies on classic plane geometry equations, namely on equations characterizing lines and the points of intersection of these lines. More precisely, the method uses the equations describing a segment' slope γ and angle α as a function of the positions (*atd*) d_1 and d_2, and altitudes h_1 and h_2 of two points situated on the segment:

$$\gamma = \frac{h_2 - h_1}{d_2 - d_1} \tag{5.1}$$

$$\alpha = \arctan\left(\frac{h_2 - h_1}{d_2 - d_1}\right) \tag{5.2}$$

and describing a point's altitude h as a function of its position (*atd*) d relative to another point on the same segment:

$$h = h_1 + \frac{h_2 - h_1}{d_2 - d_1} * (d - d_1) \tag{5.3}$$

$$h = h_1 + \gamma * (d - d_1) \tag{5.4}$$

and using the coordinates of a point X (d_x, h_x) representing the intersection of two lines, each characterized by an altitude, atd, and a slope ($h_1, d_1, \gamma_1, h_2, d_2, \gamma_2$):

$$d_X = \frac{h_1 - h_2 - \gamma_1 * d_1 + \gamma_2 * d_2}{\gamma_2 - \gamma_1} \tag{5.5}$$

$$h_X = h_1 + \frac{\gamma_1}{\gamma_2 - \gamma_1} * (h_1 - h_2 + \gamma_2 * (d_2 - d_1)) \tag{5.6}$$

The set of equations (5.1) - (5.6) are used for determining the boundaries delimiting the allowed vertical flight plans' domain, and in the construction of its corresponding segments. They require the knowledge of the precise *atd*, *altitude* and/or *gradient* values of all the waypoints associated with the segment being computed.

The provided lateral flight plan, however, presents a number of limitations. It can be observed that the values and the interpretation of the *alt1* and *alt2* parameters are dependent on the waypoints' types. Moreover, for the majority of waypoint types, at least one of the altitude limitation values is not explicitly defined. In addition, for the "*Gradient*" type waypoints, the positions (*atd*) and the altitudes of the points defining the start of the associated imposed-gradient segments are also not explicitly defined. This means that for the construction of each segment, an optimization algorithm must first determine the set of waypoints that may reside inside the *atd* domain corresponding to the segment being constructed, and then compute the explicit waypoints' altitude limitations and gradient segments' potential start positions. Generally, a segment may cover a smaller number of

waypoints than were evaluated for its construction. Therefore, an algorithm may be required to compute the *altitude* and/or *atd* values corresponding to the same waypoint multiple times, leading to computational inefficiencies. Moreover, the construction of a segment is dependent on the corresponding flight phase (climb, descent, or level flight), which cannot be easily determined algorithmically using the information provided in the input flight plan. Consequently, an optimization algorithm based on the input flight plan can be complex and computationally inefficient.

The proposed method addresses these drawbacks by employing a two-step pre-processing of the input plan, prior to the actual vertical flight plan optimization. The first pre-processing stage transforms the input flight plan into a new "pre-processed" flight plan which is characterized using the same number and type of parameters, the differences consisting of: the *alt1* and *alt2* parameters have well-defined values (*alt1* – minimal overflying altitude and *alt2* – maximal overflying altitude), and the points defining the start of the fixed gradient segments imposed by the "*Gradient*" type waypoints are explicitly inserted in the list of waypoints composing the flight plan (and characterized by the same number of waypoint parameters).

For the "*At*" and "*Gradient*" type waypoints, *alt2* is assigned the value of the corresponding *alt1* parameter. For the "*None*", "*AtOrBelow*", or "*AtOrAbove*" waypoints the *alt1* and/or *alt2* values are set to the minimal and/or maximal altitude values, respectively, in the set defined by the input lateral flight plan.

The start point of a "*Gradient*" segment is inserted into the pre-processed flight plan only if the segment resides within the flight envelope delimited by the waypoints' altitude limitations, otherwise the "*Gradient*" waypoint effectively transforms into a "regular" "*At*" waypoint, as illustrated in Figure 5.1 and Figure 5.2. The starting point's *atd* value is computed by subtracting the minimal segment length value, provided as an input parameter, from the *atd* value of the corresponding "*Gradient*" waypoint. Next, the staring point's altitude is computed using equation (5.4). Subsequently, the set of waypoints delimiting the

gradient segment are identified, and for each successive pair of waypoints, equations (5.5) and (5.6) are used to determine whether the flight envelope was breached or not and, consequently, whether the start point is to be inserted in the pre-processed flight plan or not. If it is inserted, all the waypoints situated between the start of a gradient segment and its corresponding "*Gradient*" waypoint are effectively converted into "*At*" type waypoints, and their corresponding *alt1* and *alt2* values set to the altitude of the gradient segment at their corresponding position (*atd*).

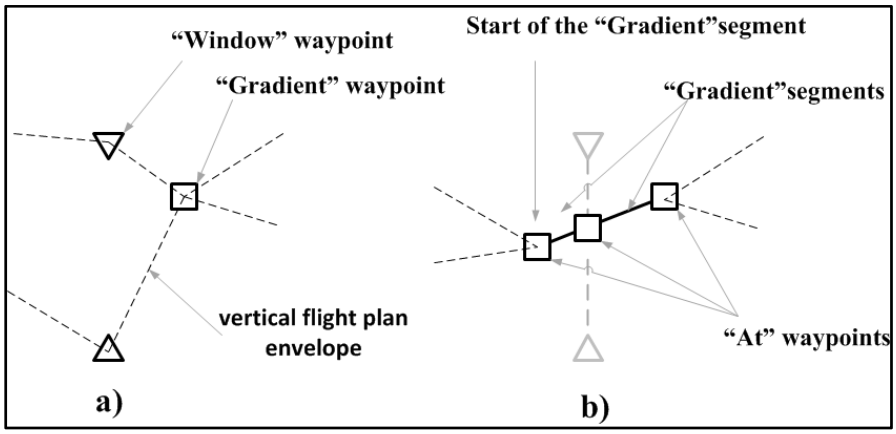

Figure 5.1 Example of successful "*Gradient*" waypoint insertion:
a) original flight plan, b) pre-processed flight plan

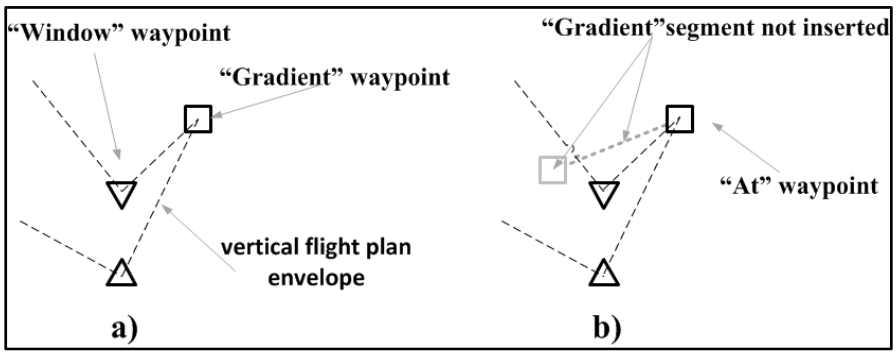

Figure 5.2 Example of failed "*Gradient*" waypoint insertion:
a) original flight plan, b) pre-processed flight plan

As mentioned above, the construction of a segment depends on the corresponding flight phase. Consequently, the second pre-processing step is used to parse the pre-processed flight

plan into a succession of domains corresponding to climb, descent or horizontal flight, and to determine the corresponding waypoints delimiting the start and end of each such domain.

A level flight (or horizontal) domain is composed of a set of successive waypoints delimited by two "*At*" waypoints determining a segment whose altitude value is constant from its first to its last waypoint.

A climb domain is composed of a set of waypoints determining a succession of segments whose gradients, or slopes are positive or zero. It starts at waypoints, situated at the end of a descent or horizontal domain, for which the *alt2* value is smaller than the *alt1* value of the succeeding waypoint, thus determining a positive gradient/slope value, and ends at the start of the succeeding descent or level flight domain.

A descent domain is composed of a set of waypoints determining a succession of segments whose gradients, or slopes are negative or zero. It starts at waypoints, situated at the end of a climb or horizontal domain, for which the value of the *alt1* is larger than the value of the succeeding waypoint's *alt2* value, thus determining a negative gradient/slope value, and ends at the start of the succeeding climb or level flight domain.

The domains' parsing is performed iteratively, with one pair of successive waypoints at a time, by comparing the relationship between the *alt1* and *alt2* constraints of each of the two waypoints. If the evaluation is conclusive, the section is assigned a corresponding climb, descent or horizontal phase. However, if the evaluation is inconclusive (for instance, in the case when one of the waypoints is type "*None*") the decision is delayed, and the evaluation is successively advanced to the next pair of waypoints, until reaching a pair of waypoints for which a conclusion can be drawn. Subsequently, the entire set of corresponding sections is assigned the same phase, determined at the end of the evaluation sequence. Once the entire set of pre-processed flight plan waypoints has been evaluated, each set of successive sections belonging to the same phase are grouped together into corresponding climb, descent or horizontal domains. The information regarding the set of vertical flight plan domains is then

assembled as a data structure listing the sequence of the domains, their type, and their corresponding initial and final waypoints and *atd* values. An example of a pre-processed flight plan and its decomposition into a corresponding set of domains is presented in Figure 5.3 below.

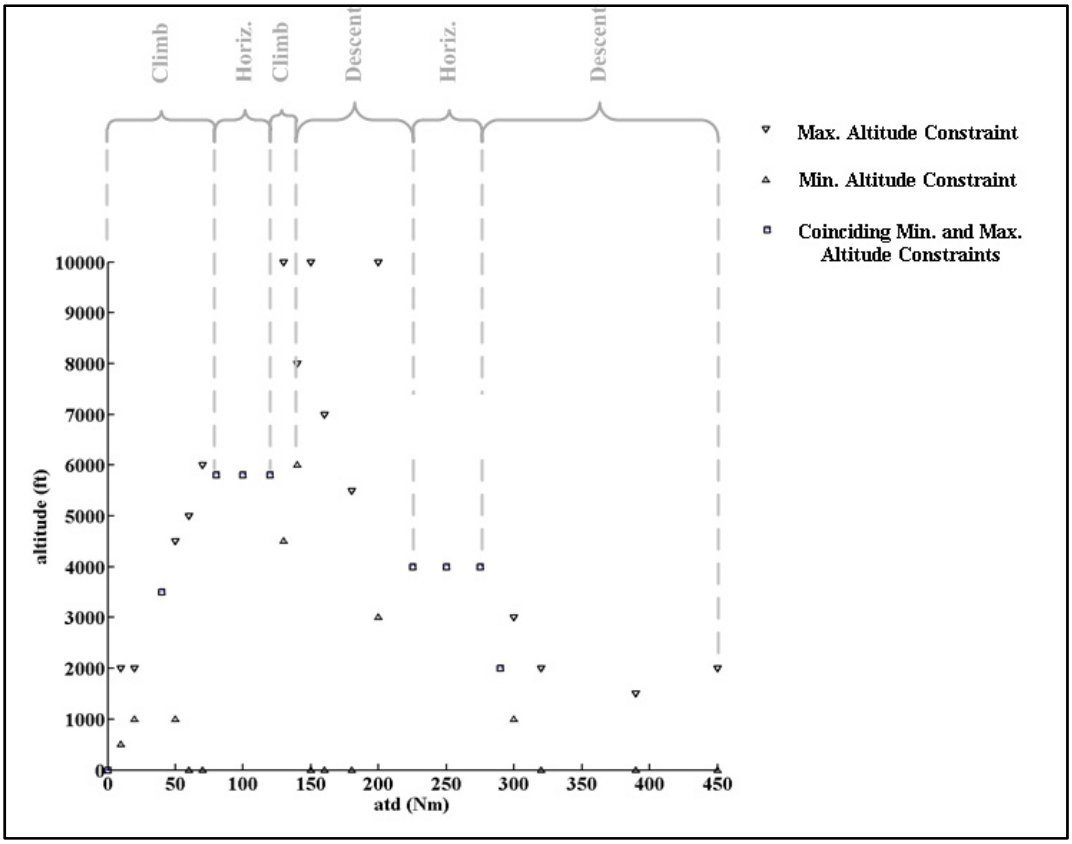

Figure 5.3 Example of a pre-processed flight plan and the corresponding domains parsing

5.2.2 Vertical Flight Plan Optimization

The optimization method presented here computes the optimized vertical flight plan using the pre-processed flight plan and the domains' parsing data. This approach presents a number of advantages, as follows: Firstly, the availability of well-defined waypoint parameter values leads to a reduction of the volume and complexity of computations required for constructing the optimized vertical flight plan segments. Secondly, the construction of the "*Gradient*"

waypoints' segments in the pre-processing phase decouples the gradient segments' insertion policies from the actual flight plan optimization. Therefore, the optimization strategy and the algorithm's implementation are rendered immune to any change of the "*Gradient*" waypoint policies. Thirdly, the information regarding the succession, and the limits of the climb, horizontal, and descent domains composing the flight plan allows the adoption of flight plan construction strategies that are best-adapted to each domain configuration (climb, descent, or horizontal), which in turns allows for more efficient algorithms.

The construction of the optimized flight plan is performed sequentially, one domain at a time, from the flight plan's first waypoint to the last. As mentioned in paragraph 5.2, if the vertical flight plan is composed of one domain and a direct segment between the first and last waypoints can be constructed, then the optimized trajectory is constructed as the direct segment connecting the first waypoint to the last. Similarly, as a result of the way they are defined, all of the horizontal domain's segments are constructed as single, direct segments connecting the corresponding domain's first and last waypoints. Figure 5.4 illustrates the flow of the general processing used for the construction of an optimized flight plan.

The vertical flight plan corresponding to a climb or a descent domain is constructed as a single segment, or as a series of segments, depending on the particular configuration of that domain. The factors that determine the domain segments' configuration are: the particular configuration of the set of waypoints composing the domain (relative *atd* positions, constraint types, and altitude restrictions), the preferred gradient values and altitude limitations for the flight phase corresponding to the domain being constructed (climb or descent), and the particular type of the domains preceding and following it.

Firstly, the presence of a preceding non-horizontal domain indicates that a horizontal segment may be required at the start of the domain. The need for the actual insertion of a horizontal segment at the start of the domain, and its minimal length, is determined as a function of the type and length of the preceding domain's last segment. If the type of the segment preceding the domain is horizontal and its length is larger than the required value, then this insertion is not required. Otherwise, the insertion of a horizontal segment is

required, with its minimal length determined accordingly. Secondly, the presence of a succeeding non-horizontal domain indicates the necessity to insert a horizontal segment at the end of the domain. Thirdly, as required by the method's limitations, pairs of successive "*At*" type waypoints (whether separated by other waypoints or not) for which a direct segment can be routed without violating the vertical flight envelope are constructed as direct segments. Fourthly, the limitation of the altitude domains on which the preferred gradient values can be employed imposes restrictions in the construction of a domain's segments.

Consequently, the domain's segments must be built sequentially, one gradient altitude domain at a time. Finally, for each segment, the particular sequence of waypoints situated after its start point (whose *atd*s are larger than the segment's start *atd* value) determine the actual range of gradient values that can be used in the construction of the segment (including the possibility of using the optimal gradient for that altitude range), and by consequence the segment's length, along with its end point's *atd* and *altitude* values. Moreover, the waypoints' altitude restrictions also determine the domain's final altitude, the set of altitudes at which a segment's gradient value can be changed, and where a horizontal segment can be inserted, and therefore, the succession of the domain's segments and their corresponding parameters.

For a "*climb*" domain the final altitude is equal to the domain's last waypoint's *alt1* value, and its horizontal segments can be constructed only at the final altitude or at a set of "*target altitudes*" composed of the *alt2* values of the domain's waypoints. The changes of gradients/slopes are allowed only at the altitudes described in the preferred climb gradient table and at the "*target altitudes*".

For a "*descent*" domain the final altitude is equal to the domain's last waypoint's *alt2* value, and its horizontal segments can be constructed only at the final altitude or at a set of "*target altitudes*" composed of the *alt1* values of the domain's waypoints. The changes of gradients/slopes are allowed only at the altitudes described in the preferred descent gradient table and at the "*target altitudes*".

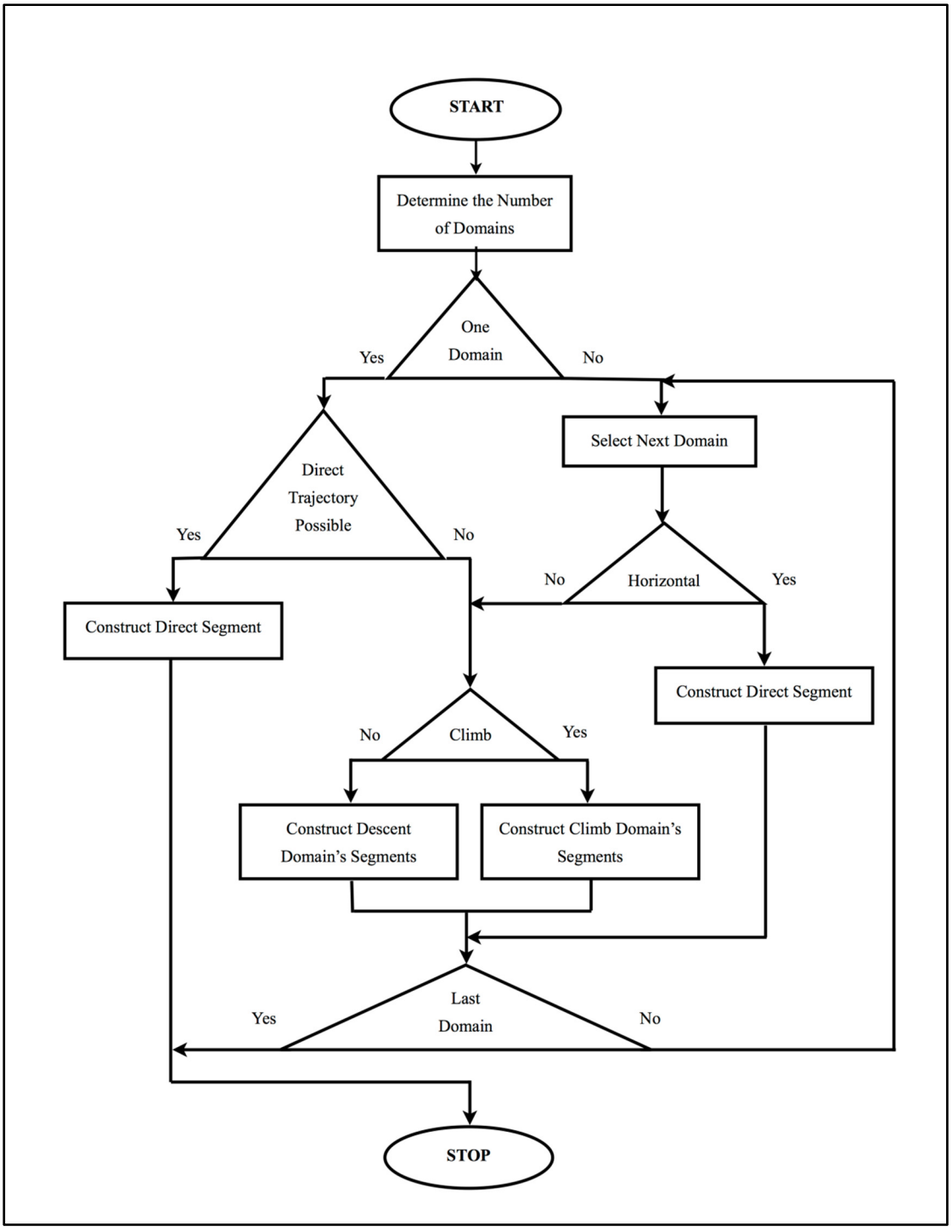

Figure 5.4 Optimal flight plan computation flowchart

Consequently, a climb or descent domain is decomposed into a set of sub-domains delimited by the presence of "*At*" type waypoints, and its segments constructed sequentially, one sub-

domain at a time. The sub-domains delimited by two "*At*" waypoints for which a direct segment can be constructed are built as direct segments. All the other sub-domains are constructed as a function of the preferred gradient and of the waypoints' configuration. Therefore, these domains are further decomposed into altitude regions following the range of altitudes described in the corresponding preferred gradient table.

On each altitude region of a sub-domain, the proposed method aims to construct, if possible, the corresponding vertical flight plan as a single segment, using a slope corresponding to a gradient value equal to or as close as possible to the preferred gradient. To this end, the range of usable slope values is determined by computing the minimal and maximal slope values that a segment can employ to reach the final altitude (h_{final}) of the altitude domain. The maximal usable slope value is computed as the minimal value of the slopes calculated for the current segment's start point *atd* and *altitude* values ($d_{current}, h_{current}$), and each of the altitude region's waypoints' *alt2* and *atd* values ($wpt_i(alt2), wpt_i(atd)$). For each waypoint situated between the current position and the end position of the altitude range domain, the equations used to compute the maximal slope ($\gamma_{wpt_i\_\max}$) are:

$$\gamma_{wpt_i\_\max} = \frac{wpt_i(alt2) - h_{current}}{wpt_i(atd) - d_{current}} \tag{5.7}$$

$$\gamma_{wpt_i\_\max} = \frac{h_{final} - h_{current}}{d_{min\_valid}(h_{final}) - d_{current}} \tag{5.8}$$

If the waypoint's *alt2* value is lower than the altitude range domain's limit then equation (5.7) is used, while equation (5.8) is used if the *alt2* value is equal to or higher. The $d_{min\_valid}(h_{final})$ represents the minimal *atd* value that can be used by any segment at the final altitude (h_{final}), and is determined by the vertical flight plan's envelope.

Similarly, the minimal usable slope value is computed as the maximal value of the slopes calculated for the current segment's starting point *atd* and *altitude* values ($d_{current}, h_{current}$). The equations used to compute the minimal slope for each waypoint situated between the current position and the end of the altitude range domain are:

$$\gamma_{wpt_i\_\min} = \frac{wpt_i(alt1) - h_{current}}{wpt_i(atd) - d_{current}} \quad \text{…and} \tag{5.9}$$

$$\gamma_{wpt_i\_\min} = \frac{h_{final} - h_{current}}{d_{max\_valid}(h_{final}) - d_{current}} \tag{5.10}$$

Equation (5.9) is used if the waypoint's *alt1* value ($wpt_i(alt1)$) is equal to or lower than the altitude range domain's limit (h_{final}), and equation (5.10) is used if the *alt1* value is higher than that limit. $d_{\max\_valid}(h_{final})$ represents the maximal *atd* value that can be used by any segment at the final altitude (h_{final}), and is determined by the vertical flight plan's envelope.

If the range of usable slopes is not void, the slope value closest to the preferred value for that altitude range is selected, a climb or descent segment is constructed and the current flight plan position is updated with the values corresponding to the end of the computed segment. If the range of usable slopes is void (the minimal slope value is larger than the maximal slope value) the final altitude is not reachable from the current point. Subsequently, the segment's final altitude is changed towards the current altitude, to the target altitude closest to the evaluated final altitude, and the process is repeated for the corresponding set of waypoints until a range of valid slope values is found or the evaluated final altitude is equal to the current segment altitude. If that occurs, a horizontal segment is inserted up to the *atd* value of the immediately following waypoint, and the process is repeated starting with the altitude range's final altitude value.

As mentioned above, the first and the last sub-domain of a climb or descent domain may require the insertion of a horizontal segment. Given the sequential manner in which the segments are constructed, the presence of these horizontal segments affects the range of valid slopes that can be used in conjunction with the segments following or preceding them, and thus, the entire set of segments composing the domain. Therefore, the initial and/or final horizontal segments may prevent the use of the preferred gradient values which would have been otherwise available. This suggests that two different strategies addressing possible trade-offs between competing, preferred gradients versus horizontal segment insertion policies can be implemented. The first one would give priority to the preferred gradient, and so either no horizontal segments or shorter horizontal segments may be inserted. The second strategy would give priority to the horizontal segments, and thus the gradient values in the construction of the corresponding vertical flight plan segments may be less than optimal.

Moreover, since the requirement regarding the insertion of a horizontal segment between two consecutive climb/descent or descent/climb segments imposes no limitation regarding how the insertion is performed (first or second domain, the entire segment in one domain, or distributed in each domain), different implementations may adopt different strategies. For instance, one implementation may insert as much as possible in the first domain, and if necessary insert the reminder of the segment in the second domain. A different implementation may choose to insert the horizontal segment in one domain, at the end of the first or the start of the second domain. Each strategy affects the geometry and thus the performance of the corresponding vertical flight plan segments (number of segments and gradient values).

5.3 Results

Two implementations of the method presented in this paper were developed in Matlab, corresponding to two preferred gradient versus climb/descent and descent/climb horizontal segment insertion strategies. The trade-offs adopted for each of the two algorithms, designated as “A” and “B”, are presented in Table 5.1.

Table 5.1 The preferred gradient versus horizontal segment insertion trade-off implemented by algorithms "A" and "B"

Trade-off	**Algorithm implementation**	
	"A"	**"B"**
Conflicting, preferred gradient versus minimal horizontal segment length constraint precedence	Minimal horizontal segment length takes precedence over the preferred gradient	Preferred gradient and earliest climb takes precedence over the minimal horizontal segment length constraint
Horizontal segment insertion	Aims to insert the horizontal segment at the end of the first domain and, if necessary, at the beginning of the second domain	Inserts the horizontal segment, if possible, at the beginning of the second domain.

Subsequently, a comparative analysis of the vertical flight plans generated for 48 test cases aimed to investigate the performance of each algorithm's implementation, and the influences of the corresponding trade-offs on the resulted flight plans. The phase and altitude-dependent preferred gradient values that were used in conjunction with the test cases are presented in Table 5.2.

Table 5.2 The phase and altitude-dependent preferred gradients

CLIMB		**DESCENT**	
altitude **(ft)**	***preferred gradient*** **(deg)**	***altitude*** **(ft)**	***preferred gradient*** **(deg)**
10000	7	15000	-3
15000	4	28000	-3.5
20000	3.5	50000	-4
25000	3		
50000	2.5		

The results showed that for 40 test cases the number of vertical flight plan segments generated by the two algorithms were identical, for seven cases the flight plans presented differences of one segment, and for one test case there was a difference of two segments. For test case 1 illustrated in Figure 5.5 and Figure 5.6, with its flight plan data given in Table 5.3, the differences were attributed to the adopted construction trade-offs.

Table 5.3 The flight plan data (*atd*, *constraint*, *alt1* and *alt2*) corresponding to Figure 5.5 and Figure 5.6

Test case 1				
Wpt	***atd*** **(Nm)**	***constraint***	***alt1*** **(ft)**	***alt2*** **(ft)**
1	0	AT	0	0
2	10	Window	16578	18818
3	20	Window	17312	17382
4	30	Window	19438	19880
5	40	Window	19962	23007
6	50	Window	21670	24243
7	60	ATorBelow	0	40744
8	70	ATorBelow	0	31359
9	80	ATorABOVE	22129	40744
10	90	Window	21664	24745
11	100	AT	18797	18797
12	110	ATorABOVE	18565	40744
13	120	Window	20112	23261
14	130	Window	283	1359
15	140	Window	25	54
16	150	Window	8	8
17	160	Window	3	3

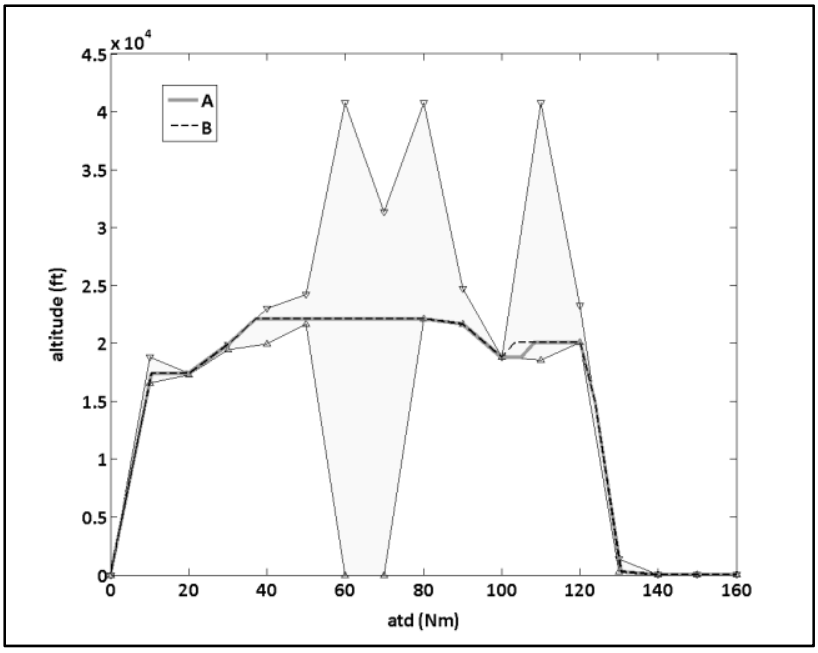

Figure 5.5 Comparative vertical flight plan segment count differences due to algorithms' adopted trade-offs: altitude profiles relative to the flight envelope

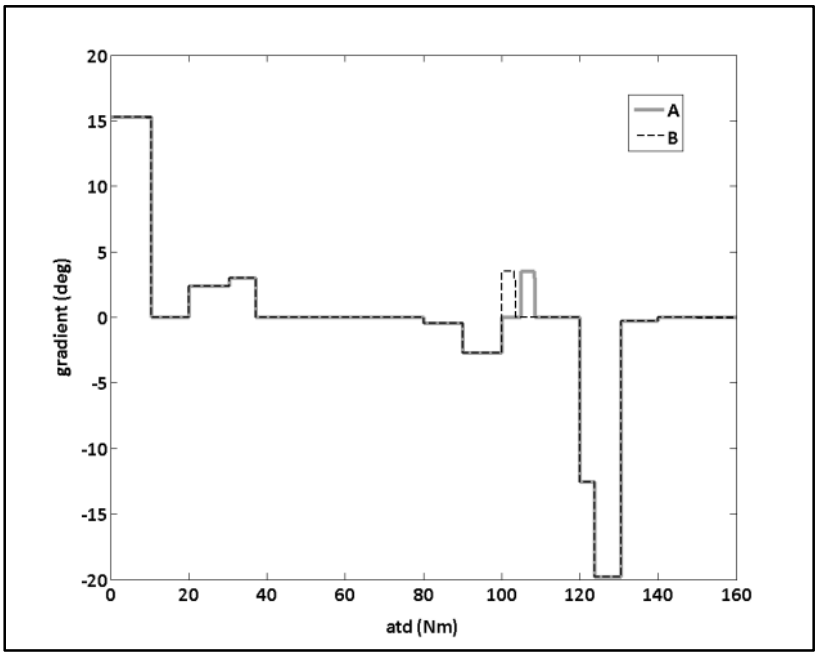

Figure 5.6 Comparative vertical flight plan segment count differences due to algorithms' adopted trade-offs: gradient profiles

This refers to algorithm "B" not inserting a horizontal segment at *atd* 100 due to its prioritizing segment gradient and earliest climb to the insertion of the horizontal segment.

For the other seven test cases that had some differences of one segment, the differences were attributed to algorithm implementation differences relative to the computation and selection of the segments' gradients, as illustrated in the case presented in Table 5.4, Figure 5.7, and Figure 5.8.

Table 5.4 The flight plan data (*atd*, *constraint*, *alt1* and *alt2*) corresponding to Figure 5.7 and Figure 5.8

Test case 2				
Wpt	***atd* (Nm)**	***constraint***	***alt1* (ft)**	***alt2* (ft)**
1	0	AT	0	0
2	10	Window	14485	18376
3	20	Window	17689	17701
4	30	Window	18938	19769
5	40	ATorBelow	0	33105
6	50	Window	21623	24519
7	60	Window	21337	24118
8	70	AT	22486	22486
9	80	Window	18638	19563
10	90	ATorABOVE	22098	33105
11	100	Window	20710	23851
12	110	ATorABOVE	18027	33105
13	120	ATorABOVE	18841	33105
14	130	Window	7588	12771
15	140	Window	3616	6368
16	150	Window	207	2716
17	160	Window	443	789

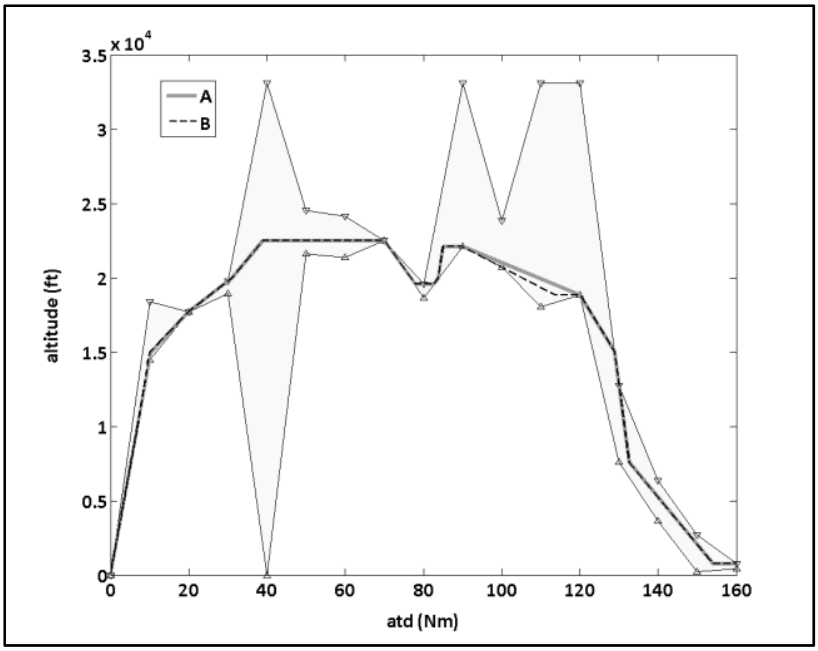

Figure 5.7 Comparative vertical flight plan segment count differences due to algorithms' segment gradient selection: altitude profiles relative to the flight envelope

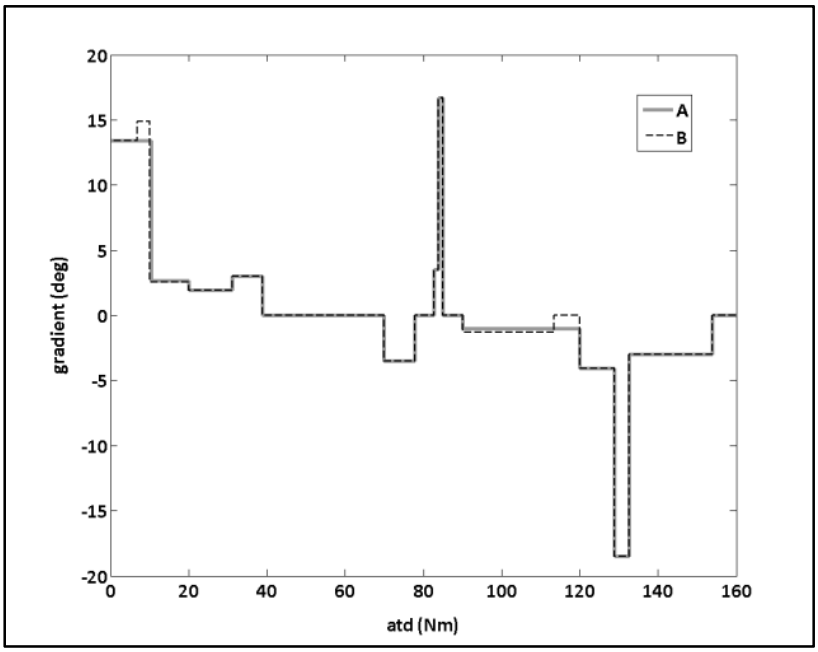

Figure 5.8 Comparative vertical flight plan segment count differences due to algorithms' segment gradient selection: gradient profiles

Of the 40 cases for which the two algorithms generated flight plans with the same number of segments, 27 showed identical segments and 13 had segments that employed different gradients due to algorithm implementation differences relative to the computation and selection of the segments' gradients, as illustrated in Table 5.5, Figure 5.9, and Figure 5.10.

Table 5.5 The flight plan data (*atd*, *constraint*, *alt1* and *alt2*) corresponding to Figure 5.9 and Figure 5.10

Test case 3				
Wpt	***atd* (Nm)**	***constraint***	***alt1* (ft)**	***alt2* (ft)**
1	0	AT	0	0
2	5.14	Window	4000	5000
3	25.14	Window	7500	9000
4	60.14	AT	21000	21000
5	110.14	AT	21000	21000
6	130.14	Window	18000	23000
7	138.14	Window	15000	20000
8	146.08	AT	14000	14000
9	154.53	Window	10000	11000
10	161.42	Window	8000	9000
11	178.32	Window	3000	4000
12	191.02	AT	167	167

Moreover, the analysis showed that even for those flight plans where the two algorithms generated a different number of segments, or segments employing different gradients, many of the segments generated by the two implementations were identical (as illustrated in Figures 5.5 to 5.10).

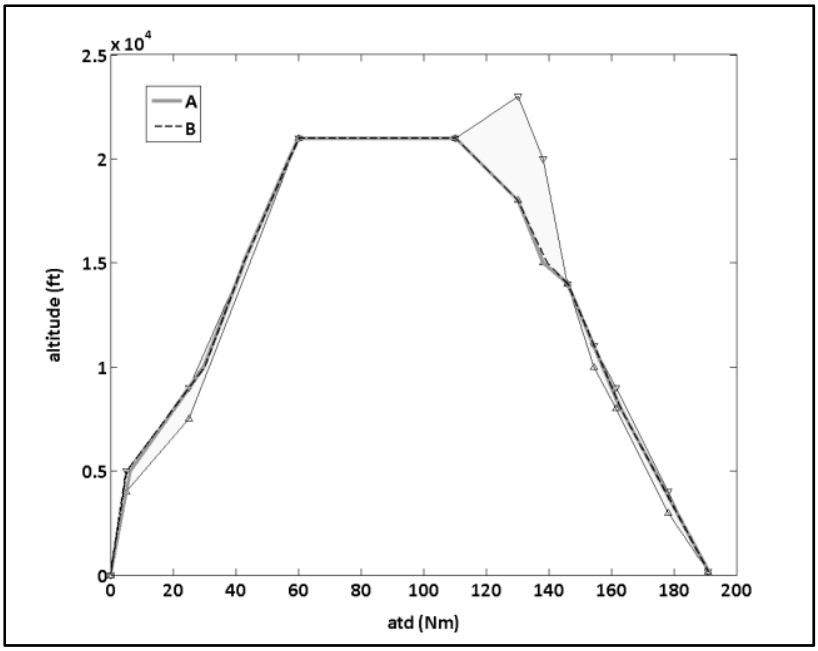

Figure 5.9 Comparative vertical flight plan differences due to algorithms' segment gradient selection: altitude profiles relative to the flight envelope

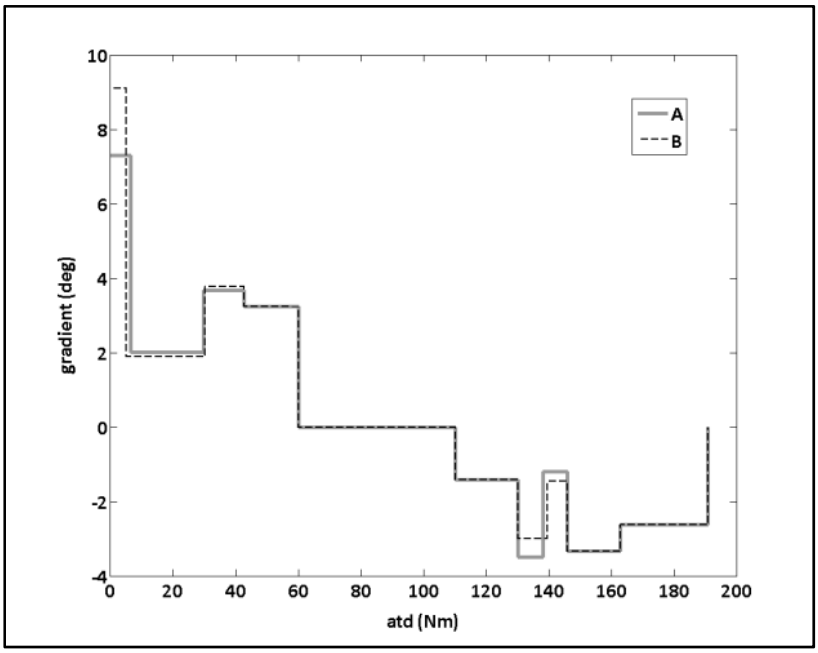

Figure 5.10 Comparative vertical flight plan differences due to algorithms' segment gradient selection: gradient profiles

The results have shown that the range of slope values that can be employed for the construction of a segment is influenced by the particular sequence of segments preceding it, due to the sequential manner in which the vertical flight plans are being constructed. Moreover, as illustrated in Figure 5.9 and Figure 5.10, the results have shown that a lower slope on one segment may determine the employment of a higher slope on the following segment, and vice versa. These results are consistent with the findings of the preliminary phases of the investigation (Beulze et al., 2015; Dancila, Beulze & Botez, 2016).

The Matlab code corresponding to the two algorithm implementations was executed on a Windows 7, AMD Phenom(tm) II X4, 2.80 Ghz platform. The minimum, maximum, and mean execution times for the set of 48 test cases, corresponding to each of the two algorithm implementations ("A" and "B") are showed in Table 5.6, below. As the pre-processing code was identical for the two implementations, the differences between the execution times were produced by the differences in the vertical flight plan optimization code implementations.

Table 5.6 Algorithm execution times for the "A" and "B" implementations, corresponding to the 48 test cases

	Implementation	
	"A"	***"B"***
Minimum time (millisec.)	3.72	2.17
Maximum time (millisec.)	44.63	47.87
Mean time (millisec.)	13.34	12.27

5.4 Conclusion

This paper presents a method for constructing an optimized vertical flight plan, minimizing the number of segments, for any given lateral flight plan defined as a sequence of waypoints characterized by their along-the-track distance, type, and altitude restrictions, as a function of a set of phase and altitude-dependent preferred gradient values. The proposed method has the advantage of constructing the optimized flight plan geometrically, using simple linear equations, without the need for time- and resource-intensive calculations based on the aircraft performance model. Moreover, the proposed method allows the adoption of construction

strategies adapted to each flight phase, and increases the computation speed by performing optimization computations only on sub-domains that require such computations. Additionally, contrary to other optimization methods (including those using the dynamic aircraft model), the ground-referenced vertical flight plan is fixed, and does not change with variable wind conditions, thus, it facilitates the flight and traffic management in congested areas. Furthermore, contrary to other optimization methods which generally propose trajectories only constrained by the aircraft's performances, the proposed method considers all altitude and flight path angle restrictions imposed by the take-off, departure, approach and landing procedures, as well as restrictions associated with any waypoint in the lateral flight plan.

A number of possible trade-offs relative to the insertion of a horizontal segment between successive climb/descent or descent/climb segments versus the selection of the gradient value were identified. Two algorithm implementations, each employing a different trade-off combination, were used to investigate their corresponding performances and the influence/differences entailed by each trade-off.

The results showed that the proposed method, and both algorithm implementations, were capable of constructing the optimized vertical flight plans. As expected, the results indicated that the particular horizontal segment insertion versus slope selection trade-off adopted in the implementation of the algorithm can influence the construction of the optimized flight plan in terms of the number of segments and slope values. However, a greater influence was exercised by the particular implementation of the segment slope selection algorithm. The investigation also showed that, as noted in the previous research conducted by the authors of this paper, due to the sequential construction of the optimal vertical flight plan the construction of a segment is dependent of the particular set of segments preceding it.

Of the 48 test cases evaluated in this research, using the two algorithms, 27 provided identical flight plans while eight test cases generated flight plans having a difference of one or two segments. However, in each test case presenting vertical flight plan differences

(number of segments and/or slope values) a large number of composing segments were identical.

Future research could include identifying and investigating new implementation trade-offs. As well, future research may investigate the use of linear optimization techniques for constructing the optimized flight plan in order to eliminate the limitations imposed by the sequential flight plan construction.

CHAPTER 6

DISCUSSION OF THE RESULTS

The objective of this Ph.D. thesis research was to investigate new methods that could be employed to improve the performances of the algorithms used for aircraft flight trajectory optimization.

During the first investigation, presented in Chapter 3, two hypotheses were investigated.

The first hypothesis was that the proposed method of selection of the geographic area used for the computation of the optimal flight trajectory provided the means to control the size of the operational area around the departure and destination airports, and the maximal trajectory distance between the two airports; thus, it provided an effective way of selection of the geographic area.

The second hypothesis was that a grid constructed to closely circumscribe this selected area would minimize the number of grid nodes considered in the trajectory optimization process, while allowing the exploration of all geographic areas that meet the criteria set relative to the trajectory maximal distance, and to the sizes of operational areas around the two airports.

The limitations imposed in this research were:

- the size of an operational area was defined as the length of a segment extending the orthodrome connecting the two airports;
- the sizes of the two operational areas were equal;
- the maximal trajectory distance was evaluated on a trajectory connecting the departure and destination airports, and it was composed of two segments intersecting on the contour of the selected ellipse.

The research was conducted in three steps. In the first step, the flat surface model was used to investigate the relationship connecting the half-distance between departure and destination airports, ellipse' semi-major axis (equal to the sum of the half-distance between the departure and destination airports, and the size of an operational area), ellipse's eccentricity, the ordinate of the position of the intersection point, and the trajectory's maximal distance. The input data (with the exception of the eccentricity, defined as a non-dimensional value), and the results were normalized to the value of the semi-major axis in order to maintain their generalization relative to the airports' positions and the size of the operational areas. The results were produced for ellipse eccentricity values of 0, 0.1, 0.5, 0.9, 0.99, and 0.999, for half-distance to semi-major axis ratios from 0 to 1 in increments of 0.1, and for intersection points' ordinates corresponding to one side of the ellipse (due to ellipse symmetry). The results showed the dependency of the maximal trajectory distance with the values of the eccentricity, and semi-major axis, thus, with the size of the operational areas. Therefore, the results showed that for a given airport configuration (distance between airports) and size of operational areas around the airports, the maximal trajectory distance was controlled by adjusting the ellipse eccentricity value, which confirmed the first hypothesis.

In the second step, the proposed method was used to analyze the performance of the "geographical routing grid", measured as the percent ratio between the number of points of the geographical routing grid and the number of points of a rectangular grid delimited by the same maximal and minimal latitude and longitude values.

The results were generated for a set of three pairs of airports corresponding to short flight distances (Montreal – Toronto, 274 Nm) and long flight distances (Montreal – Amsterdam, 2971 Nm, and Montreal – Paris, 2982 Nm), for eccentricity values between 0.1 and 0.999 (Montreal - Toronto) and between 0.8 and 0.999 (Montreal – Amsterdam and Montreal - Paris), and required sizes of operational areas around the two airports corresponding to orthodrome extensions equal to lengths of orthodromic arcs spanning 0, 0.1, 0.25, 0.5, 0.75, and 1.0 degrees. The results showed that the performance of the proposed algorithm (the reduction of the elliptical to rectangular grid size ratio) as function of the eccentricity value

was more significant for the long flight distances (i.e. from approximately 80% at eccentricity 0.8, to approximately 22% at eccentricity 0.999 in the case of Montreal – Amsterdam, thus, 57%) than for the short distances (i.e. from approximately 88% at eccentricity 0.1, to approximately 42% at eccentricity 0.999 in the case of Montreal – Toronto, thus, 46%). Moreover, the effect of the size of the operational area around the airports on the grid size ratio was smaller as the distance between the two airports increased due to its lesser contribution to the ellipse major axis' length. This fact means that the method proposed in the first paper (Dancila & Botez, 2016) was more efficient for medium and long flight distances (more than 1000 Nm) than for short flight distances (such as Montreal – Toronto , 274 Nm).

In the third step, the geographical selection areas constructed for the three pairs of airports (Montreal-Toronto, Montreal-Amsterdam, and Montreal-Paris), using a semi-major extension value (operational area size control variable) of 0.25 arc degrees and for eccentricity values of 0.9, 0.95, 0.99 and 0.999, were compared with actual flight trajectories (raw positioning data) of commercial aircrafts serving the three airports pairs. These flights were ACA429/ACA430, KLM671/KLM672 and AF342/AF345, respectively, and took place between November 22, 2014, and December 4, 2014. The results showed that for the long distance flights, the trajectories were circumscribed by ellipses with lower eccentricity values (wider ellipses) than the trajectories corresponding to the shorter flight distances. The explanation resides in the fact that a given deviation from the selected ellipse's major axis (representing the shortest distance between the two airports) has a lesser contribution on a longer flight's total distance than on a short flight total distance. Moreover, on long distance flights, the effects of the distance increase can usually be compensated by the utilization of more advantageous wind conditions.

A detailed inspection of the Montreal – Toronto flights showed that while the cruise phase trajectories were situated inside an ellipse having an eccentricity value of 0.99, the take-off and landing trajectories required an ellipse contour having an eccentricity value of 0.95 due to airport runways' orientation relative to the ellipse's major axis.

A general overview of the results presented in the first paper (Dancila & Botez, 2016) confirmed the initial hypotheses and showed that the new proposed method could improve the performances of flight trajectory optimization algorithms by providing a well adapted routing grid, or set of candidate waypoints as inputs for the optimization process. This overview also showed that the proposed method was well suited for long-haul flight trajectories, and less suited for short-haul flights.

In Chapter 4, the main hypothesis of the second paper (entitled "Vertical Flight Path Segments Sets for Aircraft Flight Plan Prediction and Optimization") was the reduction of the volume of calculations required for computing an optimal flight plan by decoupling the lateral and vertical flight plan calculations, and by the employment of pre-computed vertical flight path data; therefore, the reduction of repetitive, resource intensive calculations using the aircraft performance model. The proposed method assumed free-flight navigation scenarios, constant speed schedule and standard temperature deviation values for each flight phase (climb, cruise and descent). The method also took into account the altitude limitations specific to climb and descent phases, and the values of the crossover altitudes specific to each flight phase speed schedule. For the cruise phase, the method considered only climb-in-cruise and constant speed level flight segments. The cruising altitudes were situated at multiples of 1000 ft, up to the aircraft's maximal attainable altitude. For the descent phase, the method considered a set of descent vertical flight paths ending at the EOD altitude, and each corresponding to an estimated EOD gross weight. The consideration of multiple descent vertical flight paths (thus, multiple EOD gross weights) provided the capability to construct look-up structures, and graphs describing global vertical flight paths yielding multiple combinations of total flight times and fuel burns.

The second paper firstly provided a general presentation of the existing flight plan calculation method; the existing method computes simultaneously the lateral and vertical flight plan components using the aircraft's performance model. Secondly, this paper described the proposed, new method used for the computation and assembly of a set of

vertical flight path segments into a look-up structure, and for the generation of a corresponding vertical flight path graph. The intended objective of the vertical flight path graph was to facilitate the selection of a vertical flight plan segment and the retrieval of its performance data. Then, this paper presented the construction of a lateral and vertical flight plan using the vertical flight segments look-up structure, and their graph.

Finally, this paper analyzed the results represented by a set of nine vertical flight plan look-up structures and graphs corresponding to a total of nine combinations of maximal altitudes, number of descent paths, and sets of values of the expected aircraft EOD gross weight.
The nine look-up structures and graphs described vertical flight paths having 1 climb path, between six and eight cruise altitudes, between 36 and 44 climb-in-cruise paths, and five or 11 descent paths. Also, the total number of graph nodes varied between 249 and 443.

The results of an exhaustive "depth first" exploration of each graph allowed the identification of their corresponding total number of possible vertical flight paths (ranging from more than 1.44 million to more than 115.9 million), minimal flight times (from 5.274 to 6.355 hours), maximal flight times (from 6.405 to 7.746 hours), minimal still air distances (from 2,517.24 to 3,049.451 Nm), and maximal still air distances (from 3,046.001 to 3,687.362 Nm). These results also allowed the identification, for each graph, of the particular sequence of vertical flight path segments leading to minimal/maximal flight time or still air distance.

For each of the nine look-up structure and graph pairs, a statistical analysis identified the total number of vertical flight paths leading to each of the EOD graph nodes, the number of flight paths corresponding to an EOD gross weight which shared the same flight time and still-air distance domain with another EOD graph node (the range of the flight time/still-air domains attainable by two or more descent vertical paths), and the flight time/still-air distance domain distribution of the vertical flight paths grouped according to the end of descent weight (the range of the flight time/still-air domains attainable at the end of each descent vertical path, thus, for each total fuel burn).

An analysis of the processing time required for the generation of the look-up structure and its corresponding graph showed values between 41.554 and 54.147 seconds, which were large compared to the time required by the existing flight plan computation method (computing a single flight path). However, in the context of flight trajectory optimization, which may require the evaluation of a large number of candidate flight paths, the time required for generation of the look-up structure and graph is counteracted by the fact that this time is spent once. Each subsequent computation of a flight path uses the pre-computed look-up and graph data, thus, is much faster than existing method using the aircraft performance model, and multi-dimensional linear interpolation algorithms. The analysis has also shown that the time necessary for the generation of a look-up structure and graph could be reduced by an appropriate selection of the number of climb-in-cruise and descent vertical flight paths.

A general overview of the results presented in the second paper, showed that the new proposed method could improve the speed of the trajectory optimization calculation by providing pre-computed vertical flight path data, thus, eliminating the need for repetitive, time and resource-intensive calculations using the aircraft performance model. Moreover, the associated graph enables the identification of the vertical flight path segments that could be employed at each step of the flight trajectory calculation, as a function of the aircrafts altitude and gross weight, and facilitates the retrieval of the corresponding vertical flight path segment's data.

Although the number of climb, cruise and descent vertical flight paths segments described by the look-up structures was limited, the results showed that very large number of global vertical flight paths could generated using these structures (between 1.44 million and 119.9 million flight paths). The assembly of global vertical flight paths covered a large domain of flight time/still-air distance values that could match different lateral flight plans between a departure and destination airports. Moreover, the new proposed method makes possible the investigation of flight trajectory optimization methods based on the exploration of the vertical flight plan graph.

The objective of the research presented in the third paper (entitled "Optimal Vertical Flight Plan Construction as function of Flight Phase and Altitude"), Chapter 5, was to investigate a method for eliminating the time, and resource-intensive calculation of an optimal flight plan (using the aircraft performance model) by means of a geometrical construction of an optimal vertical flight plan as a function of a given lateral flight plan, and a set of phase and altitude-dependent preferred segment gradient values. The preferred gradient values, representing the ground-referenced vertical path slope (in ft/Nm), are pre-defined as functions of the aircraft's configuration, and performance model.

The optimization criterion is represented by the minimization of the total number of vertical flight plan segments. The two main limitations imposed in the construction of the vertical flight plan are: 1) The lateral flight plan is defined as a set of waypoints and corresponding ATD from the first flight plan waypoint. 2) Each waypoint defines its corresponding altitude and the gradient constraints values. 3) Each vertical flight path segment must follow as close as possible the preferred gradient value for the corresponding phase and altitude, and must not exceed a predefined maximal value. 4) A horizontal flight segment of a pre-defined minimal length must be inserted between consecutive climb/descent or descent/climb segments. 5) All vertical flight trajectory segments must reside within the vertical flight plan envelope delimited by connecting the maximal and minimal altitude constraints, respectively, of consecutive waypoints composing the lateral flight plan.

The methodology used for conducting the research presented in this paper addressed the following elements:

- Firstly, based on the input lateral flight plan, the pre-processed lateral flight plan listing the explicit set of waypoints (along-the-track distances), and their corresponding minimal and maximal altitudes used in the calculation of the vertical flight plan were determined.
- Secondly, the pre-processed flight plan was decomposed into a sequence of climb, horizontal, and descent flight domains.

- Thirdly, the optimal vertical flight plan was generated using geometrical calculations, one domain at a time from the first to the last domain; on each domain the vertical flight plan segments were generated sequentially, from the first to the last waypoint.
- Finally, the evaluation of the proposed method on a number of 48 test cases, was done by using two implementations that employed distinct trade-off policies. These implementation trade-of policies concerned firstly, the precedence of preferred gradient value versus the minimal length of a horizontal segment and, secondly, the insertion of the horizontal segments between successive climb and descent segments.

The results showed that for a number of 40 flight test cases, the number of vertical flight plan segments was identical for both above mentioned implementations; for a number of seven cases, the number of vertical flight plan segments computed by the two implementations was different by one segment; and for one case, the number of vertical flight plan segments was different by two segments. Upon further analysis, for only one test case the difference in the number of vertical flight segments was attributed to the difference in implemented trade-offs. For the other seven test cases the differences in the number of vertical flight segments were caused by differences in the implementation of the algorithms used for the computation and selection of the segments' gradients. The analysis also showed that the sequential construction of the vertical flight plan segments may limit the range of gradients that could be used for building a segment, i.e. employing a higher gradient on one segment may lead to the employment of a lower gradient on the next segment, and vice versa.

The new proposed method presents the advantage of constructing an optimized flight plan using geometrical calculations which are less time and resource-intensive than the ones using the aircraft performance model. A second advantage is the fact that the proposed method allows the choice of adopting distinct optimization strategies dependent on the flight phase. Moreover, the proposed method detects the sub-domains on which the optimization is not required, thus, it provides another reduction in terms of time and computing resources requirements.

CONCLUSION AND RECOMMENDATIONS

This thesis presented three new methods addressing distinct features of a flight trajectory optimization algorithm: 1) the selection of a geographic area containing the candidate waypoints and the construction of a routing grid defining the set of candidate waypoints, 2) the construction of an ensemble of vertical flight path segments to be used in the optimization process, and 3) the geometrical construction of an optimized vertical flight path.

The main benefit of the proposed method for selecting a geographic area is the ability to have an independent control on the sizes of the operational areas around the airport, and on the trajectory's maximal distance. Moreover, the proposed method ensures that all candidate waypoints meeting the two construction criteria are part of the selected geographical area. The results showed that the method was more adapted for medium and long-haul flights, as for the short flights the runway configurations may lead to take-off or landing trajectories extending the size of the operational area around the airports, and / or lower ellipse eccentricity values, thus, larger geographical areas and larger values for the maximal trajectory distances. Consequently, for short-haul flights, this method may lead to less efficient area selections and less efficient routing grids, thus, leading to a less performing optimization process. An important observation is the fact that a trajectory optimization algorithm has the flexibility to use a limited set of candidate waypoints or set of tracks situated inside the selected area, or the routing grid presented in the description of the method.

The advantages of using the ensemble of vertical flight path segments as part of the trajectory optimization are three-fold:

- Firstly, the calculation of the optimal trajectory uses pre-computed data. Therefore, the optimization algorithm is faster than the existing algorithms since it does not require repetitive, time and resource intensive computations using the aircraft performance model at each trajectory recalculation.

- Secondly, the parameters of the ensemble's vertical flight path segments have the full accuracy relative to the aircraft performance model, from which they were constructed.
- Thirdly, the graph accompanying the ensemble of vertical flight paths helps to identify the segment or the set of segments that can be used at any given time instance, and to retrieve the performance data corresponding to the selected vertical path segment.

The disadvantages of this method relate to:

- The relative long time required for the ensemble's generation (up to 54.147 seconds for the test cases presented in the second paper), which is compensated by the fact that the calculation is performed only upon changing the input configuration parameters;
- The limited number of vertical flight paths composing the ensemble;
- The vertical flight paths' generation for a single speed schedule and temperature deviation value, for each phase of flight.

The proposed method for the geometrical construction of an optimal vertical flight plan, as described in the third paper, operates on a defined lateral flight plan. However, this method can also be used in the general context of flight trajectory optimization. In this case, the trajectory optimization algorithm, at each iteration, must: 1) define the selected set of waypoints composing the candidate lateral flight plan, and/or the corresponding waypoint types and altitude restrictions; 2) perform the geometrical construction of the optimal vertical flight plan, corresponding to the candidate lateral flight plan; and 3) compute value of the cost-objective function, for the candidate flight plan composed of the candidate lateral flight plan and its optimal vertical flight plan. Subsequently, the optimal trajectory is selected from the set of candidate flight plans, by comparing the values their cost-objective functions, and by retaining the one that best matches the optimization criteria.

It can be noted that while an optimization algorithm can benefit from a performance improvement brought by using any of the three methods by itself, an even larger benefit can be achieved by employing the geographical area selection algorithm in conjunction with any of the two other methods proposed in this thesis (the construction of the ensemble of vertical flight path segments, and the geometric vertical flight path optimization methods).

Following the above set of observations, the following recommendations are made for future research:

- Exploration of the performances of a trajectory optimization algorithm that uses the geographic area selection, the routing grid construction, and the construction of an ensemble of vertical flight path segments algorithms.
- Exploration of the performances of a trajectory optimization algorithm that uses the geographic area selection, the routing grid construction, and the geometric vertical flight path optimization algorithms.
- Update the method used for the construction of an ensemble of vertical flight path segments to include descent-in-cruise vertical flight paths.
- Investigation of the necessary modifications to the method used to construct an ensemble of vertical flight path segments, corresponding to multiple speed schedules and temperature deviations.

.

APPENDIX I

FIGURES: GEOGRAPHICAL AREA SELECTION AND CONSTRUCTION OF A CORESPONDING ROUTING GRID USED FOR IN-FLIGHT MANAGEMENT SYSTEM FLIGHT TRAJECTORY OPTIMIZATION

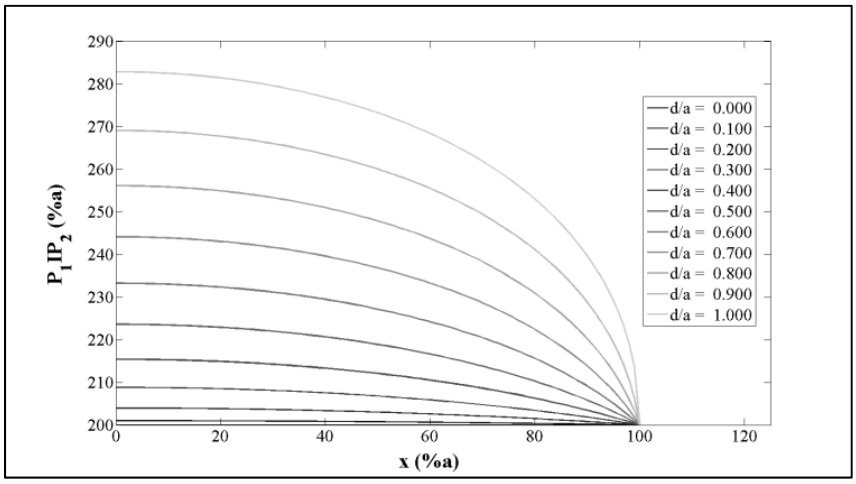

Figure-A I- 1 The total distance between the starting point P1 and the ending point P2 (P1IP2) as a function of the position of P1 and P2 (d) and the position (x) of the trajectory's point of intersection I with the ellipse, for eccentricity $e = 0$

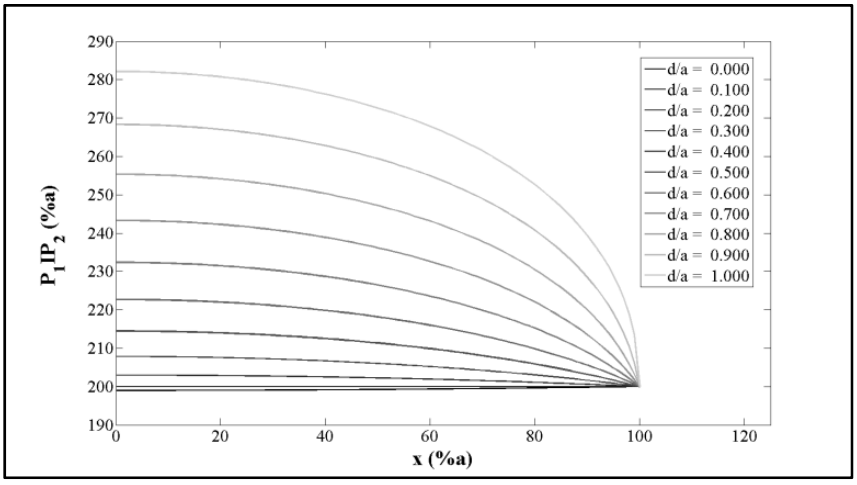

Figure-A I- 2 The total distance between the starting point P1 and the ending point P2 (P1IP2) as a function of the position of P1 and P2 (d) and the position (x) of the trajectory's point of intersection I with the ellipse, for eccentricity $e = 0.1$

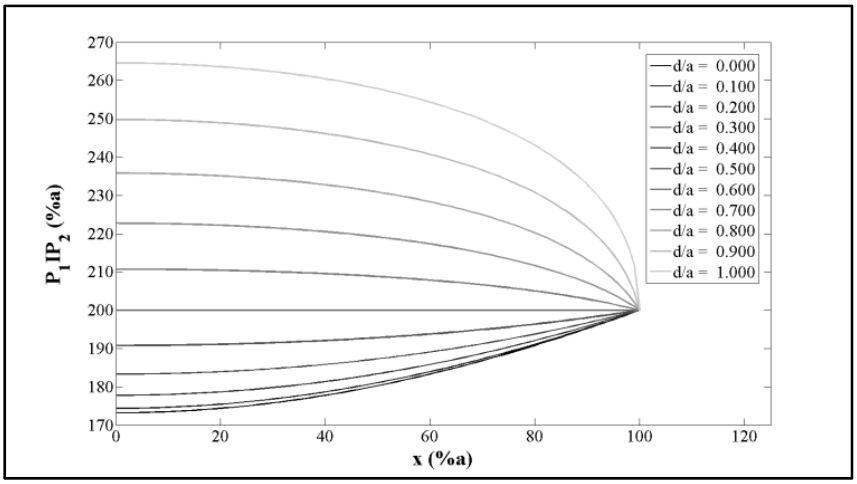

Figure-A I- 3 The total distance between the starting point P1 and the ending point P2 (P1IP2) as a function of the position of P1 and P2 (d) and the position (x) of the trajectory's point of intersection I with the ellipse, for eccentricity $e = 0.5$

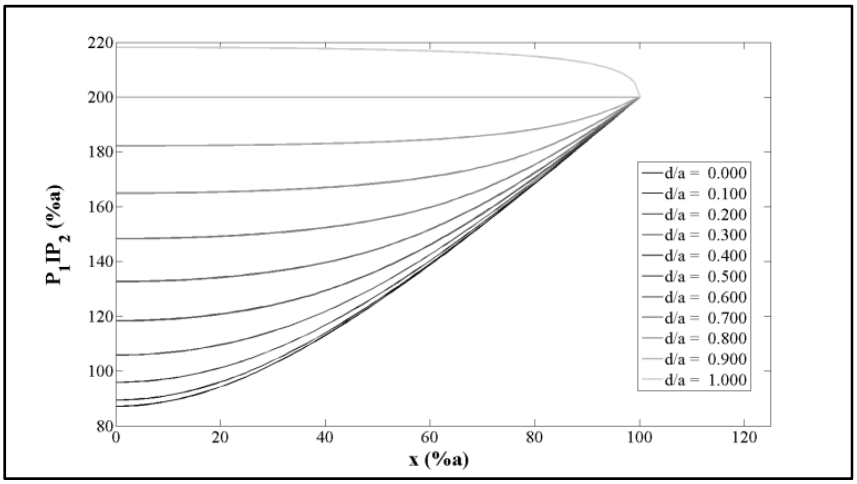

Figure-A I- 4 The total distance between the starting point P1 and the ending point P2 (P1IP2) as a function of the position of P1 and P2 (d) and the position (x) of the trajectory's point of intersection I with the ellipse, for eccentricity $e = 0.9$

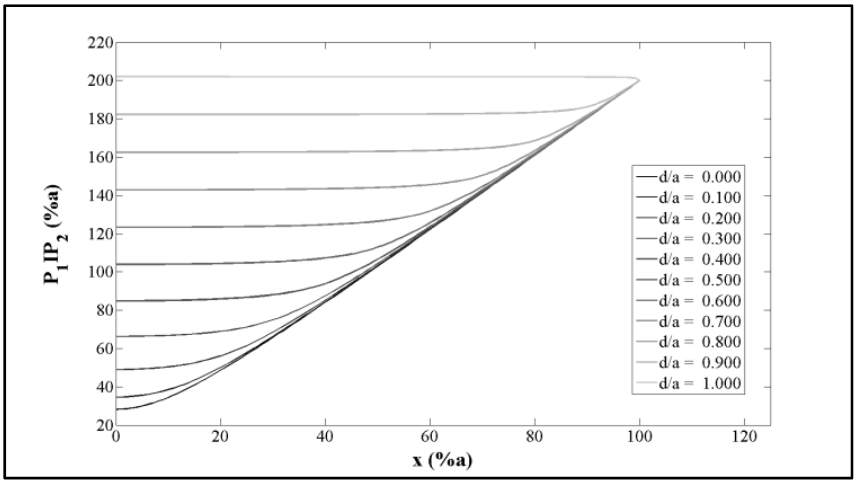

Figure-A I- 5 The total distance between the starting point P1 and the ending point P2 (P1IP2) as a function of the position of P1 and P2 (d) and the position (x) of the trajectory's point of intersection I with the ellipse, for eccentricity $e = 0.99$

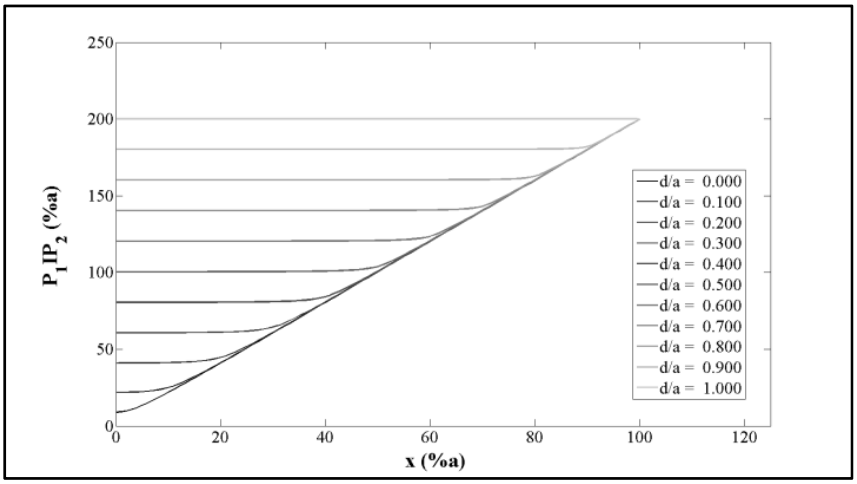

Figure-A I- 6 The total distance between the starting point P1 and the ending point P2 (P1IP2) as a function of the position of P1 and P2 (d) and the position (x) of the trajectory's point of intersection I with the ellipse, for eccentricity $e = 0.999$

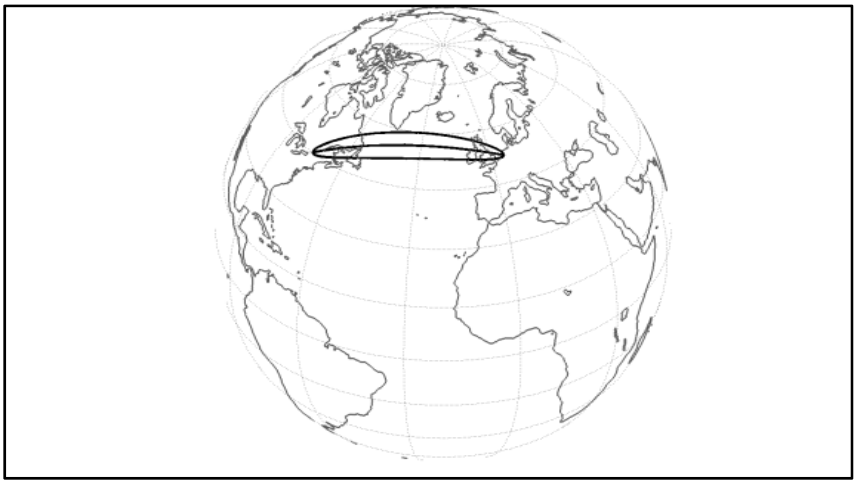

Figure-A I- 7 Example of an orthodrome and ellipse contour corresponding to a trajectory between Montreal (CYUL) and Amsterdam (EHAM) - global view

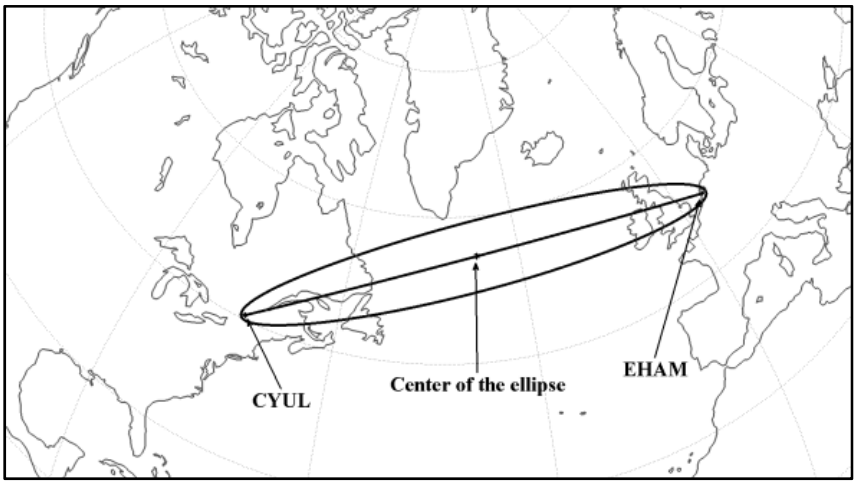

Figure-A I- 8 Example of an orthodrome and ellipse contour corresponding to a trajectory between Montreal (CYUL) and Amsterdam (EHAM) - close-up showing the principal points of the ellipse contour and the center

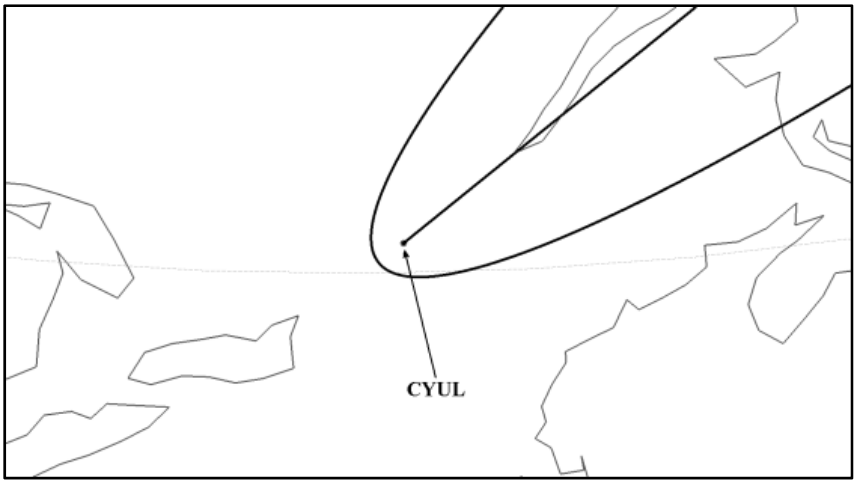

Figure-A I- 9 Example of an orthodrome and ellipse contour corresponding to a trajectory between Montreal (CYUL) and Amsterdam (EHAM) - details showing the extension area around the Montreal airport (CYUL)

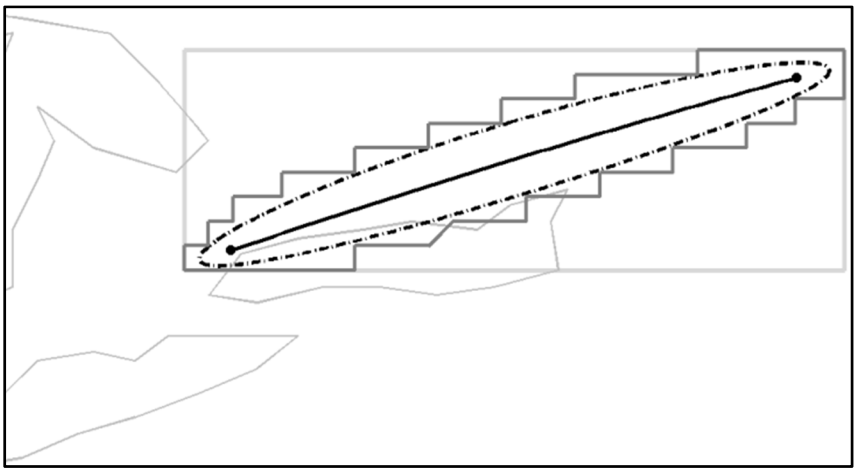

Figure-A I- 10 Comparative illustration, using a geographical projection, of the surfaces corresponding to a routing grid selected using an ellipse for which $e = 0.99$ and $c = 0.25°$, and another surface selected using a rectangular window ensuring the same minimal maneuvering surface around the departure and destination airports, for CYUL–CYYZ. The grid resolution, on both axis, is $0.5°$

Figure-A I- 11 Comparative illustration, using a geographical projection, of the surfaces corresponding to a routing grid selected using an ellipse for which $e = 0.99$ and $c = 0.25°$, and another surface selected using a rectangular window ensuring the same minimal maneuvering surface around the departure and destination airports, for CYUL–EHAM. The grid resolution, on both axis, is $0.5°$

Figure-A I- 12 Comparative illustration, using a geographical projection, of the surfaces corresponding to a routing grid selected using an ellipse for which $e = 0.99$ and $c = 0.25°$, and another surface selected using a rectangular window ensuring the same minimal maneuvering surface around the departure and destination airports, for CYUL–LFPG. The grid resolution, on both axis, is $0.5°$

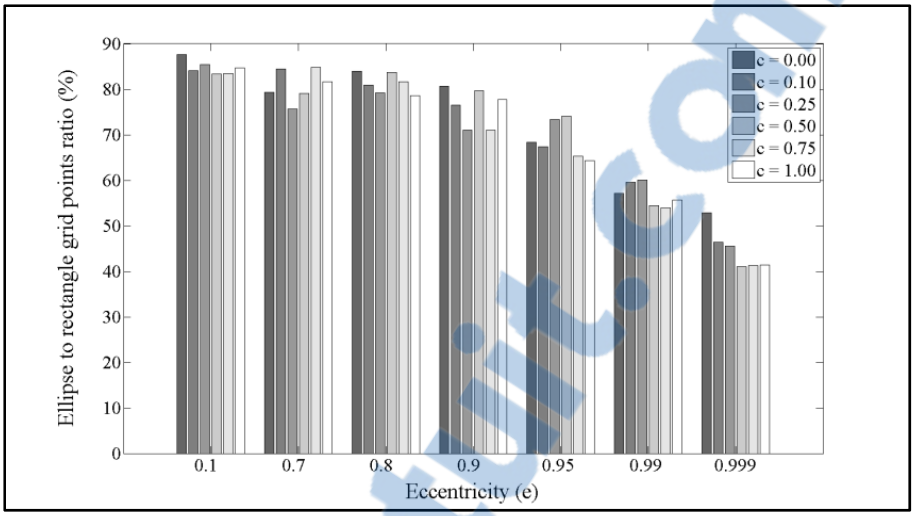

Figure-A I- 13 The percentage ratio between the reduced number of grid points selected using an elliptical contour versus those selected using the corresponding rectangle (circumscribing the selected contour) for a grid resolution of $0.5°$ and a set of eccentricity (e) and orthodrome extension (c) values, for CYUL - CYYZ (274 Nm)

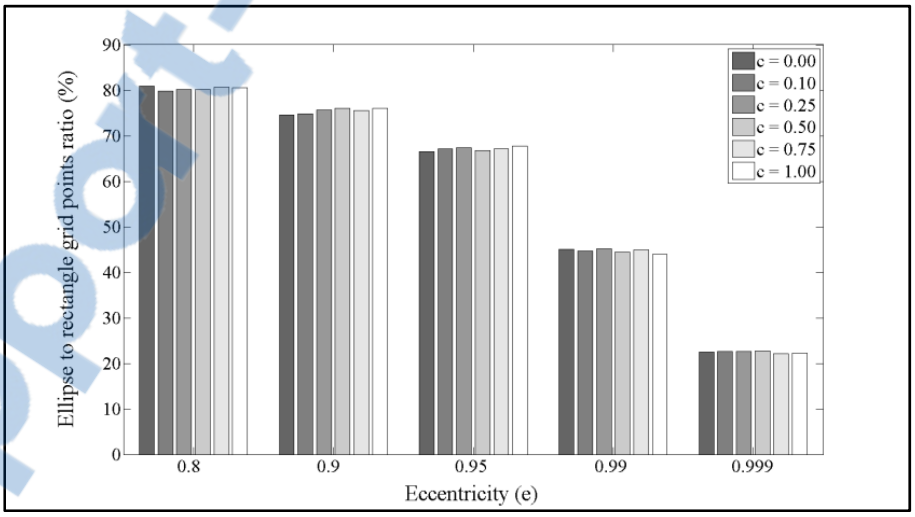

Figure-A I- 14 The percentage ratio between the reduced number of grid points selected using an elliptical contour versus those selected using the corresponding rectangle (circumscribing the selected contour) for a grid resolution of $0.5°$ and a set of eccentricity (e) and orthodrome extension (c) values, for CYUL - EHAM (2971Nm)

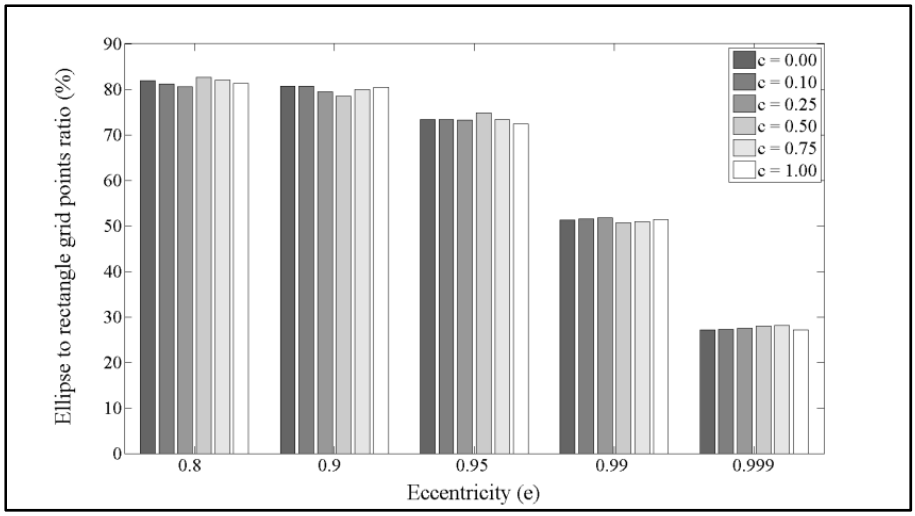

Figure-A I- 15 The percentage ratio between the reduced number of grid points selected using an elliptical contour versus those selected using the corresponding rectangle (circumscribing the selected contour) for a grid resolution of $0.5°$ and a set of eccentricity (*e*) and orthodrome extension (*c*) values, for CYUL - LFPG (2982Nm)

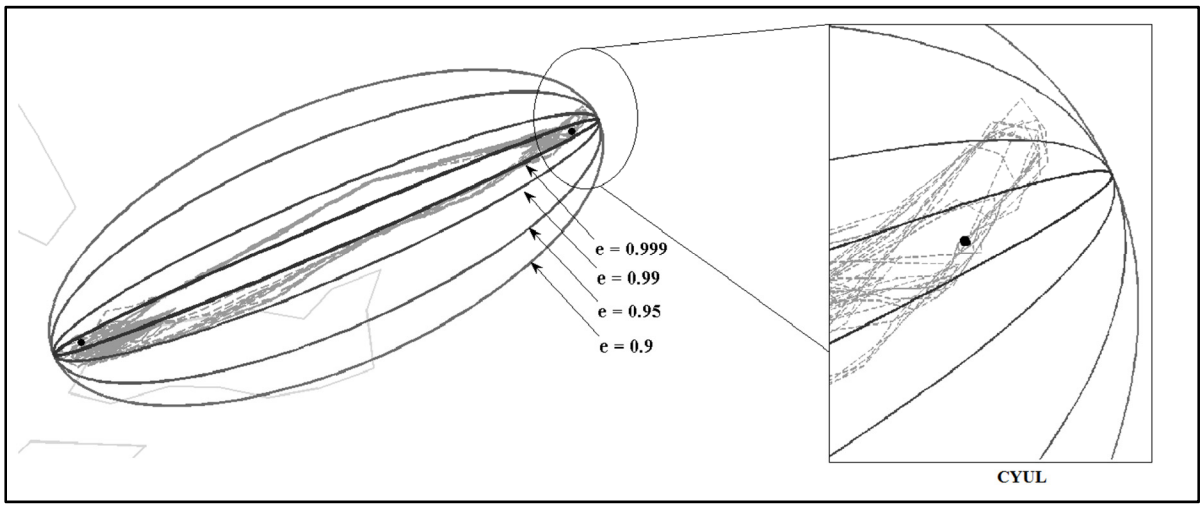

Figure-A I- 16 Lambert conformal conic projection representation of geographical contours corresponding to a semi-major axis extension value $c = 0.25°$ and eccentricities e = 0.9, 0.95, 0.99, and 0.999, and actual aircraft flight trajectories (raw positioning data) retrieved from FlightAware (2014), for pairs of flights between CYUL–CYYZ (ACA429/ACA430, corresponding to dates between 22 November 2014 and 4 December 2014, including details of the contours and flight tracks in the area surrounding CYUL

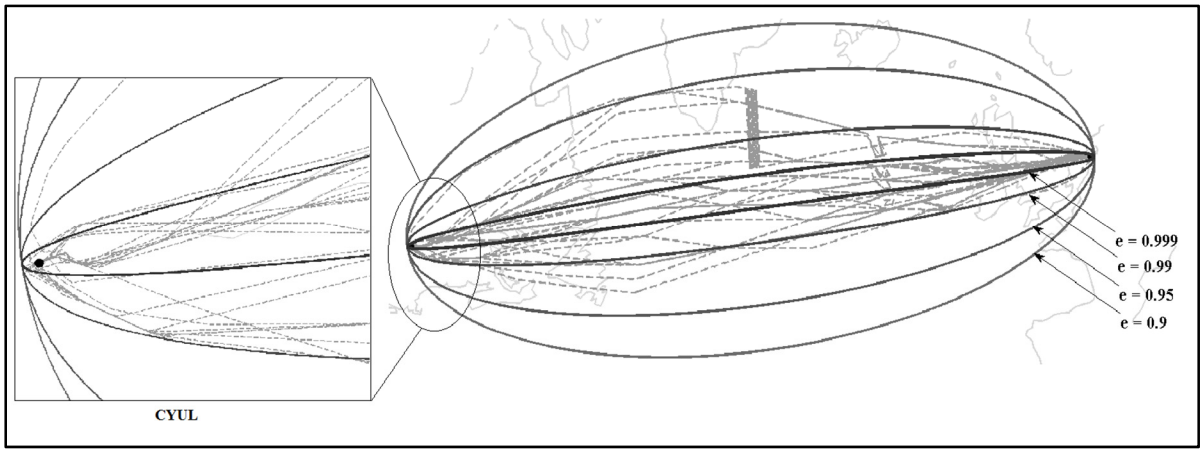

Figure-A I- 17 Lambert conformal conic projection representation of geographical contours corresponding to a semi-major axis extension value $c = 0.25°$ and eccentricities e = 0.9, 0.95, 0.99, and 0.999, and actual aircraft flight trajectories (raw positioning data) retrieved from FlightAware (2014), for pairs of flights between CYUL–EHAM (KLM671/ KLM672), corresponding to dates between 22 November 2014 and 4 December 2014, including details of the contours and flight tracks in the area surrounding CYUL

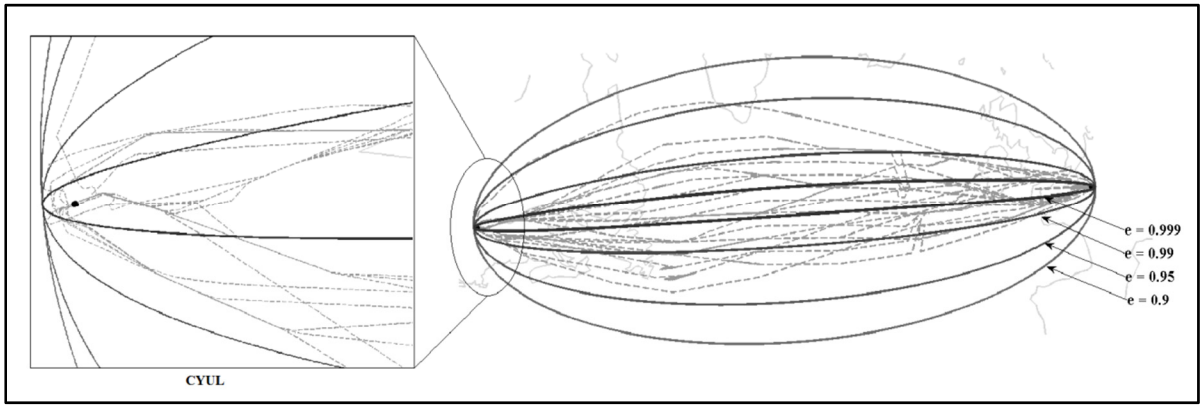

Figure-A I- 18 Lambert conformal conic projection representation of geographical contours corresponding to a semi-major axis extension value $c = 0.25°$ and eccentricities e = 0.9, 0.95, 0.99, and 0.999, and actual aircraft flight trajectories (raw positioning data) retrieved from FlightAware (2014), for pairs of flights between CYUL–LFPG (AF342/AF345), corresponding to dates between 22 November 2014 and 4 December 2014, including details of the contours and flight tracks in the area surrounding CYUL

APPENDIX II

FIGURES AND TABLES: VERTICAL FLIGHT PATH SEGMENTS SETS FOR AIRCRAFT FLIGHT PLAN PREDICTION AND OPTIMIZATION

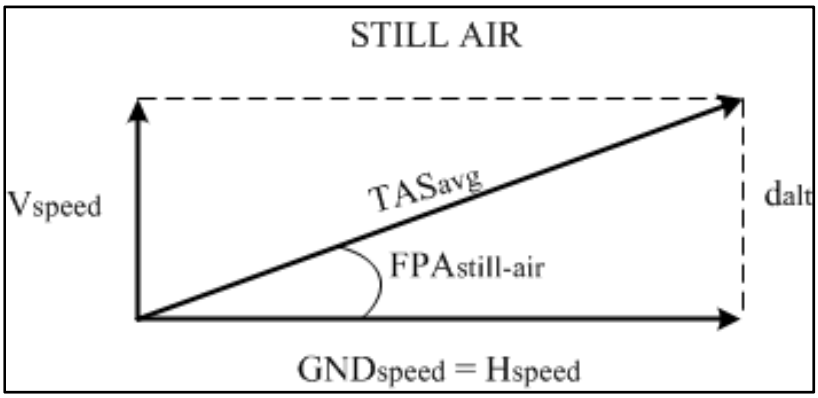

Figure-A II- 1 The relationship between the pre-computed still-air and wind-adjusted climb flight path parameters: still-air speed diagram

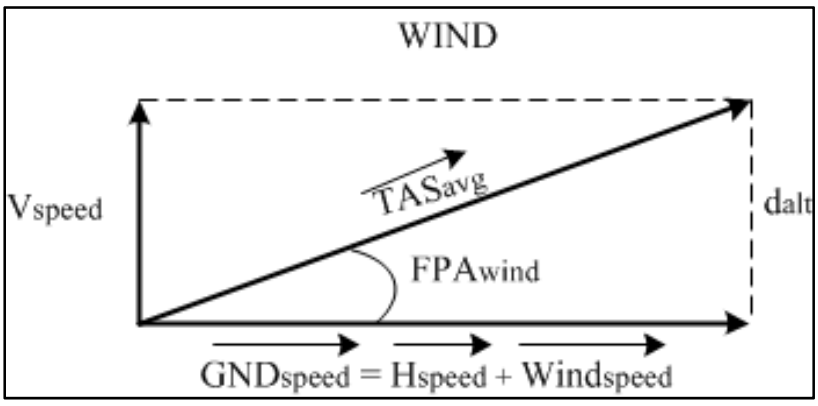

Figure-A II- 2 The relationship between the pre-computed still-air and wind-adjusted climb flight path parameters: wind-adjusted speed diagram

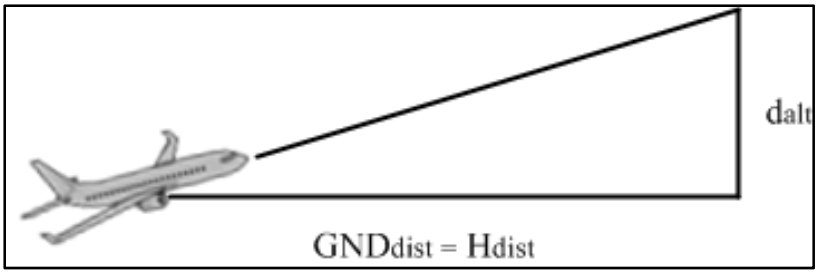

Figure-A II- 3 The relationship between the pre-computed still-air and wind-adjusted climb flight path parameters: still-air climb segment geometry

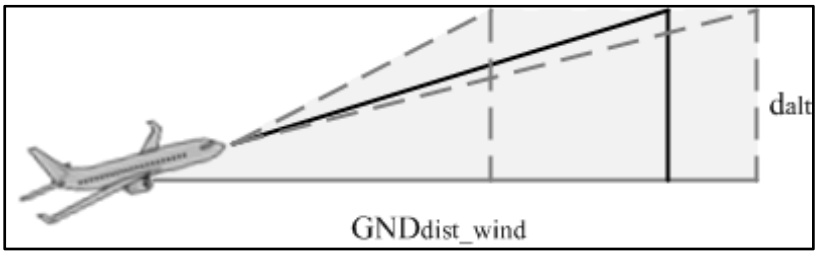

Figure-A II- 4 The relationship between the pre-computed still-air and wind-adjusted climb flight path parameters: wind-adjusted climb segment geometry

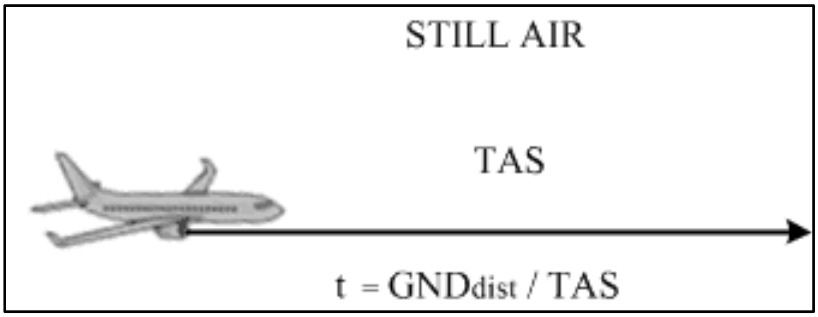

Figure-A II- 5 The relationship between the pre-computed still-air and wind-adjusted cruise, level-flight path parameters: still-air speed diagram

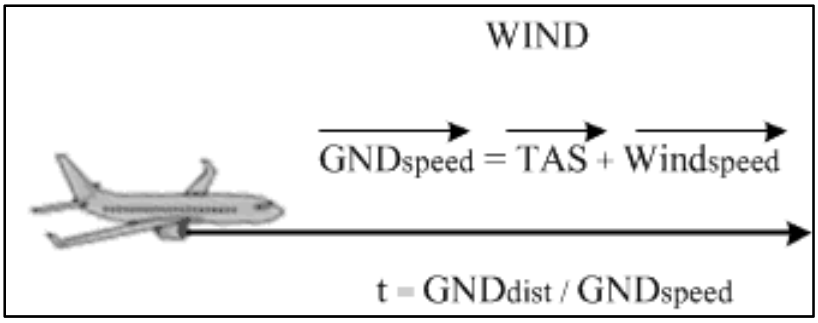

Figure-A II- 6 The relationship between the pre-computed still-air and wind-adjusted cruise, level-flight path parameters: wind-adjusted speed diagram

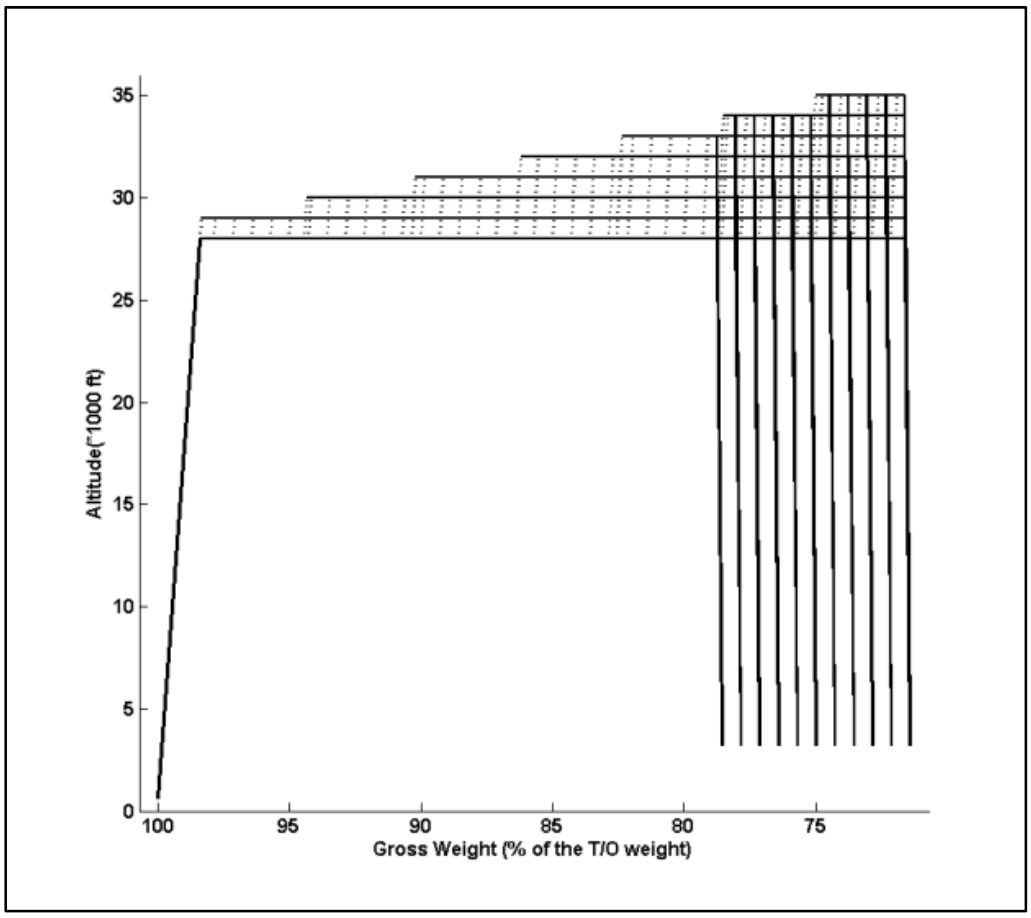

Figure-A II- 7 Vertical flight path graph corresponding to the vertical flight paths stored in the vertical flight path look-up structure: A11

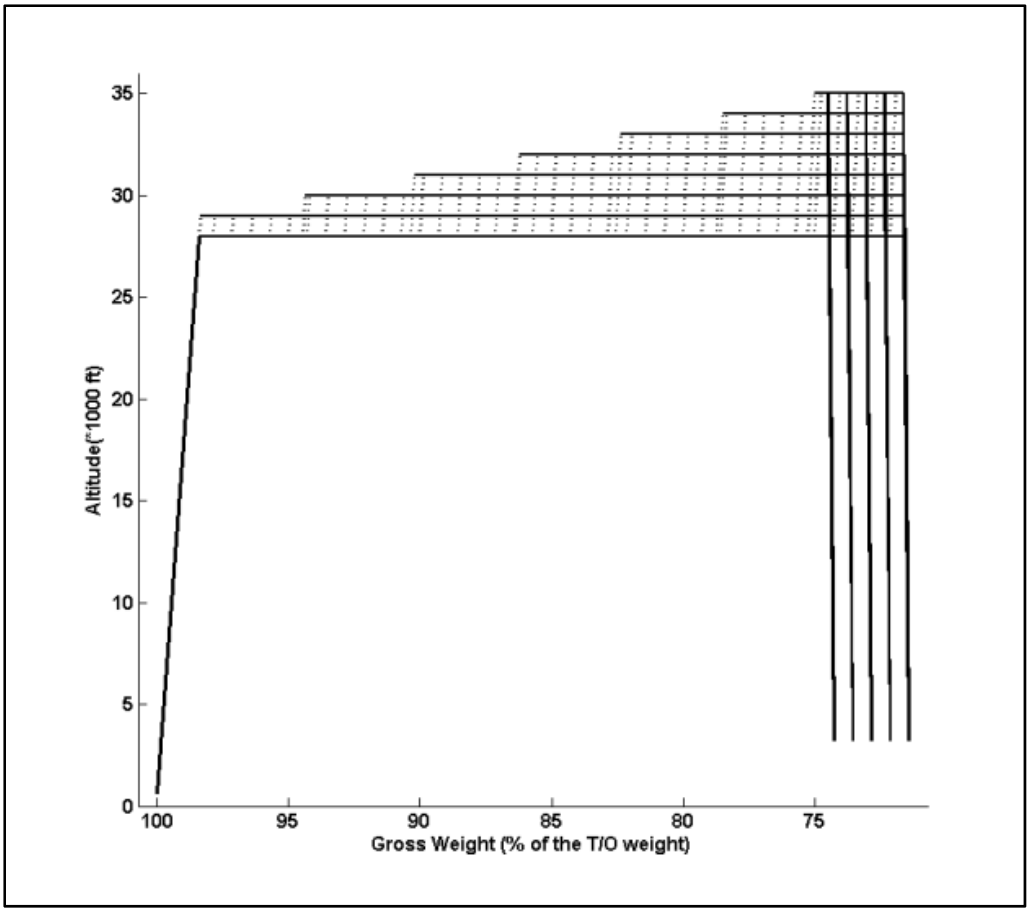

Figure-A II- 8 Vertical flight path graph corresponding to the vertical flight paths stored in the vertical flight path look-up structure: A12

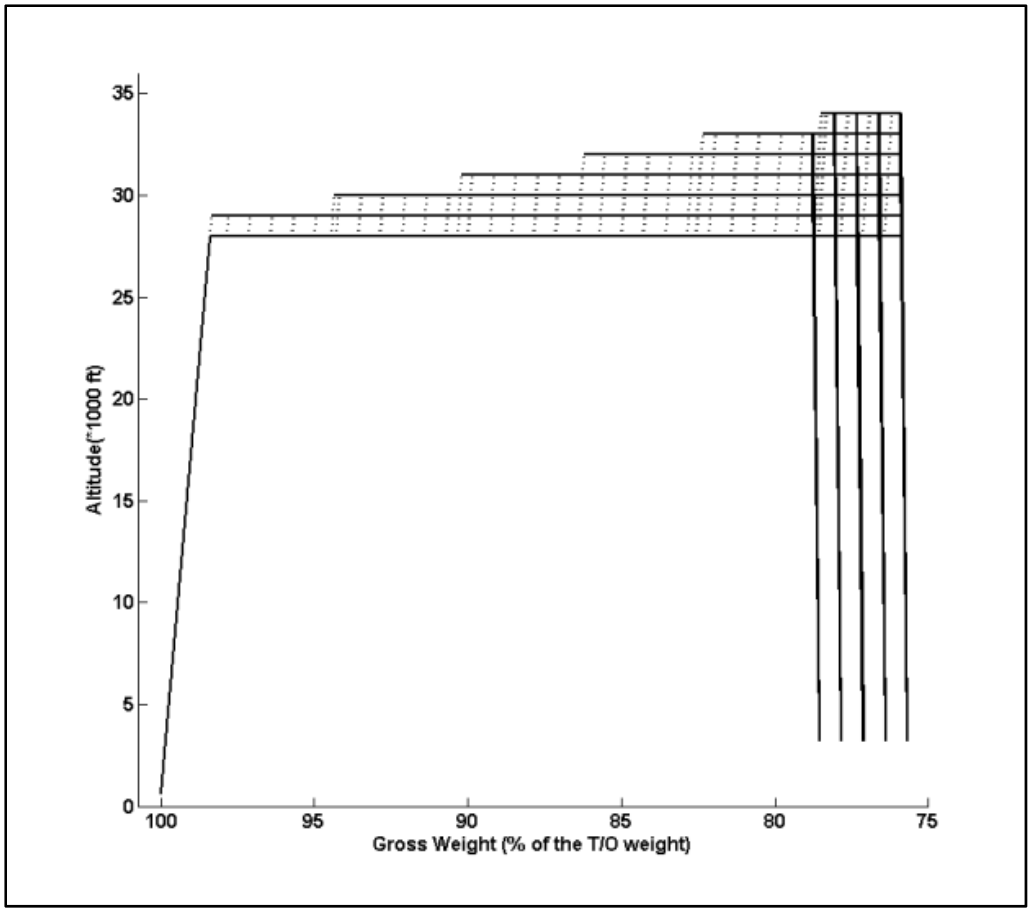

Figure-A II- 9 Vertical flight path graph corresponding to the vertical flight paths stored in the vertical flight path look-up structure: A13

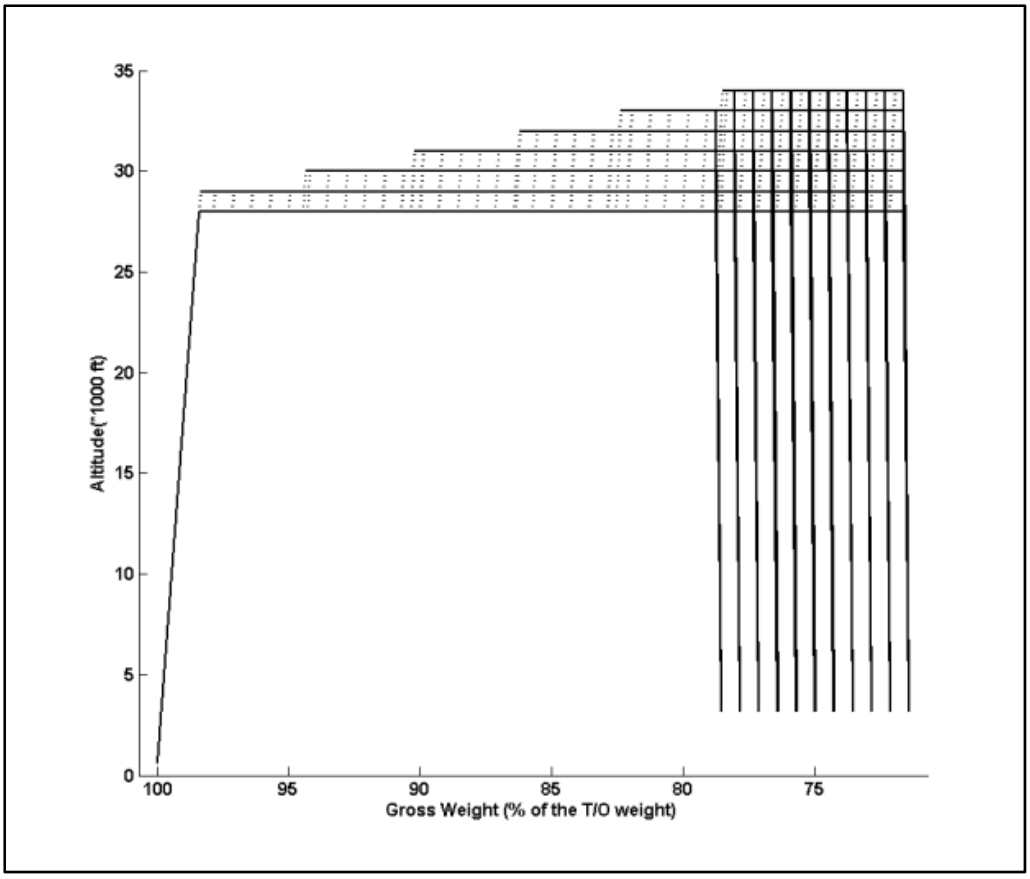

Figure-A II- 10 Vertical flight path graph corresponding to the vertical flight paths stored in the vertical flight path look-up structure: A21

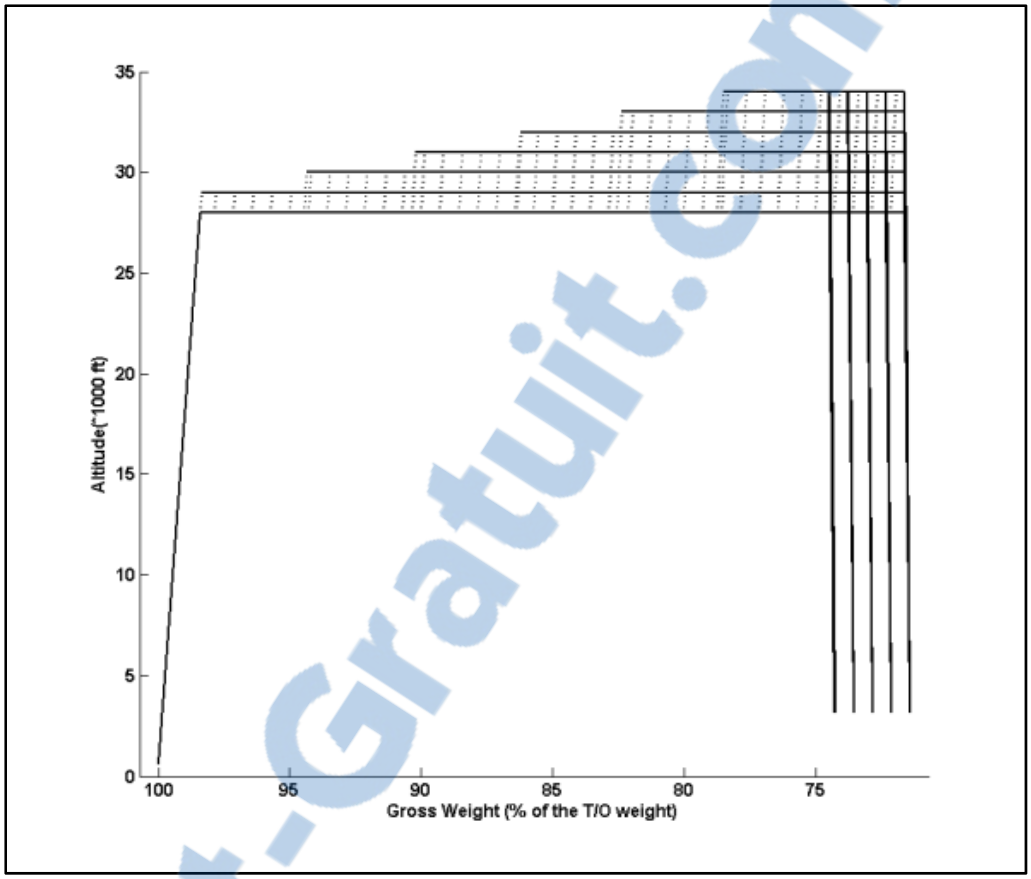

Figure-A II- 11 Vertical flight path graph corresponding to the vertical flight paths stored in the vertical flight path look-up structure: A22

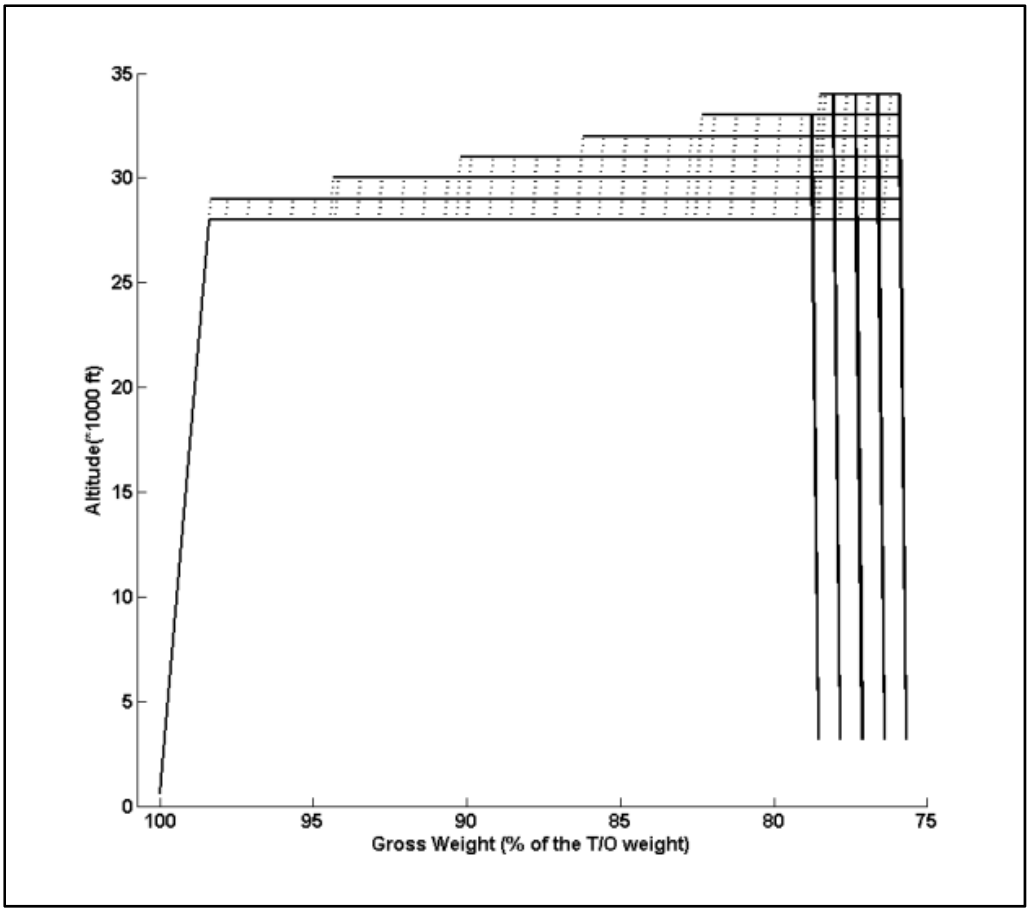

Figure-A II- 12 Vertical flight path graph corresponding to the vertical flight paths stored in the vertical flight path look-up structure: A23

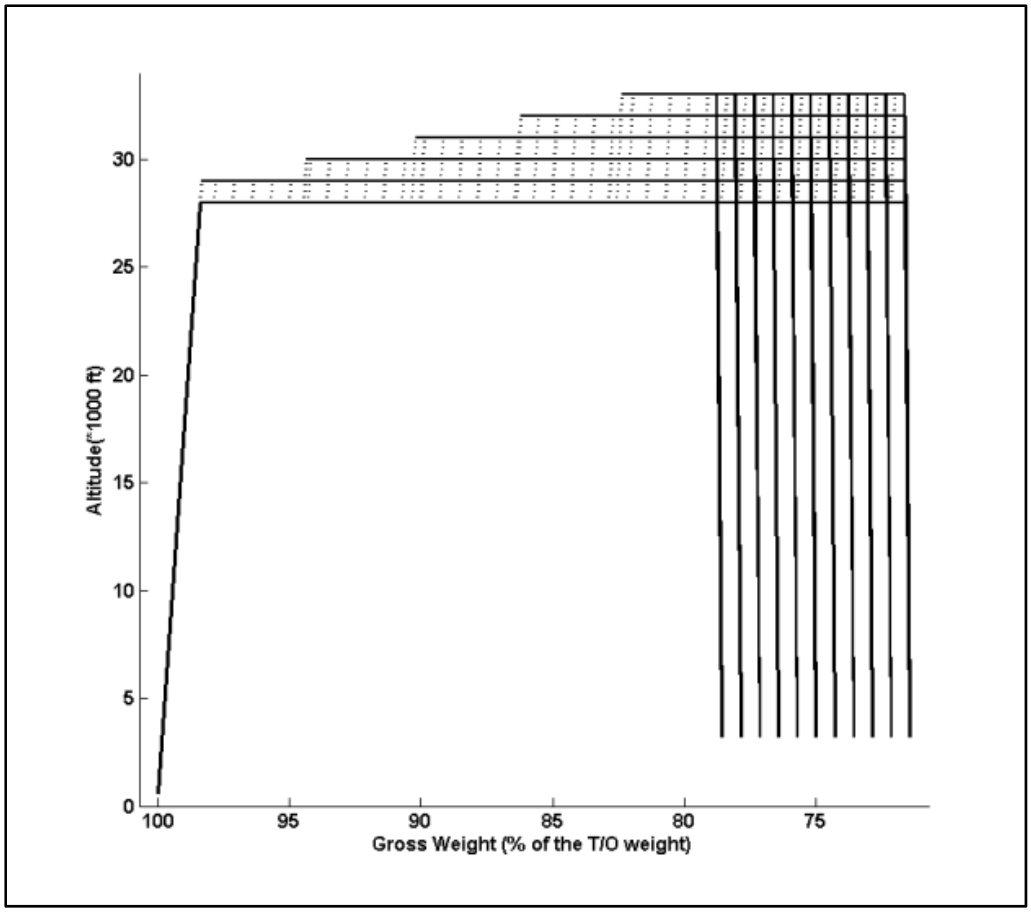

Figure-A II- 13 Vertical flight path graph corresponding to the vertical flight paths stored in the vertical flight path look-up structure: A31

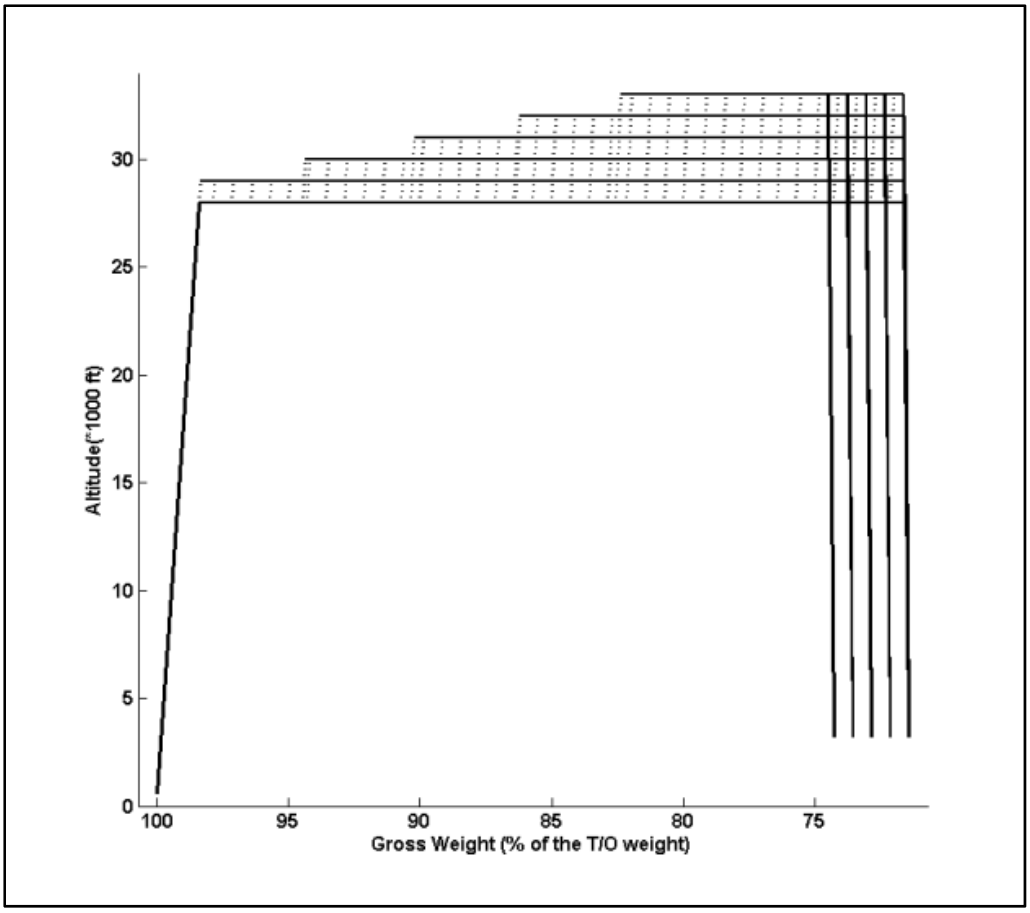

Figure-A II- 14 Vertical flight path graph corresponding to the vertical flight paths stored in the vertical flight path look-up structure: A32

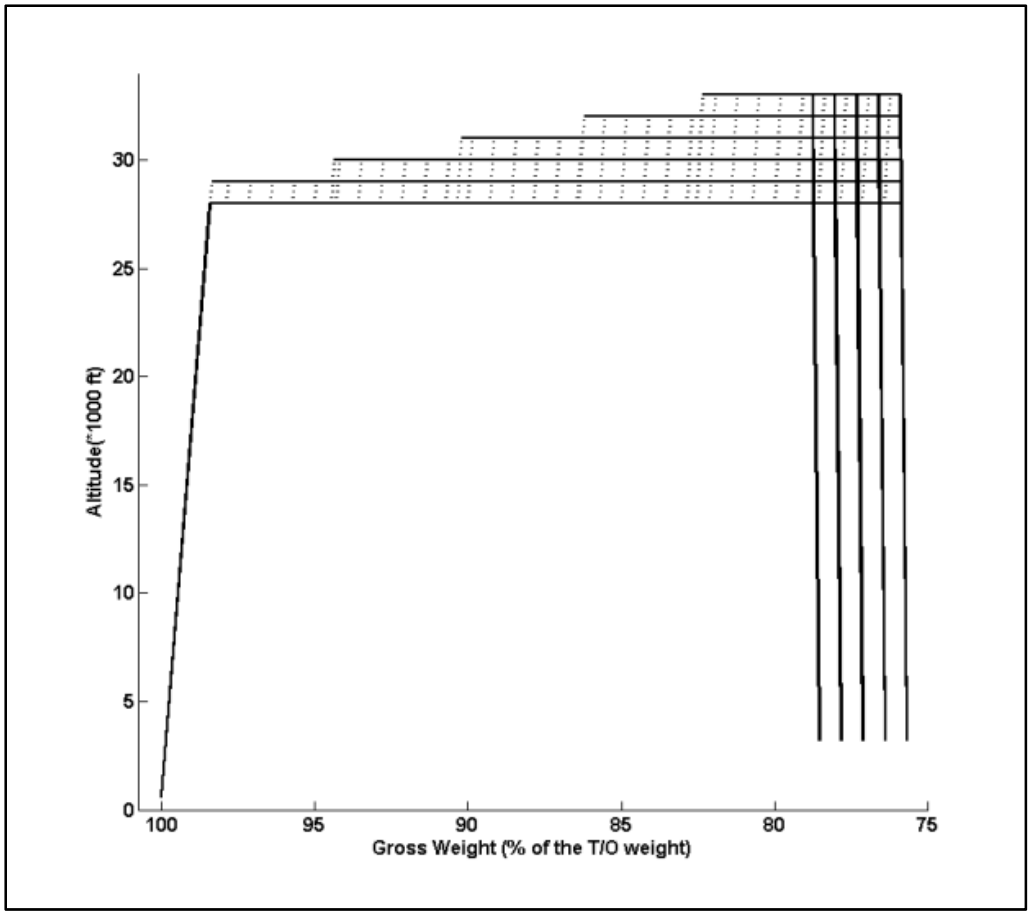

Figure-A II- 15 Vertical flight path graph corresponding to the vertical flight paths stored in the vertical flight path look-up structure: A33

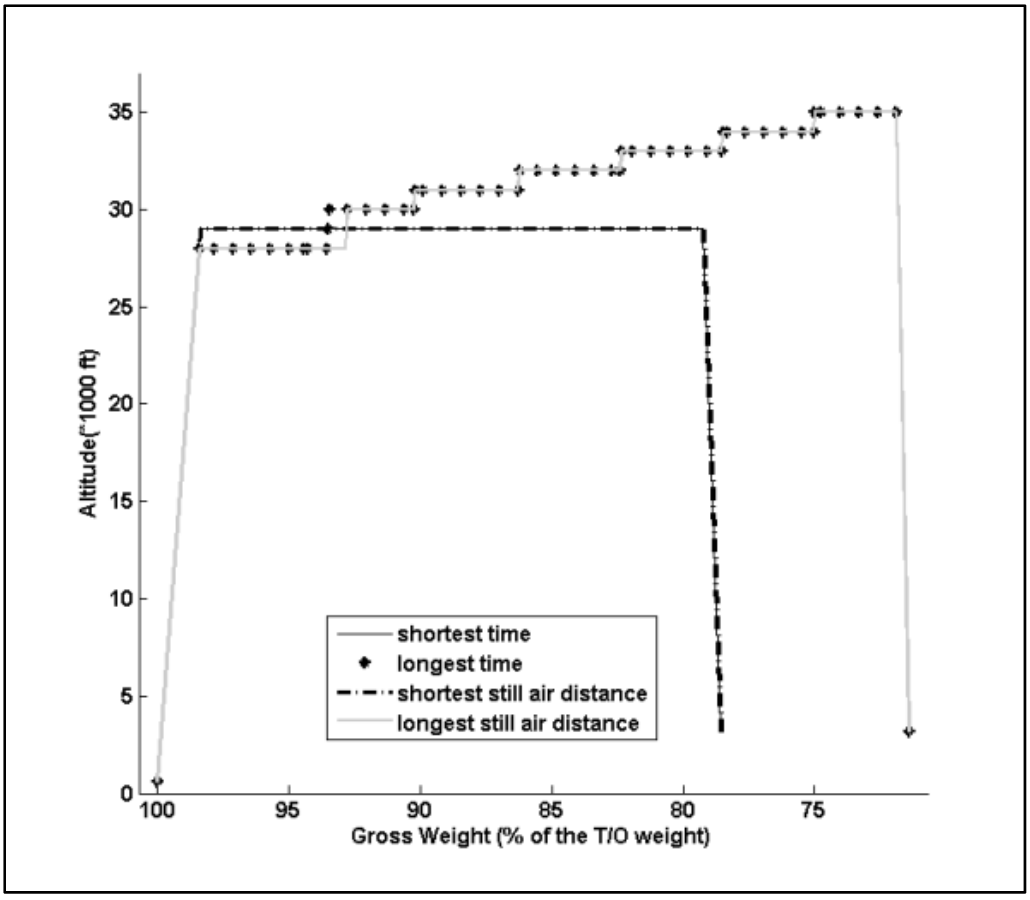

Figure-A II- 16 Vertical flight path profiles for the maximum and minimum flight-times and still-air distances: A11

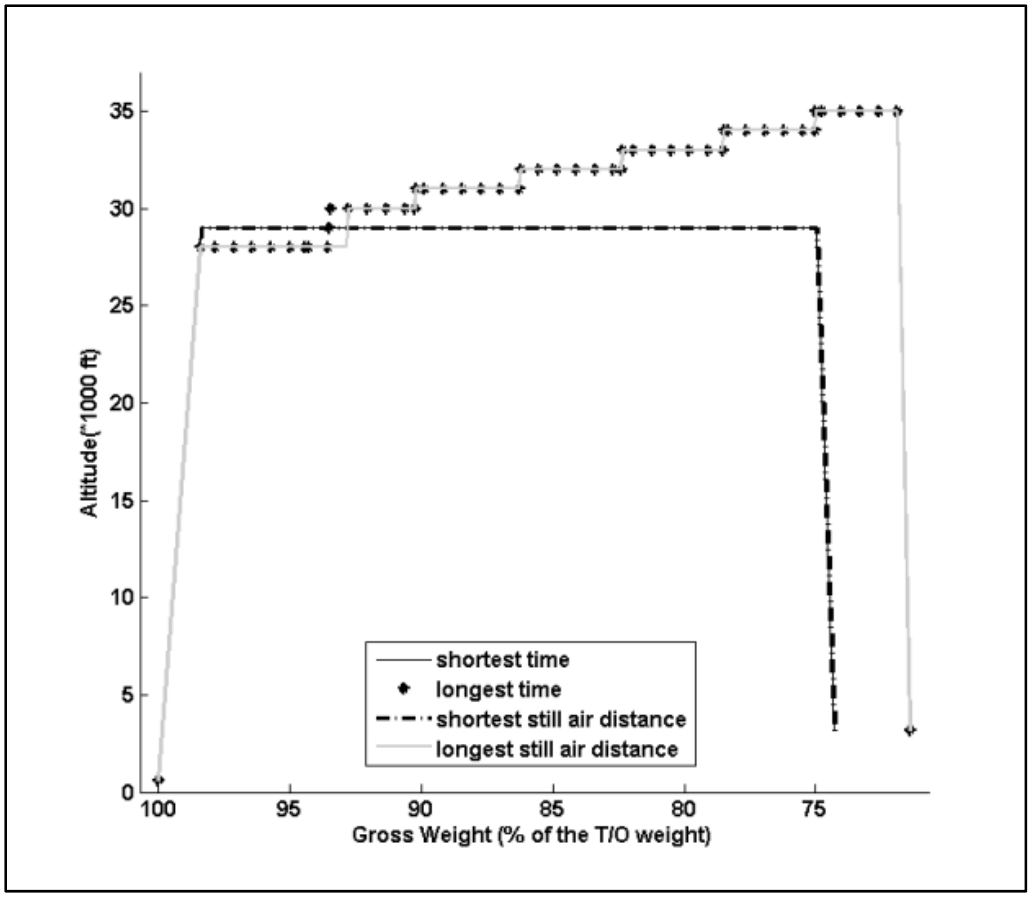

Figure-A II- 17 Vertical flight path profiles for the maximum and minimum flight-times and still-air distances: A12

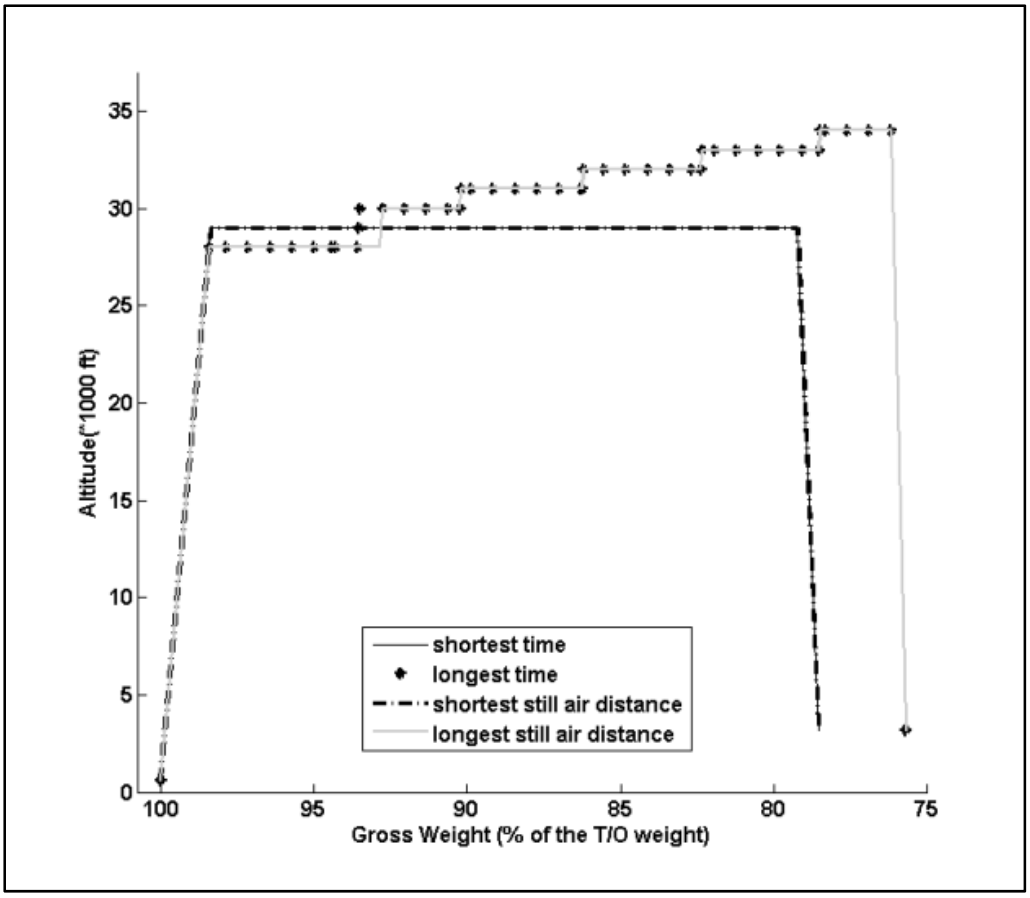

Figure-A II- 18 Vertical flight path profiles for the maximum and minimum flight-times and still-air distances: A13

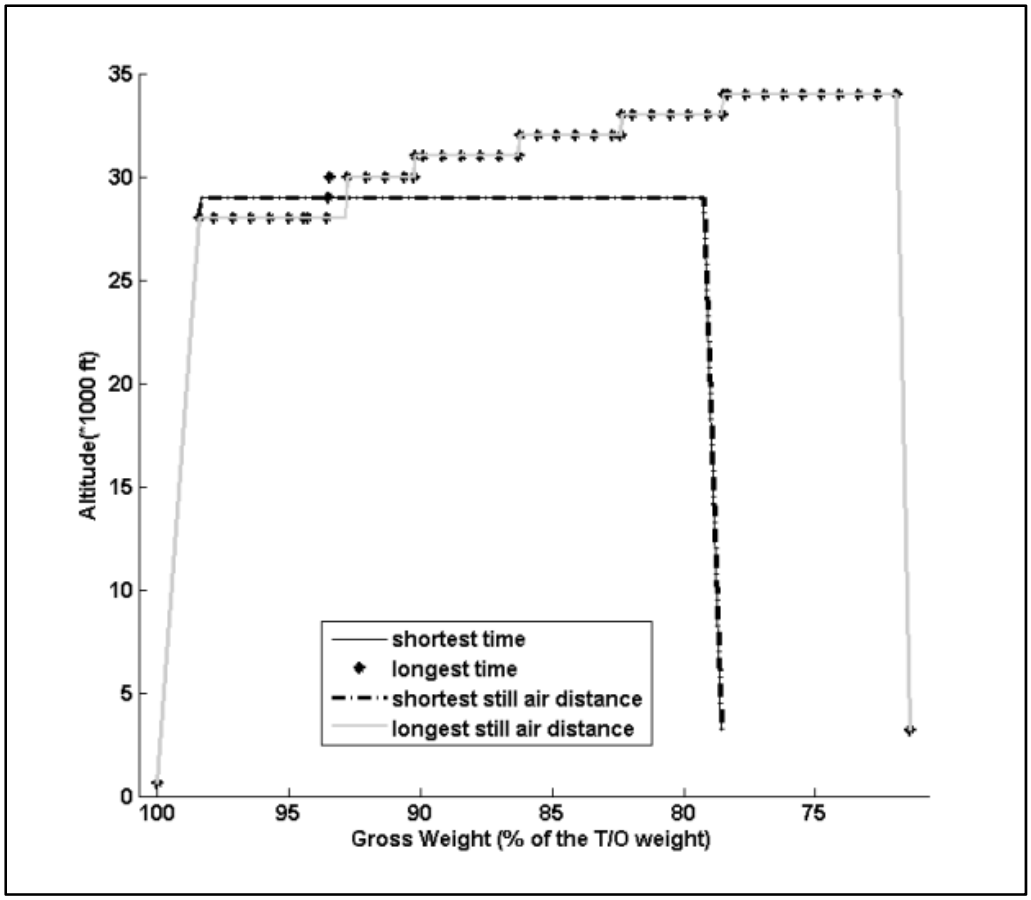

Figure-A II- 19 Vertical flight path profiles for the maximum and minimum flight-times and still-air distances: A21

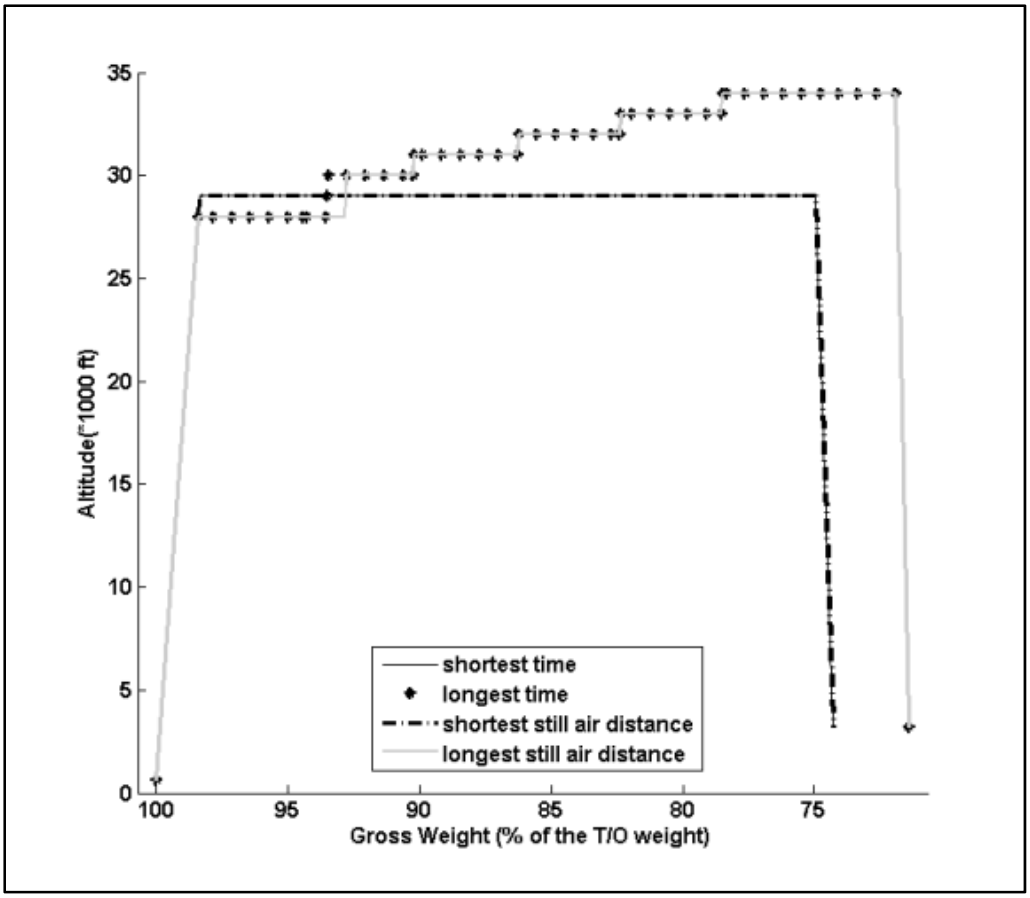

Figure-A II- 20 Vertical flight path profiles for the maximum and minimum flight-times and still-air distances: A22

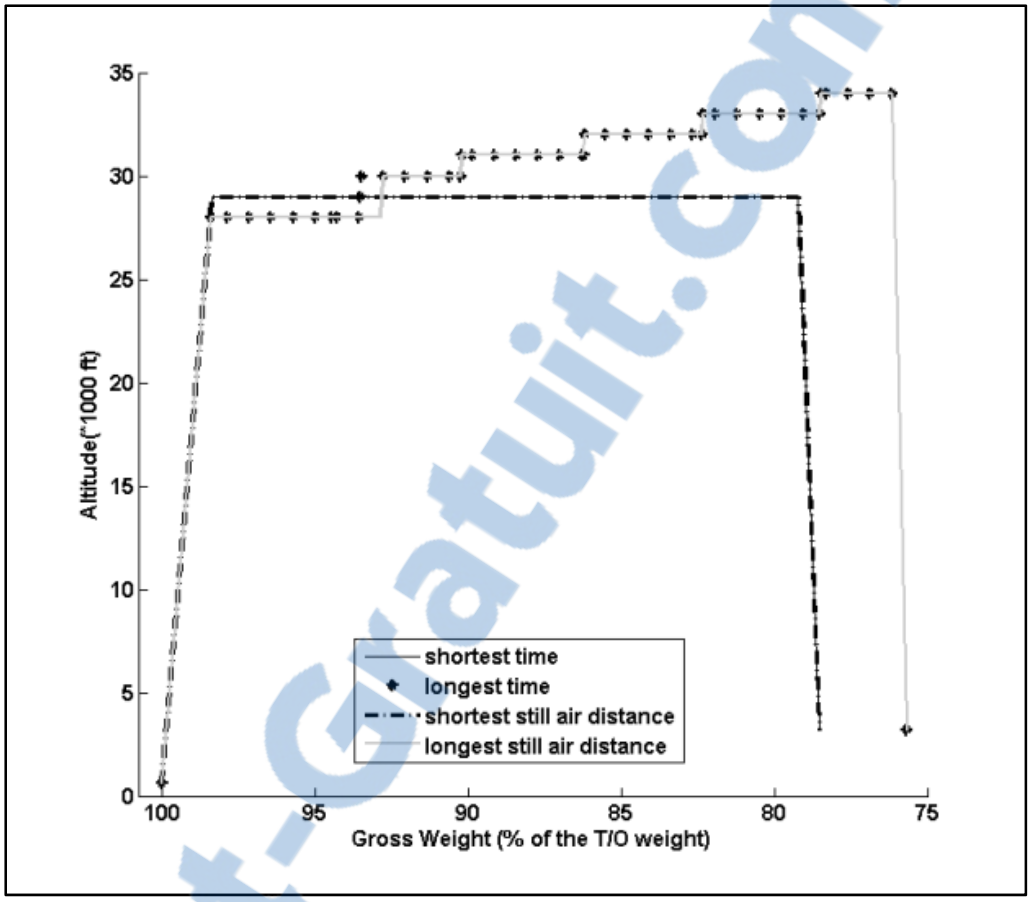

Figure-A II- 21 Vertical flight path profiles for the maximum and minimum flight-times and still-air distances: A23

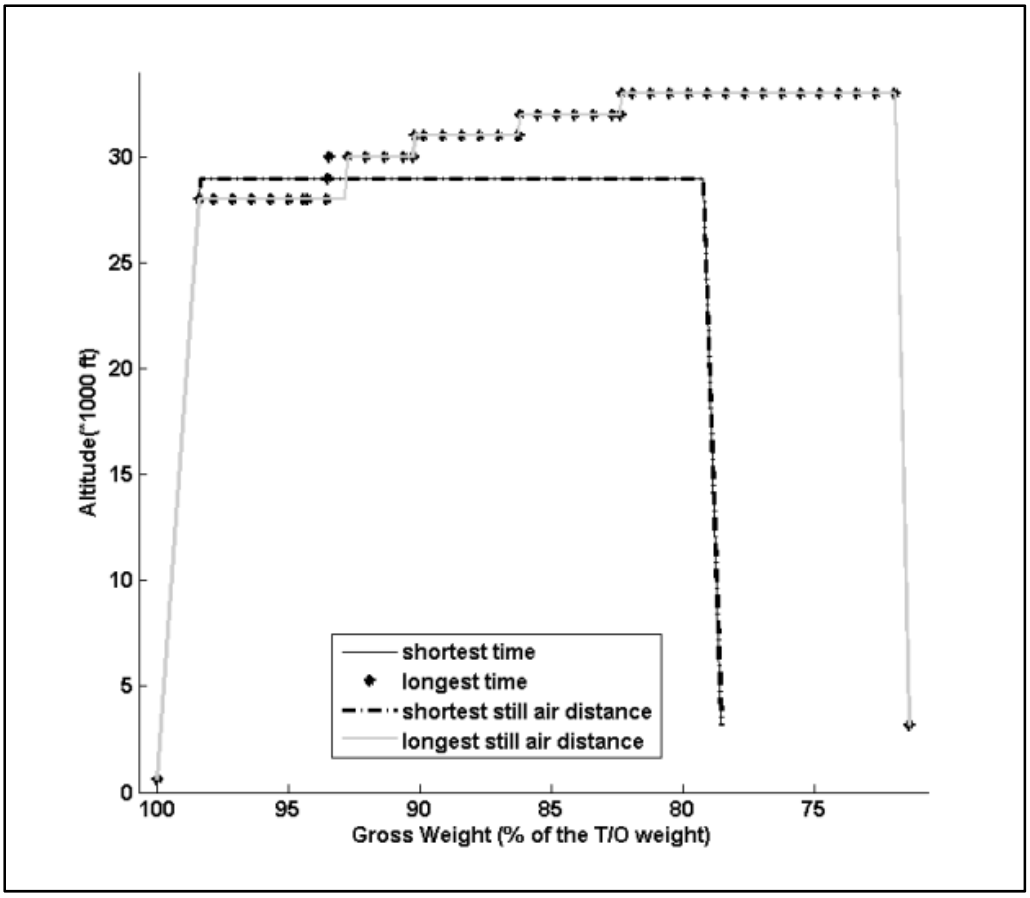

Figure-A II- 22 Vertical flight path profiles for the maximum and minimum flight-times and still-air distances: A31

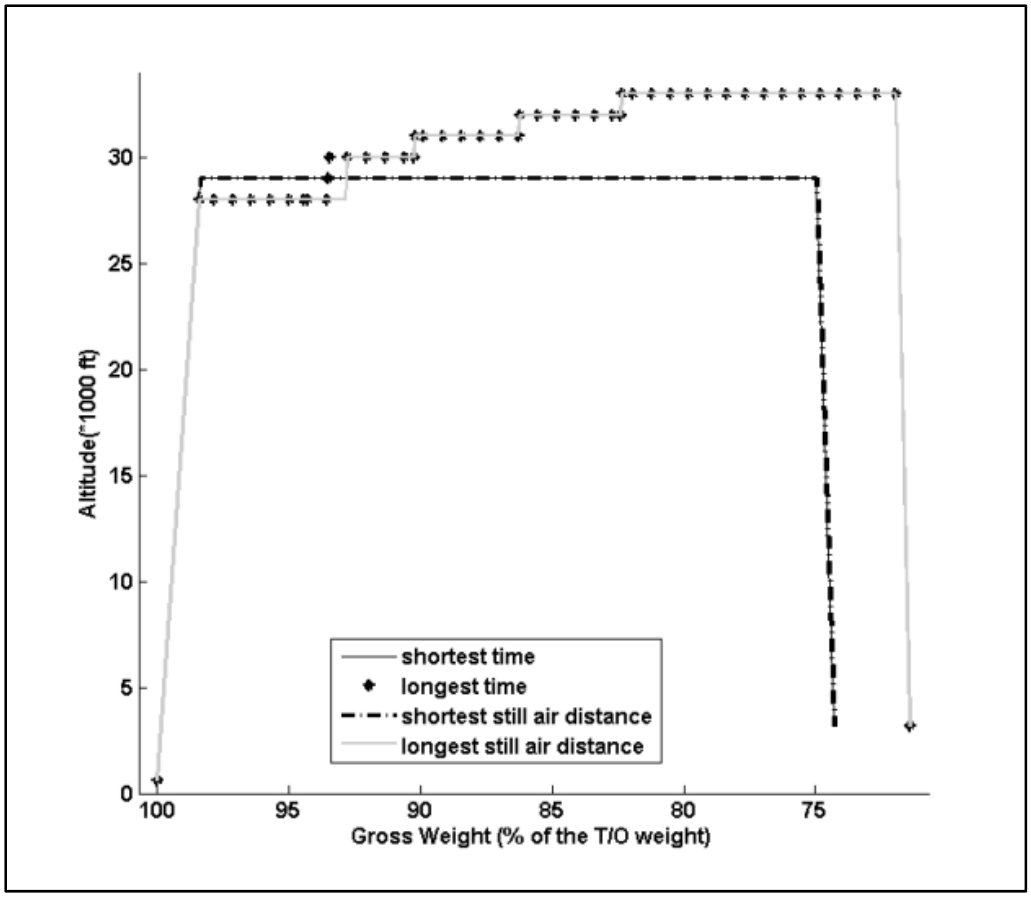

Figure-A II- 23 Vertical flight path profiles for the maximum and minimum flight-times and still-air distances: A32

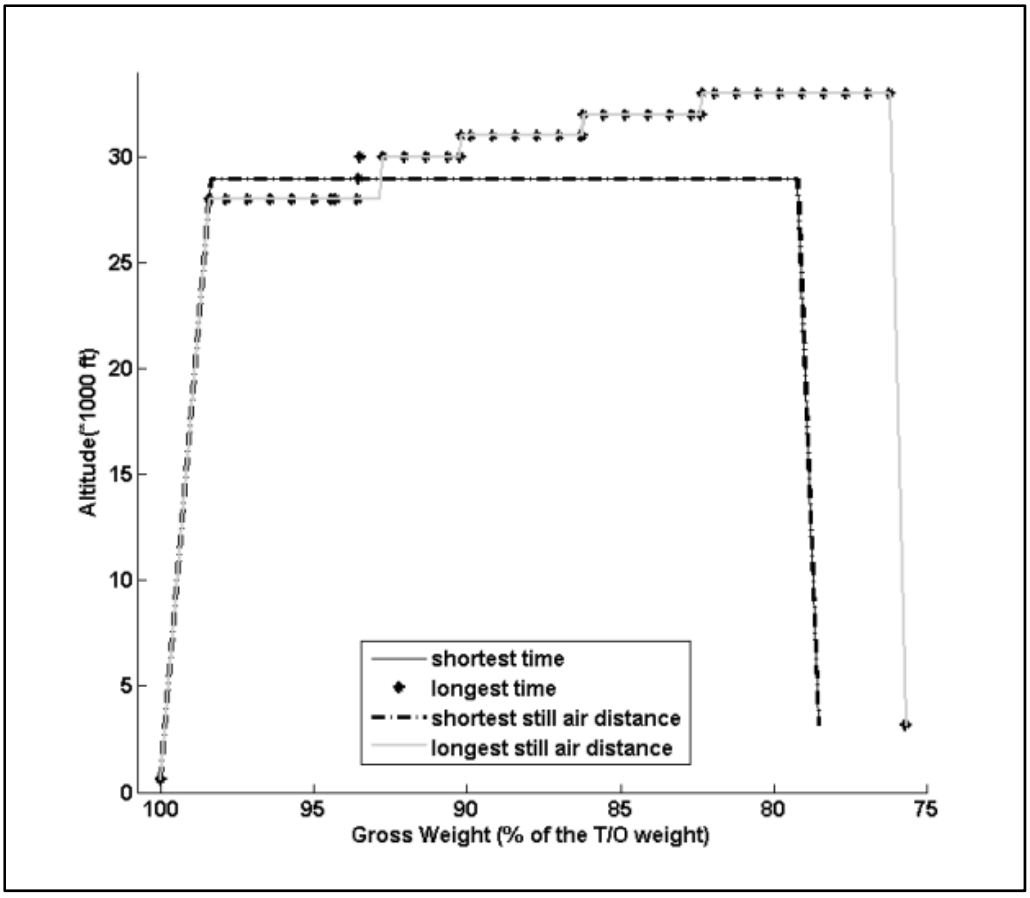

Figure-A II- 24 Vertical flight path profiles for the maximum and minimum flight-times and still-air distances: A33

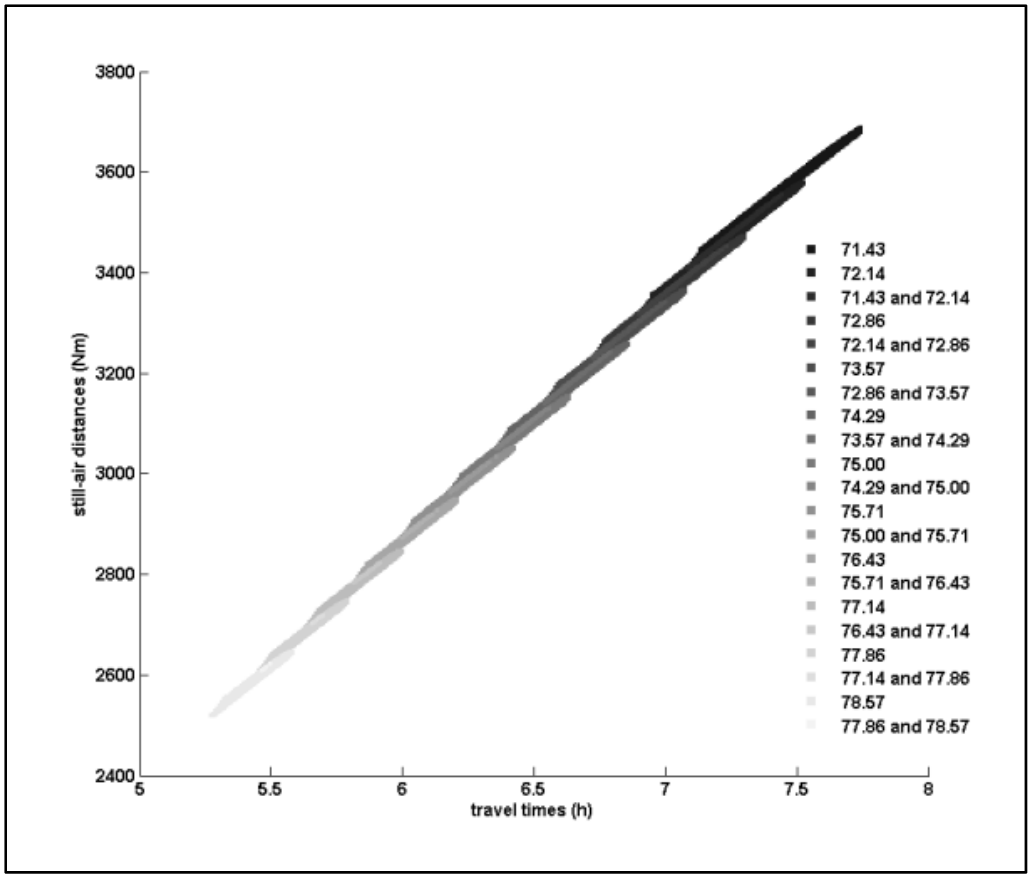

Figure-A II- 25 Vertical flight paths' flight-time and still-air distance domain distribution as function of the EOD gross weight value: A11

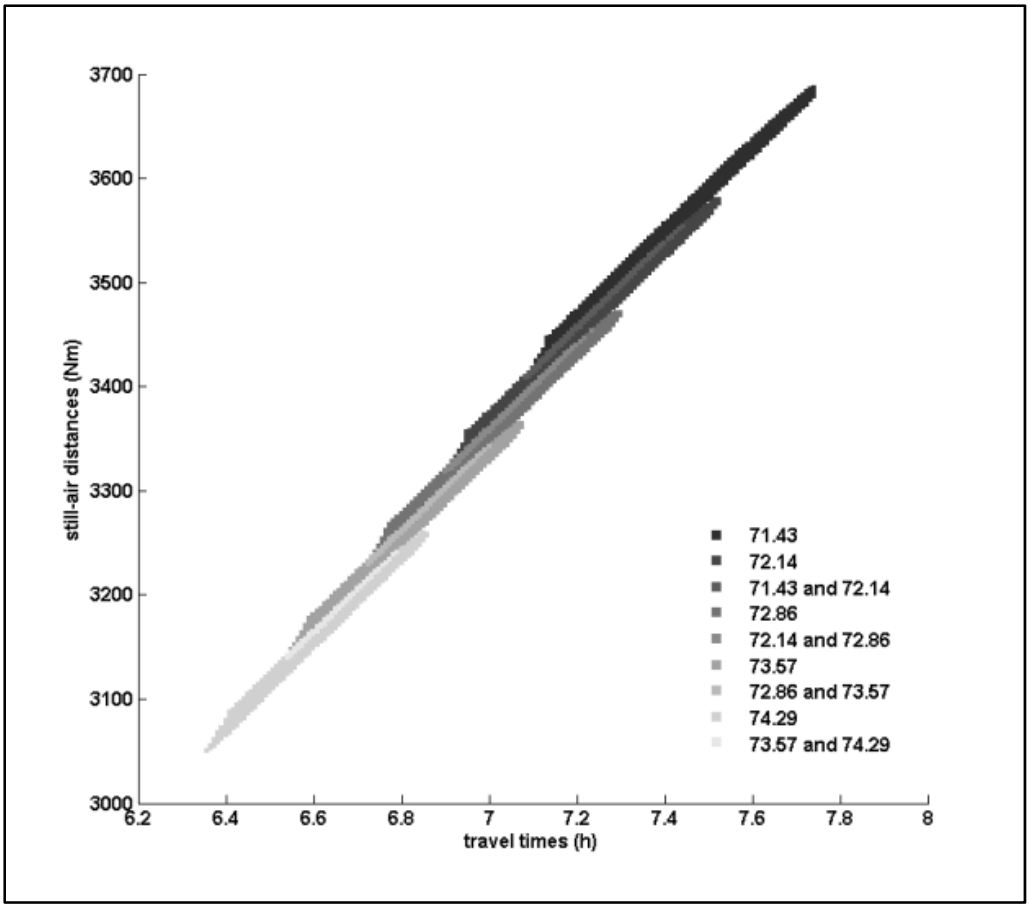

Figure-A II- 26 Vertical flight paths' flight-time and still-air distance domain distribution as function of the EOD gross weight value: A12

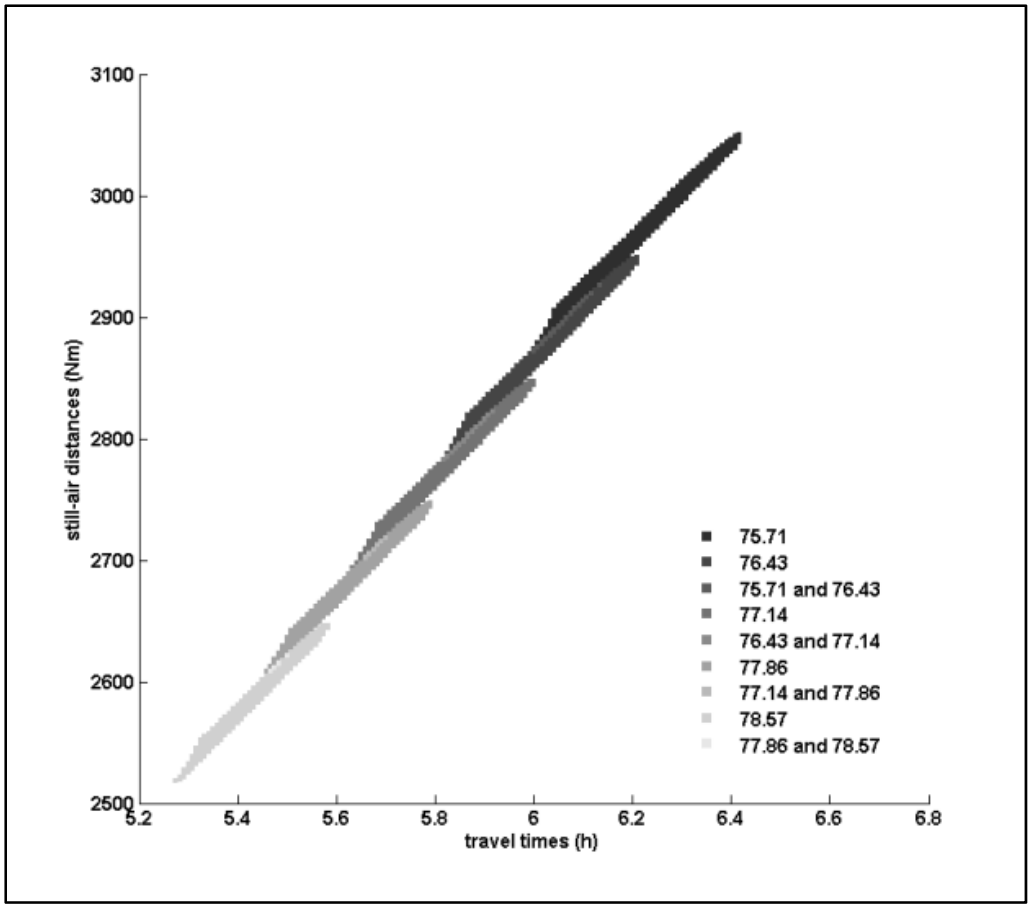

Figure-A II- 27 Vertical flight paths' flight-time and still-air distance domain distribution as function of the EOD gross weight value: A13

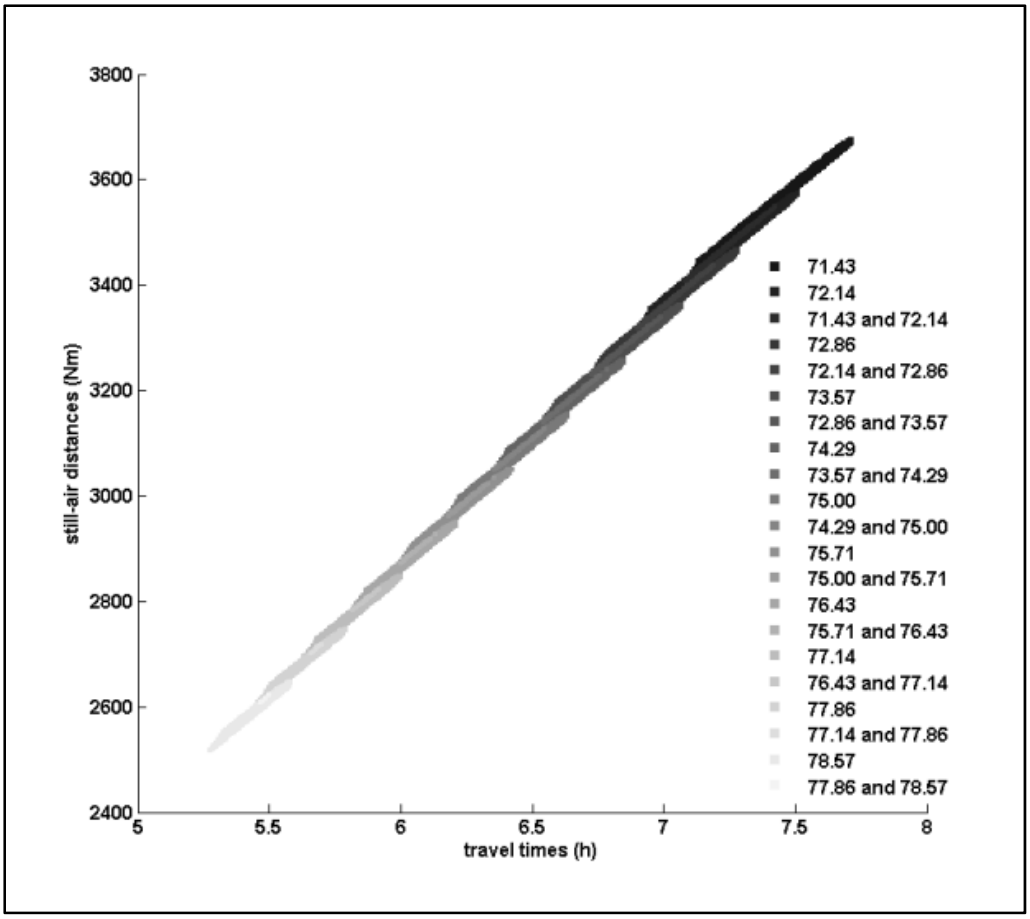

Figure-A II- 28 Vertical flight paths' flight-time and still-air distance domain distribution as function of the EOD gross weight value: A21

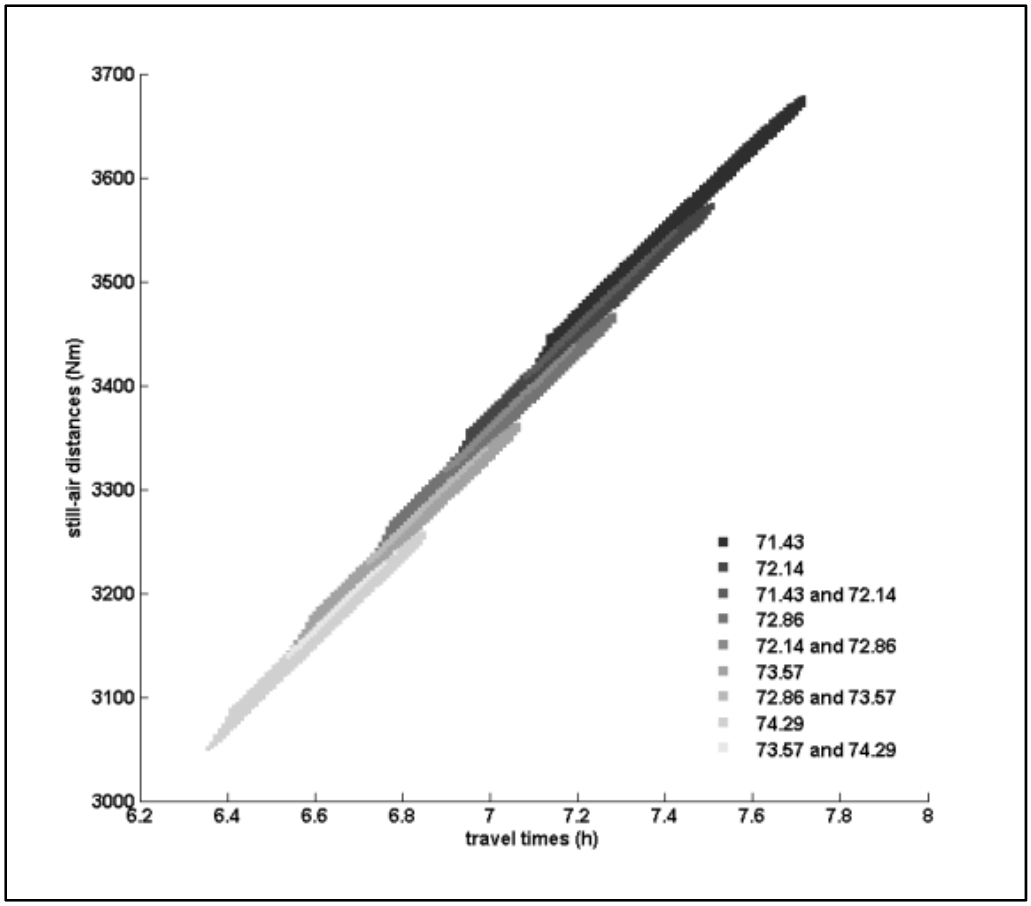

Figure-A II- 29 Vertical flight paths' flight-time and still-air distance domain distribution as function of the EOD gross weight value: A22

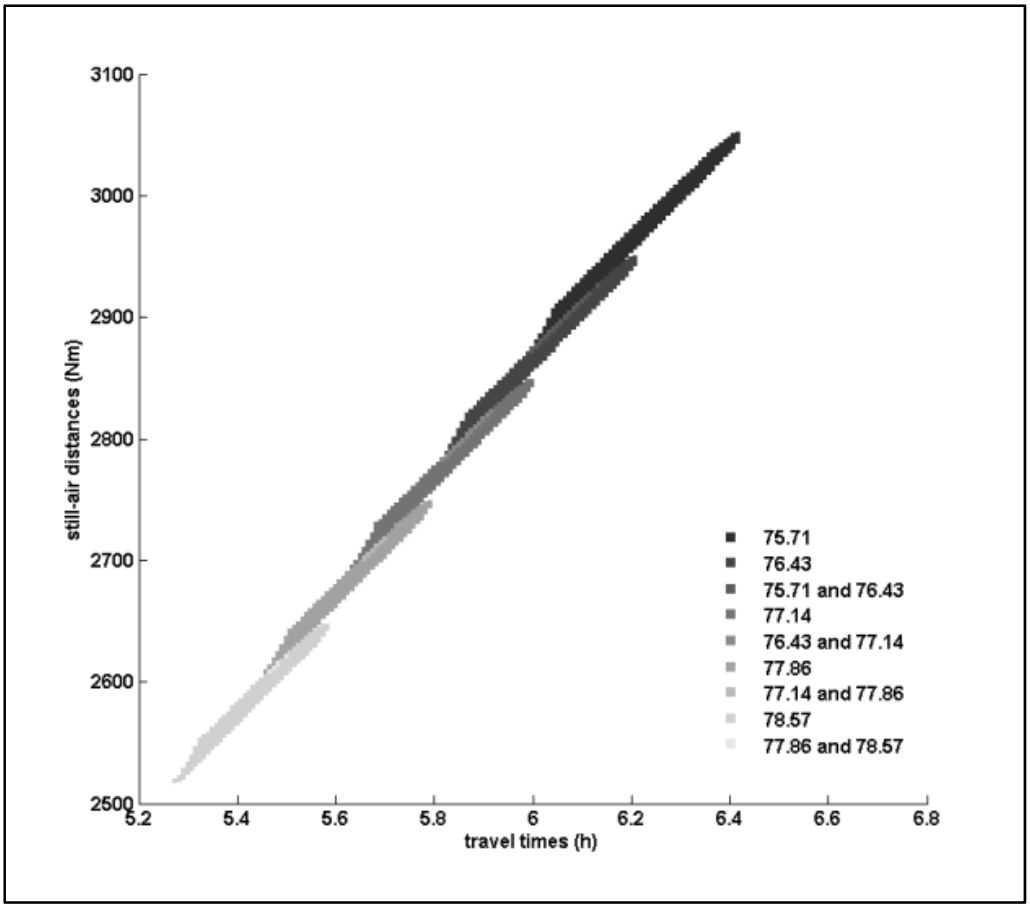

Figure-A II- 30 Vertical flight paths' flight-time and still-air distance domain distribution as function of the EOD gross weight value: A23

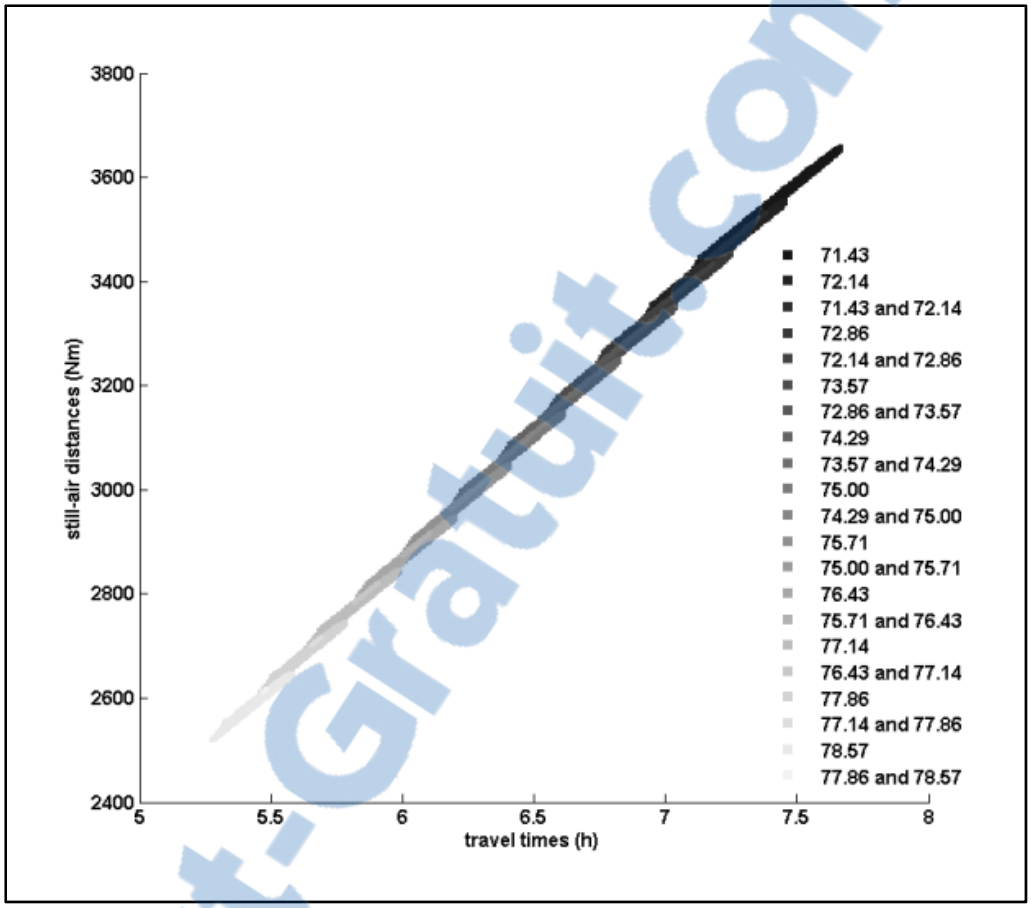

Figure-A II- 31 Vertical flight paths' flight-time and still-air distance domain distribution as function of the EOD gross weight value: A31

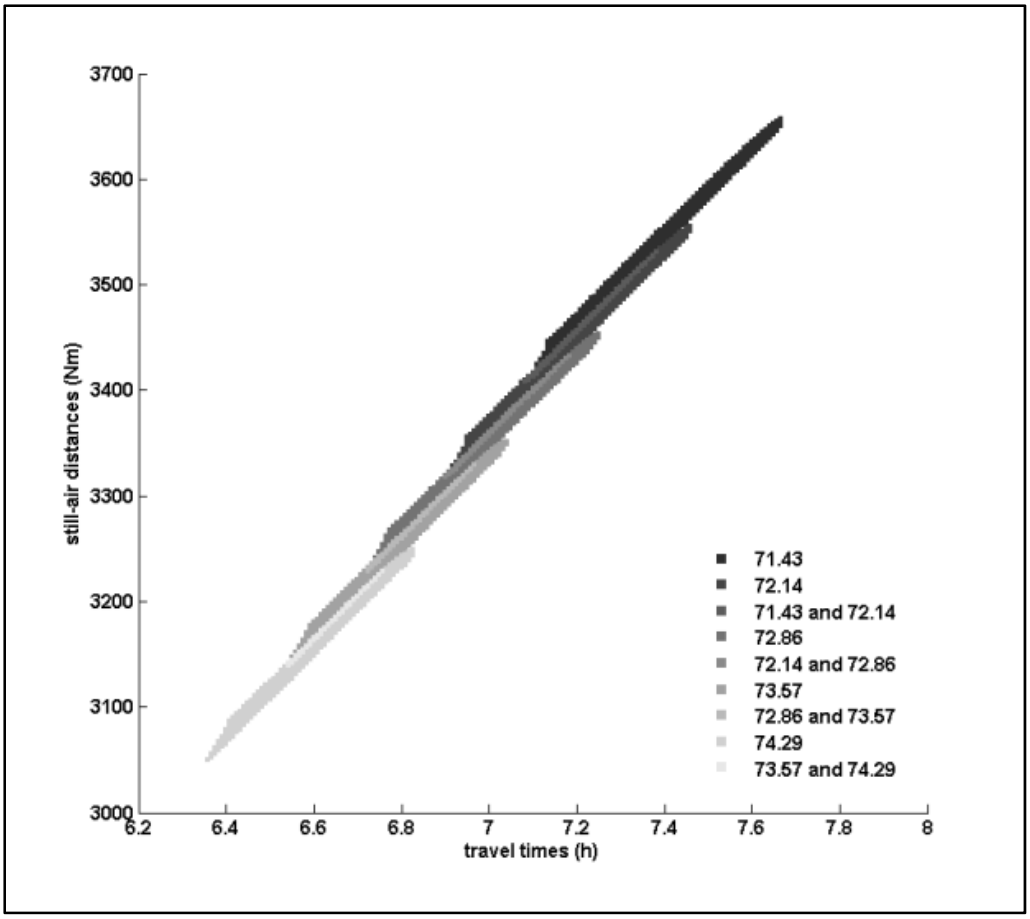

Figure-A II- 32 Vertical flight paths' flight-time and still-air distance domain distribution as function of the EOD gross weight value: A32

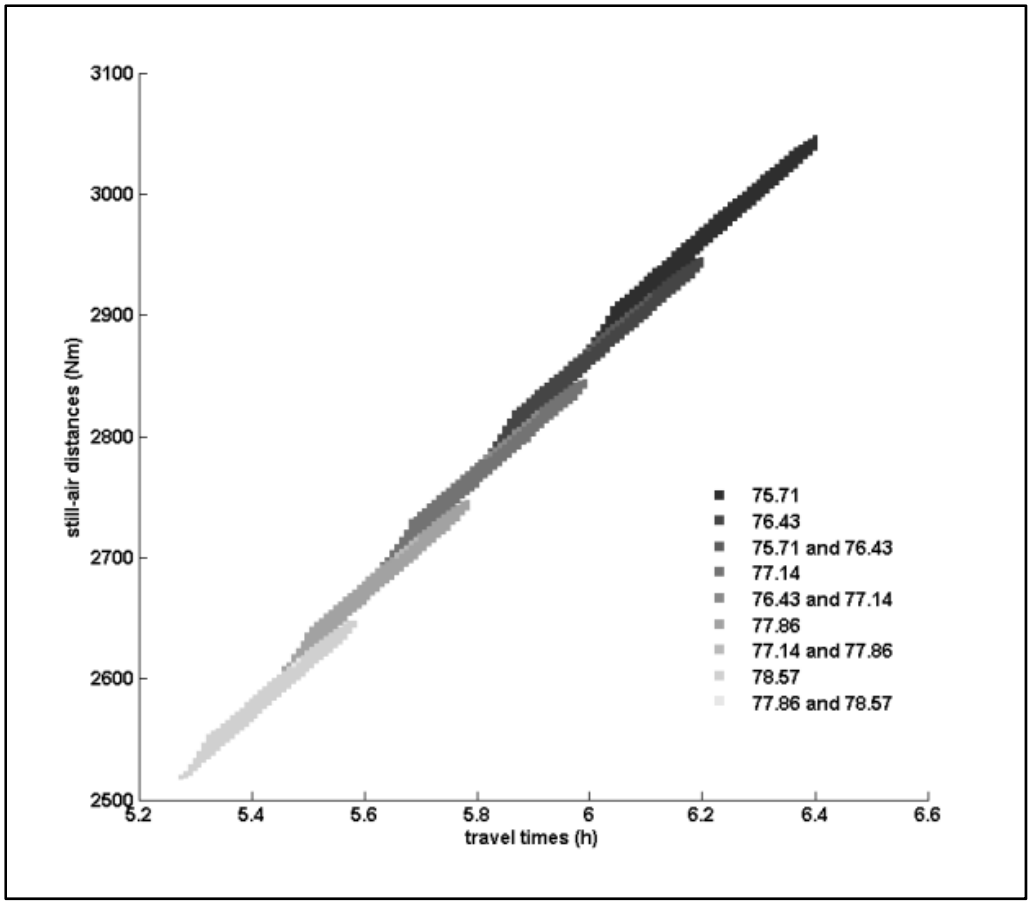

Figure-A II- 33 Vertical flight paths' flight-time and still-air distance domain distribution as function of the EOD gross weight value: A33

Table-A II- 1 Test case A11 –Statistical analysis of the number of vertical flight paths ending at an EOD gross weight that share the same flight time – still-air flight distance domain with vertical flight paths ending at each EOD gross weight, function of the EOD gross weight

EODGW(j) / EODGW(i)	71.43	72.14	72.86	73.57	74.29	75
71.43	35991369	108095	0	0	0	0
72.14	852813	27537924	59286	0	0	0
72.86	0	483300	20437355	31969	0	0
73.57	0	0	270045	14525812	16456	0
74.29	0	0	0	123031	9654533	3871
75	0	0	0	0	21766	2507121
75.71	0	0	0	0	0	8627
76.43	0	0	0	0	0	0
77.14	0	0	0	0	0	0
77.86	0	0	0	0	0	0
78.57	0	0	0	0	0	0

EODGW(j) / EODGW(i)	75.71	76.43	77.14	77.86	78.57
71.43	0	0	0	0	0
72.14	0	0	0	0	0
72.86	0	0	0	0	0
73.57	0	0	0	0	0
74.29	0	0	0	0	0
75	936	0	0	0	0
75.71	1930635	352	0	0	0
76.43	2640	1441797	121	0	0
77.14	0	1041	1030947	25	0
77.86	0	0	259	689185	3
78.57	0	0	0	9	180887

Table-A II- 2 Test case A12 – Statistical analysis of the number of vertical flight paths ending at an EOD gross weight that share the same flight time – still-air flight distance domain with vertical flight paths ending at each EOD gross weight, function of the EOD gross weight

EODGW(j) / EODGW(i)	71.43	72.14	72.86	73.57	74.29
71.43	35991369	108095	0	0	0
72.14	852813	27537924	59286	0	0
72.86	0	483300	20437355	31969	0
73.57	0	0	270045	14525812	16456
74.29	0	0	0	123031	9654533

Table-A II- 3 Test case A13 – Statistical analysis of the number of vertical flight paths ending at an EOD gross weight that share the same flight time – still-air flight distance domain with vertical flight paths ending at each EOD gross weight, function of the EOD gross weight

EODGW(j) / EODGW(i)	75.71	76.43	77.14	77.86	78.57
75.71	1930635	352	0	0	0
76.43	2640	1441797	121	0	0
77.14	0	1041	1030947	25	0
77.86	0	0	259	689185	3
78.57	0	0	0	9	180887

Table-A II- 4 Test case A21 – Statistical analysis of the number of vertical flight paths ending at an EOD gross weight that share the same flight time – still-air flight distance domain with vertical flight paths ending at each EOD gross weight, function of the EOD gross weight

EODGW(j) / EODGW(i)	71.43	72.14	72.86	73.57	74.29	75
71.43	7100569	31327	0	0	0	0
72.14	174859	5911543	17374	0	0	0
72.86	0	121869	4871279	9641	0	0
73.57	0	0	66676	3965703	4296	0
74.29	0	0	0	32980	3181710	1957
75	0	0	0	0	15313	2507120
75.71	0	0	0	0	0	8627
76.43	0	0	0	0	0	0
77.14	0	0	0	0	0	0
77.86	0	0	0	0	0	0
78.57	0	0	0	0	0	0

EODGW(j) / EODGW(i)	75.71	76.43	77.14	77.86	78.57
71.43	0	0	0	0	0
72.14	0	0	0	0	0
72.86	0	0	0	0	0
73.57	0	0	0	0	0
74.29	0	0	0	0	0
75	936	0	0	0	0
75.71	1930635	352	0	0	0
76.43	2640	1441797	121	0	0
77.14	0	1041	1030947	25	0
77.86	0	0	259	689185	3
78.57	0	0	0	9	180887

Table-A II- 5 Test case A22 – Statistical analysis of the number of vertical flight paths ending at an EOD gross weight that share the same flight time – still-air flight distance domain with vertical the EOD gross weight

EODGW(j) / EODGW(i)	71.43	72.14	72.86	73.57	74.29
71.43	7100569	31327	0	0	0
72.14	174859	5911543	17374	0	0
72.86	0	121869	4871279	9641	0
73.57	0	0	66676	3965703	4296
74.29	0	0	0	32980	3181710

Table-A II- 6 Test case A23 – Statistical analysis of the number of vertical flight paths ending at an EOD gross weight that share the same flight time – still-air flight distance domain with vertical flight paths ending at each EOD gross weight, function of the EOD gross weight

EODGW(j) / EODGW(i)	75.71	76.43	77.14	77.86	78.57
75.71	1930635	352	0	0	0
76.43	2640	1441797	121	0	0
77.14	0	1041	1030947	25	0
77.86	0	0	259	689185	3
78.57	0	0	0	9	180887

Table-A II- 7 Test case A31 – Statistical analysis of the number of vertical flight paths ending at an EOD gross weight that share the same flight time – still-air flight distance domain with vertical flight paths ending at each EOD gross weight, function of the EOD gross weight

EODGW(j) / EODGW(i)	71.43	72.14	72.86	73.57	74.29	75
71.43	1040264	8301	0	0	0	0
72.14	28847	905576	4916	0	0	0
72.86	0	18139	783993	3194	0	0
73.57	0	0	11621	674590	1459	0
74.29	0	0	0	6745	576485	739
75	0	0	0	0	3481	488838
75.71	0	0	0	0	0	1835
76.43	0	0	0	0	0	0
77.14	0	0	0	0	0	0
77.86	0	0	0	0	0	0
78.57	0	0	0	0	0	0

EODGW(j) / EODGW(i)	75.71	76.43	77.14	77.86	78.57
71.43	0	0	0	0	0
72.14	0	0	0	0	0
72.86	0	0	0	0	0
73.57	0	0	0	0	0
74.29	0	0	0	0	0
75	249	0	0	0	0
75.71	410850	94	0	0	0
76.43	688	341762	43	0	0
77.14	0	128	280854	8	0
77.86	0	0	35	227444	2
78.57	0	0	0	8	180887

Table-A II- 8 Test case A32 – Statistical analysis of the number of vertical flight paths ending at an EOD gross weight that share the same flight time – still-air flight distance domain with vertical flight paths ending at each EOD gross weight, function of the EOD gross weight

EODGW(j) / EODGW(i)	71.43	72.14	72.86	73.57	74.29
71.43	1040264	8301	0	0	0
72.14	28847	905576	4916	0	0
72.86	0	18139	783993	3194	0
73.57	0	0	11621	674590	1459
74.29	0	0	0	6745	576485

Table-A II- 9 Test case A33 – Statistical analysis of the number of vertical flight paths ending at an EOD gross weight that share the same flight time – still-air flight distance domain with vertical flight paths ending at each EOD gross weight, function of the EOD gross weight

EODGW(j) / EODGW(i)	75.71	76.43	77.14	77.86	78.57
75.71	410850	94	0	0	0
76.43	688	341762	43	0	0
77.14	0	128	280854	8	0
77.86	0	0	35	227444	2
78.57	0	0	0	8	180887

Table-A II- 10 Vertical flight path modules' and total average execution times (in seconds)

Vertical flight path module	Average execution time (s)				
	A11	A12	A13	A21	A22
Maximum altitude function of gw	3.134	3.144	3.139	3.134	3.154
Climb flight path and TOC	0.595	0.599	0.599	0.596	0.590
Descent flight paths and TODs	3.109	3.030	3.763	2.953	2.861
Step-Climb flight paths	9.437	10.202	8.465	9.059	9.731
Level-flight fuel burn tables initialization	0.034	0.034	0.034	0.034	0.034
Level-flight fuel burn tables construction	36.898	36.801	36.887	29.341	29.325
Vertical flight path graph construction	0.302	0.343	0.241	0.281	0.307
Algorithm's execution time evaluation method					
As a sum of the composing vertical flight path modules' execution times	53.512	54.155	53.130	45.402	46.004
Algorithm code – integrating the vertical flight path modules	53.747	54.147	53.153	45.361	45.816

Vertical flight path module	Average execution time (s)			
	A23	A31	A32	A33
Maximum altitude function of gw	3.147	3.126	3.142	3.153
Climb flight path and TOC	0.603	0.592	0.593	0.594
Descent flight paths and TODs	3.561	2.854	2.769	3.534
Step-Climb flight paths	8.409	8.629	9.2	7.969
Level-flight fuel burn tables initialization	0.034	0.034	0.034	0.034
Level-flight fuel burn tables construction	29.360	26.095	25.951	25.873
Vertical flight path graph construction	0.241	0.247	0.276	0.215
Algorithm's execution time evaluation method				
As a sum of the composing vertical flight path modules' execution times	45.357	41.580	41.967	41.377
Algorithm code – integrating the vertical flight path modules	45.312	41.184	41.846	41.554

LIST OF REFERENCES

Agard, S. B. & Gehring, F. W. (1965). Angles and quasiconformal mappings. *Proceedings of the London Mathematical Society*, s3-14A (1), 1-21. DOI: 10.1112/plms/s3-14A.1.1

Ardema, M. D. & Asuncion, B. C. (2009). Flight path optimization at constant altitude. In Buttazzo, G. & Frediani, A. (Eds), *Variational Analysis and Aerospace Engineering* (pp. 21-32). New York, NY: Springer-Verlag. DOI: 10.1007/978-0-387-95857-6_2

Asselin, M. (1997). *AIAA Education Series: An Introduction to Aircraft Performance. Reston*, VA: American Institute of Aeronautics and Astronautics. DOI: 10.2514/4.861529

Benavides, J. V., Kaneshige, J., Sharma, S., Panda, R. & Steglinski, M. (2014, June). *Implementation of a trajectory prediction function for trajectory based operations*. Paper presented at AIAA Atmospheric Flight Mechanics Conference, Atlanta, GA (p. 2198). DOI: 10.2514/6.2014-2198

Beulze, B., Dancila, B., Botez, R., Bottollier-Lemallaz, S. & Herda, S. (2015, June). *Presentation of three methods results comparison for Vertical Navigation VNAV trajectory optimization for the Flight Management System FMS*. Paper presented at 15th AIAA Aviation Technology, Integration, and Operations Conference, Dallas, TX USA.

Bijlsma, S. J. (2009). Optimal Aircraft Routing in General Wind Fields, *Journal of Guidance, Control, and Dynamics*, *32*(3), pp. 1025-1029.

Bilimoria, K. D. & Shepard, M. L. (1989, August). *Optimization of aircraft cruise performance*. Paper presented at AIAA Atmospheric Flight Mechanics Conference, Boston, MA, (pp. 338-347). DOI: 10.2514/6.1989-3386

Bonami, P., Olivares, A., Soler, M. & Staffetti, E. (2013). Multiphase Mixed-Integer Optimal Control Approach to Aircraft Trajectory Optimization, *Journal of Guidance, Control, and Dynamics*, *36*(5), pp. 1267-1277.

Bonnefoy, P. & Hansman, R. J. (2010, September). *Operational Implications of Cruise Speed Reductions for Next Generation Fuel Efficient Subsonic Aircraft*. Paper presented at 27th International Congress of the Aeronautical Sciences, Nice, France (sn). Retrieved from http://www.icas.org/ICAS_ARCHIVE/ICAS2010/PAPERS/503.PDF

Botez, R. M. & Fays, J. (2013, February). *Aircraft trajectories generation by use of no fly zones self-management for a flight management system*. Paper presented at AIAC15: 15th Australian International Aerospace Congress, Melbourne, Australia (pp. 60-73).

Retrieved from https://www.researchgate.net/profile/Ruxandra_Botez/publication/270961331_Aircraft_trajectories_generation_by_use_of_No_Fly_Zones_self_management_for_a_Flight_Management_System/links/54c431160cf256ed5a93ed4a/Aircraft-trajectories-generation-by-use-of-No-Fly-Zones-self-management-for-a-Flight-Management-System.pdf

Bousson, K. & Machado, P. (2010). 4D Flight Trajectory Optimization Based on Pseudospectral Methods. *International Journal of Mechanical, Aerospace, Industrial, Mechatronic and Manufacturing Engineering*, *4*(9), pp. 879-885. Retrieved from http://www.waset.org/publications/11036/4d-flight-trajectory-optimization-based-on-pseudospectral-methods

Bowring, B. R. (1983). The geodesic inverse problem. *Journal of Geodesy*, *57*(1), 109-120.

Brunilde, G., Lapasset, L., Delahaye, D., Rabut, C. & Brenier, Y. (2013, July). *Generating optimal aircraft trajectories with respect to weather conditions*. Paper presented at ISIATM 2013, 2nd International Conference on Interdisciplinary Science for Innovative Air Traffic Management, Toulouse, France. Retrieved from https://hal-enac.archives-ouvertes.fr/hal-00867818/

Bureau of Transportation Statistics (2017). Airline Fuel Cost and Consumption (US Carriers - Scheduled). Retrieved from https://www.transtats.bts.gov/fuel.asp on July 11, 2017

Cano, M., Dorado, M. M. & Sánchez-Escalonilla, P. (2007, October). *Complexity analysis in the next generation of air traffic management system*. Paper presented at Digital Avionics Systems Conference, 2007. DASC'07. IEEE/AIAA 26th. Dallas, TX (pp. 3-D). DOI: 10.1109/DASC.2007.4391890

Caron, G. M. & Hadjaz, A. (2011, June). *Beta-mesh - A dynamic 3D mesh modelization*. Paper presented at American Control Conference (ACC) 2011, San Francisco, CA (pp. 2148-2153). DOI: 10.1109/ACC.2011.5991291

Dancila, B. D. (2011). *Altitude optimization algorithm for cruise, constant speed and level flight segments*. (Master's thesis, École de Technologie Supérieure, Montréal, QC).

Dancila, B. D., Botez, R. M. & Labour, D. (2012, August). *Altitude optimization algorithm for cruise, constant speed and level flight segments*. Paper presented at AIAA Guidance, Navigation, and Control Conference, Mineapolis, MI, USA.

Dancila, B. D., Botez, R. & Labour, D. (2013). Fuel burn prediction algorithm for cruise, constant speed and level flight segments. *The Aeronautical Journal*, *117*(1191), pp. 491-504.

Dancila, B. D. & Botez, R. (2014, June). *Construction of an aircraft's VNAV flight envelope for in-FMS flight trajectory computation and optimization*. Paper presented at 14th

AIAA Aviation Technology, Integration, and Operations Conference, Atlanta, GA, USA.

Dancila, B. D. & Botez, R. M. (2016). Geographical area selection and construction of a corresponding routing grid used for in-flight management system flight trajectory optimization. *Proceedings of the Institution of Mechanical Engineers, Part G: Journal of Aerospace Engineering*, *231*(5), pp. 809-822. DOI: 10.1177/09544100 16643104

Dancila, B. D., Beulze, B. & Botez, R. M. (2016, August). *Geometrical Vertical Navigation Trajectory Optimization–Comparative Performance Evaluation of Phase versus Phase and Altitude-Dependent Preferred Gradient Selection*. Paper presented at 20th IFAC Symposium on Automatic Control in Aerospace - ACA 2016, Sherbrooke, Quebec, Canada.

Dancila, R., Botez, R. & Ford, S. (2014). Fuel burn and emissions evaluation for a missed approach procedure performed by a B737-400. *The Aeronautical Journal*, *118*(1209), pp. 1329-1348.

de Grado, J. G. & Tascon, C. S. (2011, June). *On the development of a digital meteorological model for simulating future air traffic management automation*. Paper presented at Enabling Technologies: Infrastructure for Collaborative Enterprises (WETICE), 2011 20th IEEE International Workshops on, Paris, France (pp. 223-228). DOI: 10.1109/WETICE.2011.40

Deakin, R. E. (2004, April). *A guide to the mathematics of map projections*. Paper presented at the Victorian Tasmanian Survey Conference Across the Strait, Launceston Tasmania, Australia. Retrieved from https://www.researchgate.net/profile/ Rod_Deakin/publication/228492443_A_GUIDE_TO_THE_MATHEMATICS_OF_ MAP_PROJECTIONS/links/0fcfd50bc384bae723000000.pdf

Devulapalli, R. (2012). *An efficient algorithm for commercial aircraft trajectory optimization in the air traffic system*. (Doctoral disertation, University of Minnesota, Minneapolis). Retrieved from ProQuest Dissertations & Theses Global. (1081743480).

Dunn, C. D. (2008, May). *Weather data processing: Display of aviation weather*. Paper presented at Integrated Communications, Navigation and Surveillance Conference, 2008, ICNS 2008, Bethesda, MD (pp. 1-9). DOI: 10.1109/ICNSURV.2008.4559187

Durrieu, G., Faugère, M., Girbal, S., Pérez, D. G., Pagetti, C., & Puffitsch, W. (2014, February). *Predictable flight management system implementation on a multicore processor*. Paper presented at Embedded Real Time Software (ERTS'14), Toulouse, France. Retrieved from https://hal.archives-ouvertes.fr/hal-01121700/

Engels, J., & Grafarend, E. (1995). The oblique Mercator projection of the ellipsoid of revolution IE a 2, b. *Journal of Geodesy*, *70*(1), 38-50. DOI: 10.1007/BF00863417

Environment Canada, (2013). Analyses and Modelling - Environment Canada [HTML]. Retrieved from https://weather.gc.ca/mainmenu/modelling_menu_e.html

Erzberger, H., McLean, J.D. & Barman, J.F. (1975). *Fixed-range optimum trajectories for short-haul aircraft* (Report No. NASA-TN-D-8115, A-5874). Retrieved from https://ntrs.nasa.gov/archive/nasa/casi.ntrs.nasa.gov/19760005964.pdf

Erzberger, H. & Lee, H. (1978). *Characteristics of constrained optimum trajectories with specified range* (Report No. NASA-TM-78519, A-7592). Retrieved from https://ntrs.nasa.gov/archive/nasa/casi.ntrs.nasa.gov/19780022129.pdf

Erzberger, H. & McLean, J.D. (1981). Fuel-conservative guidance system for powered-lift aircraft. *Journal of Guidance, Control and Dynamics*, *4*(3), pp. 253-261.

Erzberger, H. & Paielli, R. A. (2002). Concept for next generation air traffic control system. *Air Traffic Control Quarterly*, *10*(4), pp. 355-378.

Federal Aviation Administration. (2007). *Aircraft Weight and Balance Handbook* (FAA-H-8083-1A). Oklahoma City, OK: U.S. Department of Transporation, Federal Aviation Administration, Airmen Testing Standards Branch.

Félix Patrón, R. S., Botez, R. M. & Labour, D. (2012, October). *Vertical profile optimization for the Flight Management System CMA-9000 using the golden section search method*. Paper presented at IECON 2012 - 38th Annual Conference on IEEE Industrial Electronics Society, Montréal, QC (pp. 5482-5488). DOI: 10.1109/IECON.2012.6389517

Félix Patrón, R. S., Kessaci, A., Botez, R. M. & Labour, D. (2013, August). *Flight trajectories optimization under the influence of winds using genetic algorithms*. Paper presented at AIAA Guidance, Navigation, and Control (GNC) Conference, Boston, MA (p. 4620). DOI: 10.2514/6.2013-4620

Félix Patrón, R. S., Botez, R. M. & Labour, D. (2013). New altitude optimisation algorithm for the flight management system CMA-9000 improvement on the A310 and L-1011 aircraft. *The Aeronautical Journal*, *117*(1194), 787-805. DOI: 10.1017/S000192 4000008459

Félix Patrón, R. S., Oyono Owono, A. C., Botez, R. M. & Labour, D. (2013, August). *Speed and altitude optimization on the FMS CMA-9000 for the Sukhoi Superjet 100 using genetic algorithms*. Paper presented at 2013 Aviation Technology, Integration, and Operations Conference, Los Angeles, CA (p. 4257). DOI: 10.2514/6.2013-4257

Félix Patrón, R. S. & Botez, R. M. (2014, November). *Flight trajectory optimization through genetic algorithms coupling vertical and lateral profiles*. Paper presented at ASME 2014 International Mechanical Engineering Congress and Exposition, Proceedings (IMECE), Montreal, QC.

Félix Patrón, R. S., Kessaci, A. & Botez, R. M. (2014). Horizontal flight trajectories optimisation for commercial aircraft through a flight management system. *The Aeronautical Journal*, *118*(1210), 1499-1518. DOI: 10.1017/S0001924000010162

Félix Patrón, R. S., Berrou, Y. & Botez, R. M. (2015). New methods of optimization of the flight profiles for performance database-modeled aircraft. *Proceedings of the Institution of Mechanical Engineers, Part G: Journal of Aerospace Engineering*, *229*(10), 1853-1867. DOI: 10.1177/0954410014561772

FlightAware. (2014). "FlightAware - Live Flight Tracking." Retrieved from flightaware.com on December 5th, 2014.

Gagné, J., Murrieta Mendoza, A., Botez, R. M. & Labour, D. (2013, August). *New method for aircraft fuel saving using Flight Management System and its validation on the L-1011 aircraft*. Paper presented at 2013 Aviation Technology, Integration, and Operations Conference, Los Angeles, CA (p. 4290). DOI: 10.2514/6.2013-4290

Gerretsen, A. & Swierstra, S. (2003). *Sensitivity of aircraft performance to variability of input data* (EUROCONTROL Doc. CoE-TP-02005). Retrieved from http://pom.tls.cena.fr/PREDICT/Documents/Perf%20Sensitivity%20report.pdf

Ghazi, G., Botez, R. M. & Tudor, M. (2015, September). *Performance Database Creation for Cessna Citation X Aircraft in Climb Regime using an Aero-Propulsive Model developed from Flight Tests*. Paper presented at Sustainability 2015: International Conference on Environmental Sustainability in Air Vehicle Design and Operations of Helicopters and Airplanes, Montreal, QC.

Gil, J. (2011). *Optimisation de la trajectoire de vol en croisière en prenant en compte l'influence du vent*. (Project Report s/n). Montréal, QC: École de Technologie Supérieure.

Girardet, B., Lapasset, L., Delahaye, D., Rabut, C. & Brenier, Y. (2013, July). *Generating Optimal Aircraft Trajectories with respect to Weather Conditions*. Paper presented at ISIATM 2013, 2nd International Conference on Interdisciplinary Science for Innovative Air Traffic Management, Toulouse: France. Retrieved from https://hal-enac.archives-ouvertes.fr/hal-00867818/document

Grabbe, S., Sridhar, B. & Cheng, N. (2006, August). *Central East Pacific Flight Routing*. Paper presented at AIAA Guidance, Navigation, and Control Conference and Exhibit, Keystone, CO (p. 6773) DOI: 10.2514/6.2006-6773

Grafarend, E. W. & Krumm, F. W. (2006). Map projections: cartographic information systems (1st ed.). Berlin Heidelberg, Germany: Springer-Verlag.

Granger, G., Durand, N. & Alliot, J. M. (2001, December). *Optimal resolution of en route conflicts*. Paper presented at ATM 2001, 4th USA/Europe Air Traffic Management Research and Development Seminar, Santa Fe, NM. Retrieved from http://www.atmseminar.org/seminarContent/seminar4/papers/p_127_DSTCDM.pdf

Hagelauer, P. & Mora-Camino, F. (1998), A soft dynamic programming approach for on-line aircraft 4D-trajectory optimization. *European Journal of Operational Research*, *107*(1), pp. 87-95. DOI: 10.1016/S0377-2217(97)00221-X

Haraldsdottir, A., Berge, M. E., Kang, L. S., Schoemig, E. G., Alcabin, M. S., Repetto, B. W. & Carter, M. L. (2006, October). *Required Navigation Performance and 3D Paths in HighTraffic ATM Operations*. Paper presented at 25th Digital Avionics Systems Conference, 2006 IEEE/AIAA, Portland, OR (pp. 1-13). DOI: 10.1109/DASC.2006.313712

Herndon, A.A., Cramer, M. & Nicholson, T. (2009, October). *Analysis of advanced flight management systems (FMS), flight management computer (FMC) field observations, trials; lateral and vertical path integration*. Paper presented at Digital Avionics Systems Conference, 2009. DASC '09. IEEE/AIAA 28th, Orlando, FL (pp.1.C.2). DOI: 10.1109/DASC.2009.5347572

Hopper, J. (2011, October). *Analysis of a wind compensation tool for the Relative Position Indicator (RPI)*. Paper presented at Digital Avionics Systems Conference (DASC), 2011 IEEE/AIAA 30th, Seattle, WA (pp. 2A3). DOI: 10.1109/DASC.2011.6095982

Huang, G.Q., Lu Y.P. & Nan Y. (2012). A survey of numerical algorithms for trajectory optimization of flight vehicles. *Science China Technological Sciences*, *55*(9), pp. 2538–2560. DOI: 10.1007/s11431-012-4946-y

International Civil Aviation Organization. (2013). *NAT Doc 007: NORTH ATLANTIC OPERATIONS AND AIRSPACE MANUAL*. (Edition 2013). Neuilly-sur-Seine, France: European and North Atlantic Office of ICAO. Retrieved from http://www.icao.int/EURNAT/EUR and NAT Documents/NAT Documents/NAT Doc 007/_NAT Doc007_Edition 2013 with bkmrks.pdf [on February 16, 2015]

Irvine, E. A., Hoskins, B. J., Shine, K. P., Lunnon, R. W. & Froemming, C. (2012). Characterizing North Atlantic weather patterns for climate-optimal aircraft routing. *Meteorological Applications*. *20*(1), pp 80-93. DOI: 10.1002/met.1291

Jackson, M. R. C., Gonda, J., Mead, R. & Saccone, G. (2009, May). *The 4D trajectory data link (4DTRAD) service-Closing the loop for air traffic control*. Paper presented at

Integrated Communications, Navigation and Surveillance Conference, 2009. ICNS'09, Arlington, VA (pp. 1-10). DOI: 10.1109/ICNSURV.2009.5172860

Jardin, M. R. & Bryson Jr., A. E. (2012), Methods for Computing Minimum-Time Paths in Strong Winds. *Journal of Guidance, Control, and Dynamics*, *35*(1), pp. 165-171. DOI: 10.2514/1.53614

Jensen, L., Hansman, R. J., Venuti, J. C. & Reynolds, T. (2013, August). *Commercial airline speed optimization strategies for reduced cruise fuel consumption*. Paper presented at 2013 Aviation Technology, Integration, and Operations Conference, Los Angeles, CA (p. 4289). DOI: 10.2514/6.2013-4289

Jensen, L., Hansman, R. J., Venuti, J. & Reynolds, T. (2014, June). *Commercial airline altitude optimization strategies for reduced cruise fuel consumption*. Paper presented at 14th AIAA Aviation Technology, Integration, and Operations Conference, Atlanta, GA (p. 3006). DOI: 10.2514/6.2014-3006

Kamgarpour, M., Dadok, V. & Tomlin, C. (2010, December). *Trajectory Generation for Aircraft Subject to Dynamic Weather Uncertainty*. Paper presented at Decision and Control (CDC), 2010 49th IEEE Conference on, Atlanta, GA (pp. 2063-2068). DOI: 10.1109/CDC.2010.5717889

Karney, C. F. F. (2011). *Geodesics on an ellipsoid of revolution*. Retrieved from https://arxiv.org/pdf/1102.1215.pdf

Karney, C. F. F. (2013). Algorithms for geodesics. *Journal of Geodesy*, *87*(1), pp. 43-55. DOI: 10.1007/s00190-012-0578-z

Kayton, M. & Fried, W. R. (1997). Avionics navigation systems (Second Edition). New York, NY: John Wiley & Sons, Inc.

Kim, B. Y., Fleming, G. G., Lee, J. J., Waitz, I. A., Clarke, J. P., Balasubramanian, S., ... & Gupta, M. L. (2007). System for assessing Aviation's Global Emissions (SAGE), Part 1: Model description and inventory results. *Transportation Research Part D: Transport and Environment*, *12*(5), 325-346. DOI: 10.1016/j.trd.2007.03.007

Kjenstad, K. (2011). Construction and computation of geometries on the ellipsoid. *International Journal of Geographical Information Science*, *25*(9), pp. 1413-1437. DOI: 10.1080/13658816.2010.518968

Knapp, D. I., Jameson, T., Measure, E. & Butler, A. (2008, January). *Optimized flight routing based on weather impacts grids*. Poster session at 13th Conference on Aviation, Range and Aerospace Meteorology, New Orleans, LA (pp. P1-11). Retrieved from https://ams.confex.com/ams/pdfpapers/132215.pdf

Krozel, J., Mitchell, J. S. B., Prete, J., Smith, P. & Andre, A. D. (2007, October). *Designing 4-D trajectories for super-dense operations given weather constraints*. Paper presented at Digital Avionics Systems Conference, 2007. DASC'07. IEEE/AIAA 26th, Dallas, TX (pp. 1-A.5). DOI: 10.1109/DASC.2007.4391821

Lee, A. G., Weygandt, S. S., Schwartz, B. & Murphy, J. R. (2009, August). *Performance of trajectory models with wind uncertainty*. Paper presented at AIAA Modeling and Simulation Technologies Conference, Chicago, IL (p. 5834). DOI: 10.2514/6.2009-5834

Leick, A. (1985). Mathematical models within geodetic frame. *Journal of surveying engineering*, *111*(2), pp. 105-117. DOI: 10.1061/(ASCE)0733-9453(1985)111:2(105)

Liden, S. (1985, June). *Practical considerations in optimal flight management computations*. Paper presented at American Control Conference, 1985, Boston, MA (pp. 675-681).

Liden, S. (1992a). Optimum 4D guidance for long flights. *Digital Avionics Systems Conference, 1992. Proceedings., IEEE/AIAA 11th*, pp. 262-267.

Liden, S. (1992b). Optimum cruise profiles in the presence of winds. *Digital Avionics Systems Conference, 1992. Proceedings., IEEE/AIAA 11th*, pp. 254-261. DOI: 10.1109/DASC.1992.282147

Lovegren, J. A. & Hansman, R. J. (2011). *Estimation of Potential Aircraft Fuel Burn Reduction in Cruise Via Speed and Altitude Optimization Strategies* (Report No. ICAT-2011-03). Retrieved from http://dspace.mit.edu/bitstream/handle/1721.1/62196/Lovegren_ICAT-2011.pdf?sequence=1

Marceau Caron, G. & Hadjaz, A. (2011, 29 June-1 July). *Beta-mesh - A dynamic 3D mesh modelization*. Paper presented at the American Control Conference (ACC), 2011, San Francisco, CA, (pp. 2148-2153). DOI: 10.1109/ACC.2011.5991291

Miyazawa, Y., Wickramasinghe, N. K., Harada, A. & Miyamoto, Y. (2013, August). *Dynamic Programming Application to Airliner Four Dimensional Optimal Flight Trajectory*. Paper presented at AIAA Guidance, Navigation, and Control (GNC) Conference, Boston, MA (p. 4969). DOI: 10.2514/6.2013-4969

Mondoloni, S., Paglione, M. & Green, S. (2002, September). *Trajectory modeling accuracy for air traffic management decision support tools*. Paper presented at ICAS 2002 Congress, Toronto, ON (pp. 491-10). Retrieved from http://icas.org/ICAS_ARCHIVE/ICAS2002/PAPERS/R45.PDF

Mondoloni, S., Swierstra, S. & Paglione, M. (2005, October – November). *Assessing trajectory prediction performance-metrics definition*. Paper presented at Digital

Avionics Systems Conference, 2005. DASC 2005. The 24th, Washington, DC (pp. 3-C.1). DOI: 10.1109/DASC.2005.1563347

Murrieta Mendoza, A. (2013). *Vertical and lateral flight optimization algorithm and missed approach cost calculation* (Masters's thesis, École de Technologie Supérieure, Montréal, QC). Retrieved from http://espace.etsmtl.ca/1188/1/MURRIETA_ MENDOZA_Alejandro.pdf

Murrieta Mendoza, A. & Botez, R. M. (2014a, November). *Lateral Navigation Optimization Considering Winds and Temperatures for Fixed Altitude Cruise Using Dijsktra's Algorithm*. Paper presented at ASME 2014 International Mechanical Engineering Congress and Exposition, Montreal, QC (pp. V001T01A054). DOI: 10.1115/ IMECE2014-37570.

Murrieta Mendoza, A. & Botez, R. (2014b, June). *Vertical navigation trajectory optimization algorithm for a commercial aircraft*. Paper presented at AIAA/3AF Aircraft Noise and Emissions Reduction Symposium, Atlanta, GA (p. 3019). DOI: 10.2514/6.2014-3019

Murrieta Mendoza, A., Beuze, B., Ternisien, L. & Botez, R. (2015, June). *Branch & Bound Based Algorithm For Aircraft VNAV Profile Reference Trajectory Optimization*. Paper presented at 15th AIAA Aviation Technology, Integration, and Operations Conference, Dallas, TX (p. 2280). DOI: 10.2514/6.2015-2280

Murrieta Mendoza, A., Botez, R. M. & Félix Patrón, R. S. (2015). *Flight Altitude Optimization Using Genetic Algorithms Considering Climb and Descent Costs in Cruise with Flight Plan Information*, (SAE Technical Paper No. 2015-01-2542). DOI: 10.4271/2015-01-2542

Murrieta Mendoza, A., Demange, S., George, F. & Botez, R. (2015, February). *Performance DataBase creation using a level D simulator for Cessna Citation X aircraft in cruise regime*. Paper presented at The 34th IASTED International Conference on Modelling, Identification and Control, MIC 2015, Innsbruck, Austria. DOI: 10.2316/P.2015.826-028

Murrieta Mendoza, A., Botez, R. M. & Ford, S. (2016). New Method to Compute the Missed Approach Fuel Consumption and its Emissions, *The Aeronautical Journal*, *120*(1228), pp. 910-929. DOI: 10.1017/aer.2016.37

Ng, H. K., Sridhar, B. & Grabbe, S. (2012, October), *A Practical Approach for Optimizing Aircraft Trajectories in Winds*. Paper presented at Digital Avionics Systems Conference (DASC), 2012 IEEE/AIAA 31st, Williamsburg, VA (pp. 3D6-1). DOI: 10.1109/DASC.2012.6382319

Nilim, A., El Ghaoui, L. & Duong, V. (2002). *Robust dynamic routing of aircraft under uncertainty. Digital Avionics Systems Conference, 2002. Proceedings. The 21st*, *1*(), pp. 1A5. DOI: 10.1109/DASC.2002.1067888

Nuic, A., Poinsot, C., Iagaru, M. G., Gallo, E., Navarro, F. A. & Querejeta, C. (2005,October – November). *Advanced aircraft performance modeling for ATM: enhancements to the BADA model*. Paper presented at Digital Avionics Systems Conference, 2005. DASC 2005. The 24th, Washington, DC (pp. 2-B). Retrieved from http://publish.eurocontrol.int/eec/gallery/content/public/document/eec/conference/paper/2005/018_Enhancements_to_the_BADA_model.pdf

Ojha, S. K. (1995). *AIAA Education Series: Flight Performance of Aircraft*. Washington, DC: American Institute of Aeronautics and Astronautics. Inc.

Paglione, M., Garcia-Avello, C., Swierstra, S., Vivona, R. & Green, S. (2005, 30 October – 3 November). *A collaborative approach to trajectory modeling validation*. Paper presented at Digital Avionics Systems Conference, 2005. DASC 2005. The 24th, Washington, DC (pp. 3-C.2). DOI: 10.1109/DASC.2005.1563350

Palopo, K., Windhorst, R. D., Suharwardy, S. & Lee, H. T. (2010). Wind-optimal routing in the national airspace system. *Journal of Aircraft*, *47*(5), 1584-1592. DOI: 10.2514/1.C000208

Panou, G., Delikaraoglou, D. & Korakitis, R. (2013). Solving the geodesics on the ellipsoid as a boundary value problem. *Journal of Geodetic Science*, *3*(1), 40-47. DOI: 10.2478/jogs-2013-0007

Pappas, G., Tomlin, C., Lygeros, J., Godbole, D. & Sastry, S. (1997, December). A next generation architecture for air traffic management systems. *Decision and Control, 1997., Proceedings of the 36th IEEE Conference on*, *3*(), 2405-2410. DOI: 10.1109/CDC.1997.657516

Prevot, T., Palmer, E., Smith, N. & Callantine, T. (2001, September). *Future air traffic management: A perspective on distributed automation*. Paper presented at CSAPC ’01, 8th Conference on Cognitive Science Approaches to Process Control, Munich, Germany. Retrieved from https://human-factors.arc.nasa.gov/publications/Prevot-01-Future-ATM-Perspective-CSAPC2001.pdf

Prevot, T. (2009, October). *NextGen technologies for mid-term and far-term air traffic control operations*. Paper presented at Digital Avionics Systems Conference, 2009. DASC'09. IEEE/AIAA 28th, Orlando, FL (pp. 2-A.4). DOI: 10.1109/DASC. 2009.5347556

Rippel, E., Bar-Gill, A. & Shimkin, N. (2005). Fast Graph-Search Algorithms for General-Aviation Flight Trajectory Generation. *Journal of Guidance, Control, and Dynamics*, *28*(4), 801-811. DOI: 10.2514/1.7370

Rivas, D., Valenzuela, A. & de Augusto, J. L. (2012). Computation of global trajectories of commercial transport aircraft. *Proceedings of the Institution of Mechanical Engineers, Part G: Journal of Aerospace Engineering*, *227*(1), 142-158. DOI: 10.1177/0954410011427107

Rodionova, O., Sbihi, M., Delahaye, D. & Mongeau, M. (2014). North Atlantic aircraft trajectory optimization. *IEEE Transactions on Intelligent Transportation Systems*, *15*(5), 2202-2212. DOI: 10.1109/TITS.2014.2312315

RTCA Inc. (2002). *Minimum Operational Peformance Standards for Required Navigation Performance for Area Navigation*. Standard RTCA DO-283. Washington, DC: RTCA, Inc.

Schreur, J. M. (1995). B737 flight management computer flight plan trajectory computation and analysis. *American Control Conference, Proceedings of the 1995*, *5*(), 3419-3424. DOI: 10.1109/ACC.1995.532246

SESAR Joint Undertaking (2015). *European ATM Master Plan: Executive View* (EDITION 2015). Luxemburg: Publications Office of the European Union. DOI: 10.2829/240873

Sidibé, S. & Botez, R. (2013). Trajectory optimization of FMS-CMA 9000 by dynamic programming. Paper presented at *60th Aeronautics Conference and AGM (Aero13) : Aerospace Clusters : Where are we Headed*?. (pp. 631-641). Toronto, ON: Canadian Aeronautics and Space Institute.

Sjöberg, L. E. (2009). New solutions to classical geodetic problems on the ellipsoid. In Siders, M. G. (Ed.), *Observing our Changing Earth* (IAG SYMPOSIA, *Vol. 133*, pp. 781-784). Berlin, Heidelberg: Springer-Verlag. DOI: 10.1007/978-3-540-85426-5_89

Sorensen, J.A., Morello, S.A, & Erzberger, H. (1979, December). *Application of trajectory optimization principles to minimize aircraft operating costs*. Paper presented at18th IEEE Conference on Decision and Control including the Symposium on Adaptive Processes, Fort Lauderdale, FL (pp. 415-421). DOI: 10.1109/CDC.1979.270208

Sorensen, J.A. (1979). *Concepts for generating optimum vertical flight profiles* (Report number CR-159181). Retrieved from https://ntrs.nasa.gov/archive/nasa/casi.ntrs.nasa.gov/19800009767.pdf

Sorensen, J. A. & Waters, M. H. (1981). *Generation of optimum vertical profiles for an advanced flight management system* (NASA Contract Report CR-165674). Retrieved from https://ntrs.nasa.gov/archive/nasa/casi.ntrs.nasa.gov/19810011523.pdf

Souders, C. G., McGettigan, S., May, J. & Dash, E. R. (2007, January). *The Next Generation Air Transportation System Weather Concept of Operations*. Paper presented at 23rd Conference on IIPS for Meteorology, Oceanography, and Hydrology, American Meteorological Society, American Meteorological Society, San Antonio, TX.

Steiner, M., Bateman, R., Benjamin, S., Brown, B., Carmichael, B., Davidson, G., … Weygandt, S. (2007, August). *Integration of probabilistic weather information with air traffic management decision support tools—A conceptual vision for the*, Paper presented at 33rd Conference on Radar Meteorology, American Meteorological Society, Cairns, Australia (pp. 12B4) Retrieved from https://www.researchgate.net/profile/Matthias_Steiner/publication/237523806_Integration_of_probabilistic_weather_information_with_air_traffic_management_decision_support_tools-A_conceptual_vision_for_the_future/links/5529398a0cf2779ab79053bd.pdf

Suchkov, A., Swierstra, S. & Nuic, A. (2003, June), *Aircraft Performance Modeling For Air Traffic Management Applications*. Paper presented at 5th USA/Europe ATM R&D Seminar, Budapest, Hungary. Retrieved from http://atmseminar.org/seminarContent/seminar5/papers/p_039_DS.pdf

Suzuki, S., Tsuchiya, T. & Andreeva, A. (2009). Trajectory optimization for safe, clean and quiet flight. *Proceedings of the 1st ENRI International Workshop on ATM/CNS (EIWAC)*, 31-35.

Swierstra, S., & Green, S. (2003, June). *Common trajectory prediction capability for decision support tools*. Paper presented at 5th USA/Eurocontrol ATM R&D Seminar, Budapest, Hungary. Retrieved from http://atmseminarus.org/seminarContent/seminar5/papers/p_059_DS.pdf

Tomlin, C., Pappas, G. J. & Sastry, S. (1998). Conflict resolution for air traffic management: A study in multiagent hybrid systems. *IEEE Transactions on Automatic Control*, *43*(4), 509-521. DOI: 10.1109/9.664154

Tomlin, C. J., Pappas, G. J., Košecká, J., Lygeros, J. & Sastry, S. S. (1998). Advanced air traffic automation: A case study in distributed decentralized control. In B. Siciliano & K. P. Valavanis (Eds.), *Control Problems in Robotics and Automation* (LNCIS, *Vol. 230*, pp. 261-295). Berlin, Heidelberg: Springer Berlin Heidelberg. DOI: 10.1007/BFb0015088

Tong, K.O., Schoemig, E.G., Boyle, D.A., Scharl, J. & Haraldsdottir, A. (2007, October). *Descent profile options for continuous descent arrival procedures within 3D path concept*. Paper presented at Digital Avionics Systems Conference, 2007. DASC'07. IEEE/AIAA 26th., Dallas, TX (pp. 3-A). DOI: 10.1109/DASC.2007.4391872

Visintini, A. L., Glover, W., Lygeros, J. & Maciejowski, J. (2006). Monte Carlo optimization for conflict resolution in air traffic control. *IEEE Transactions on Intelligent Transportation Systems*, *7*(4), 470-482. DOI: 10.1109/TITS.2006.883108

Warren, A. (2000, June). *Trajectory prediction concepts for next generation air traffic management*. Presented at 3rd USA/Europe ATM R&D Seminar, Napoli, Italy (p. 171). Retrieved from http://atmseminarus.org/seminarContent/seminar3/papers/p_091_AGOADM.pdf

Wichman, K. D., Klooster, J. K., Bleeker, O. F. & Rademaker, R. M. (2007, October). *Flight validation of downlinked flight management system 4D trajectory*. Paper presented at Digital Avionics Systems Conference, 2007. DASC'07. IEEE/AIAA 26th, Dallas, TX (pp. 1-D.1). DOI: 10.1109/DASC.2007.4391833

Wilburn, J. N., Perhinschi, M. G. & Wilburn, B. K. (2013a, August). *Implementation of a 3-Dimensional Dubins-Based UAV Path Generation Algorithm*. Paper presented at AIAA Guidance, Navigation, and Control (GNC) Conference, Boston, MA (p. 5232). DOI: 10.2514/6.2013-5232

Wilburn, J. N., Perhinschi, M. G. & Wilburn, B. K. (2013b, August). *Implementation of composite clothoid paths for continuous curvature trajectory generation for UAVs*. Paper presented at AIAA Guidance, Navigation, and Control (GNC) Conference, Boston, MA (p. 5230). DOI: 10.2514/6.2013-5230

Wilson, I. & Hafner, F. (2005, October – November*). Benefit assessment of using continuous descent approaches at Atlanta*. Paper presented at Digital Avionics Systems Conference, 2005. DASC 2005. The 24th, Washington, DC (pp. 2-B). DOI: 10.1109/DASC.2005.1563318

Wirth, L., Oettershagen, P., Ambühl, J. & Siegwart, R. (2015, March). *Meteorological path planning using dynamic programming for a solar-powered UAV*. Paper presented at Aerospace Conference, 2015 IEEE, Big Sky, MT (pp. 1-11). DOI: 10.1109/AERO.2015.7119284

World Meteorological Organization. (2003). *Guide to the WMO Table Driven Code Form Used for the Representation and Exchange of Regularly Spaced Data In Binary Form: FM 92 GRIB Edition 2*. Geneva, Switzerland: WMO. Retrieved from https://www.wmo.int/pages/prog/www/WMOCodes/Guides/GRIB/GRIB2_062006.pdf

Zillies, J., Kuenz, A., Schmitt, A., Schwoch, G., Mollwitz, V., & Edinger, C. (2014, April), *Wind optimized routing: An opportunity to improve european flight efficiency?*. Paper presented at Integrated Communications, Navigation and Surveillance Conference (ICNS), 2014, Herndon, VA (pp. X3-1). DOI: 10.1109/ICNSurv.2014.6820029